2017

Using Remote Sensing to Estimate Crop Water Use to Improve Irrigation Water Management

Arturo Reyes-Gonzalez
South Dakota State University

USING REMOTE SENSING TO ESTIMATE CROP WATER USE TO IMPROVE

IRRIGATION WATER MANAGEMENT

BY

ARTURO REYES-GONZÁLEZ

A dissertation submitted in partial fulfillment of the requirements for the

Doctor of Philosophy

Major in Biological Science

South Dakota State University

2017

USING REMOTE SENSING TO ESTIMATE CROP WATER USE TO IMPROVE IRRIGATION WATER MANAGEMENT

This dissertation is approved as a creditable and independent investigation by a candidate for the Doctor of Philosophy in Biological Science degree and is acceptable for meeting the dissertation requirements for this degree. Acceptance of this does not imply that the conclusions reached by the candidates are necessary the conclusions of the major department.

Todd Trooien Ph.D.   Date
Major Advisor
Department of Agricultural and Biosystems Engineering

Jeppe Kjaersgaard Ph.D.   Date
Dissertation Advisor
Minnesota Department of Agriculture

Van Kelley Ph.D.   Date
Head
Department of Agricultural and Biosystems Engineering

Dean, Graduate School   Date

ACKNOWLEDGEMENT

Thank God for blessing me

I would like to express my sincere appreciation to Dr. Jeppe Kjaersgaard for his help, guidance, and comments contributed to the quality of this dissertation. I also thank to my graduate committee members, Drs. Todd Trooien, Christopher Hay, and Laurent Ahiablame for their guidance and comments to improve the quality of my dissertation.

I would also like to thank Mike Schmidt for his cooperation in providing the field site. Also thank Ryan Vanderleest and Nathan Edwards for providing meteorological datasets.

Much thanks to the National Council for Science and Technology of México (CONACYT) and the National Institute of Forestry, Agriculture, and Livestock Research (INIFAP) for funding my doctoral scholarship. Additional funding was provided by the South Dakota Experiment Station and the South Dakota Water Resource Institute, thank you.

Special thanks to my wife, Maria, daughter, Jenny, son, Jesus, for their invaluable patience, support, and love during my studies. I want to thank my mom Lucina and my sister Fanny for their prayers and love.

TABLE OF CONTENT

ABBREVIATIONS

AM	Ante meridiem
ALEXI	Atmosphere Land Exchange Inverse
ASCE	American Society of Civil Engineers
BREBS	Bowen Ratio Energy Balance System
CIMEC	Calibration using Inverse Modeling of Extreme Conditions
CWSI	Crop water stress index
DAE	Day after emergence
DOY	Day of year
"d"	Index of agreement
dT	Near surface air temperature difference
E	Evaporation
EB	Energy balance
EC	Eddy cvariance
e.g.	For example
ET	Evapotranspiration
ET_a	Actual evapotranspiration
ET_a-METRIC	Actual evapotranspiration estimated with METRIC
ET_a-atm	Actual evapotranspiration estimated with atmometer
ET_c	Crop evapotranspiration
ETM+	Enhanced Thematic Mapper Plus
ET_{ins}	Instantaneous evapotranspiration
ET_r	Reference evapotranspiration

ET_r-atm	Reference evapotranspiration from atmometer
ET_r-P-M	Reference evapotranspiration from Penman-Monteith equation
ET_rF	Reference evapotranspiration fraction
ET_{24}	Evapotranspiration for 24-hour period
FC	Field capacity
G	Soil heat flux
H	Sensible heat flux
INIFAP	Instituto Nacional de Investigaciones Forestales, Agrícolas y Pecuarias
IRTs	Infrared thermometers
K_c	Crop coefficient
LAI	Leaf area index
LAS	Large Aperture Scintillometer
LE	Latent heat flux
MBE	Mean bias error
METRIC	Mapping EvapoTranspiration at high Resolution using Internal Calibration
NDVI	Normalized Difference Vegetation Index
NIR	Near-infrared band
OLI	Operational Land Imager
PWP	Permanent wilting point
QC	Quality control
RH	Relative humidity
R_n	Net radiation
Rs	Solar radiation

RMSE	Root mean square error
r^2	Coefficient of determination
SAVI	Soil adjusted vegetation index
SEBAL	Surface Energy Balance Algorithm for Land
SEBS	Surface Energy Balance Systems
SSEB	Simplified Surface Energy balance
Std. Dev.	Standard deviation
T	Transpiration
Ta	Air temperature
Td	Dew point temperatue
TIM	Trapezoid Interpolation Model
TIRS	Thermal Infrared Sensor
T_s	Surface temperature
TSEB	Two-source Energy Balance Model
UAV	Unmanned aerial vehicles
USGS	United States Geological Survey
VIs	Vegetation indices
V	Vegetation stage
VWC	Volumetric water content
R	Reproductive stage

LIST OF FIGURES

LIST OF TABLES

ABSTRACT

USING REMOTE SENSING TO ESTIMATE CROP WATER USE TO IMPROVE

IRRIGATION WATER MANAGEMENT

ARTURO REYES-GONZÁLEZ

2017

Irrigation water is scarce. Hence, accurate estimation of crop water use is necessary for proper irrigation managements and water conservation. Satellite-based remote sensing is a tool that can estimate crop water use efficiently.

Several models have been developed to estimate crop water requirement or actual evapotranspiration (ET_a) using remote sensing. One of them is the Mapping EvapoTranspiration at High Resolution using Internalized Calibration (METRIC) model. This model has been compared with other methods for ET estimations including weighing lysimeters, pan evaporation, Bowen Ratio Energy Balance System (BREBS), Eddy Covariance (EC), and sap flow. However, comparison of METRIC model outputs to an atmometer for ET_a estimation has not yet been attempted in eastern South Dakota. The results showed a good relationship between ET_a estimated by the METRIC model and estimated with atmometer ($r^2 = 0.87$ and RMSE = 0.65 mm day^{-1}). However, ET_a values from atmometer were consistently lower than ET_a values from METRIC.

The verification of remotely sensed estimates of surface variables is essential for any remote-sensing study. The relationships between LAI, T_s, and ET_a estimated using the remote sensing-based METRIC model and *in-situ* measurements were established.

The results showed good agreement between the variables measured *in situ* and estimated by the METRIC model. LAI showed $r^2 = 0.76$, and RMSE = 0.59 m^2 m^{-2}, T_s had $r^2 = 0.87$ and RMSE 1.24 °C and ET$_a$ presented $r^2 = 0.89$ and RMSE = 0.71 mm day^{-1}.

Estimation of ET$_a$ using energy balance method can be challenging and time consuming. Thus, there is a need to develop a simple and fast method to estimate ET$_a$ using minimum input parameters. Two methods were used, namely 1) an energy balance method (EB method) that used input parameters of the Landsat image, weather data, a digital elevation map, and a land cover map and 2) a K$_{c\text{-NDVI}}$ method that use two input parameters: the Landsat image and weather data. A strong relationship was found between the two methods with r^2 of 0.97 and RMSE of 0.37 mm day^{-1}. Hence, the K$_{c\text{-NDVI}}$ method performed well for ET$_a$ estimations, indicating that K$_{c\text{-NDVI}}$ method can be a robust and reliable method to estimate ET$_a$ in a short period of time.

Estimation of crop evapotranspiration (ET$_c$) using satellite remote sensing-based vegetation index such as the Normalized Difference Vegetation Index (NDVI). The NDVI was calculated using near-infrared and red wavebands. The relationship between NDVI and tabulated K$_c$'s was used to generate K$_c$ maps. ET$_c$ maps were developed as an output of K$_c$ maps multiplied by reference evapotranspiration (ET$_r$). Daily ET$_c$ maps helped to explain the variability of crop water use during the growing season. Based on the results we can conclude that ET$_c$ maps developed from remotely sensed multispectral vegetation indices are a useful tool for quantifying crop water use at regional and field scales.

This dissertation resulted in three manuscripts submitted for publication.

- Reyes-González, A., Kjaersgaard, J., Trooien, T., Hay, C., and Ahiablame, L. Comparative Analysis of METRIC model and atmometer methods for estimating actual evapotranspiration. *International Journal of Agronomy*, submitted April 2017.

- Reyes-González, A., Kjaersgaard, J., Trooien, T., Hay, C., and Ahiablame, L. Assessing the relationship between leaf area index, surface temperature, and actual evapotranspiration estimated using the remote sensing-based METRIC model and *in-situ* measurements. *Applied Engineering in Agriculture*, submitted May 2017.

- Reyes-González, A., Kjaersgaard, J., Trooien, T., Hay, C., and Ahiablame, L. Comparison of actual evapotranspiration estimated with energy balance and vegetation index methods. *Journal of Irrigation and Drainage Engineering*, submitted June 2017.

CHAPTER 1: General Introduction

1.1   Evapotranspiration

Evapotranspiration (ET) is the largest component of the hydrologic cycle after

precipitation (Irmak, 2011; Shoko, Dube, Sibanda, & Adelabu, 2015). However, for

irrigated areas in arid and semi-arid regions ET may be is the largest component. ET is

the loss of water from the land surface to the atmosphere through two separate processes,

viz. evaporation (E) from soil and water surfaces and transpiration (T) from vegetative

surfaces (R. G. Allen, Pereira, Raes, & Smith, 1998; Gowda, Chavez, et al., 2008). Both

processes are driven by the available energy and the drying potential of the air, but

transpiration depends also on the capacity of plants to replenish the leaf tissue with water

coming from the root zone (Irmak, 2011). Evaporation of water from the soil and

transpiration from the stomatal cavities of plants account for more than 98 percent of the

crop water use of most plant species (USDA-SCS, 1993). When the crop is small, water

is lost by soil evaporation, but once the crop is well developed and completely cover the

soil, transpiration becomes the main process (R. G. Allen et al., 1998). Crops lose their

water through stomata. Stomata are little pores on the leaf surface that regulates the

transpiration (R. G. Allen et al., 1998). Energy is required to evaporate water from the

stomatal cavity (R. G. Allen et al., 1998; Tasumi, 2003). The largest energy source is

from solar radiation. ET can be limited by either the amount of available energy or water

available in the soil profile (R. G. Allen et al., 1998; USDA-SCS, 1993).

There are several factors that affect the ET rates such as weather factor (e.g., solar

radiation, air temperature, wind speed, and the vapor pressure), crop factor (e.g., crop

type, crop variety, and growth stages), and soil factor (e.g., hydraulic properties, water retention capacity, and soil salinity) (R. G. Allen et al., 1998). ET varies according to several factors, understanding these variations, an accurate estimation of ET is essential for improving irrigation water management. Thus, ET continues to be of foremost importance in irrigation agriculture.

Various methods have been developed to estimate ET directly or indirectly such as weighing lysimeters, pan evaporation, soil water balance, atmometer, Bowen Ratio Energy Balance System (BREBS), Eddy covariance (EC), and sap flow (R. G. Allen, Pereira, Howell, & Jensen, 2011). However those methods are *in situ* point measurement and do not provide information at regional scale (Gowda, Chavez, et al., 2008; Knipper, Hogue, Scott, & Franz, 2017; Shoko et al., 2015) also some of them requires maintenance and are expensive (He et al., 2017; Maeda, Wiberg, & Pellikka, 2011; Xu et al., 2015). To overcome this problem, remote sensing techniques are alternative to estimate ET at regional scale in less time and with less cost (R. Allen, A. Irmak, R. Trezza, J. M. Hendrickx, et al., 2011; J Kjaersgaard, Allen, & Irmak, 2011). ET varies in both space and time. It is variable in space because of the wide spatial variability of precipitation, hydraulic properties of soil, and vegetation types. It is variable in time because of variability of climate and development or senescence of vegetation (R. Allen, Trezza, Tasumi, & Kjaersgaard, 2014). For these reasons satellite images are a useful tool for determining and mapping the spatial and temporal variability of ET (R. Allen et al., 2014).

To estimate ET at regional scale, two types of remote sensing approaches have been developed (R. G. Allen et al., 2011; Gowda, Chavez, et al., 2008; Neale, Jayanthi, &

Wright, 2005; Trezza, Allen, & Tasumi, 2013). The first approach computes ET using the

energy balance (EB) method, obtaining ET as a residual of the energy balance equation

(R. G. Allen, Tasumi, & Trezza, 2007) computed as:

$$LE = R_n - G - H \tag{1}$$

where LE is the latent heat flux (W m^{-2}), or ET$_a$ (mm day^{-1}), R_n is the net

radiation (W m^{-2}), G is the soil heat flux (W m^{-2}), and H is the sensible heat flux (W m^{-2}).

The second approach estimates ET using vegetation indices (VI) derived from

canopy reflectance values to compute crop coefficient (K$_c$) values (Glenn, Neale,

Hunsaker, & Nagler, 2011; Gontia & Tiwari, 2010). The K$_c$ values are multiplied by the

reference evapotranspiration (ET$_r$) to estimate actual evapotranspiration (ET$_a$), which is

computed as follows:

$$ET_a = K_c \times ET_r \tag{2}$$

The second approach can be an alternative to estimate crop water requirements at

regional and field scale in regions where digital elevation, land cover map, and thermal

infrared data are not available for ET$_a$ estimations.

1.2   The METRIC Model

In the last decades several models have been used to estimate ET$_a$ at different

scales using remotely sensed data (Gowda, Chavez, et al., 2008). The models include

Surface Energy Balance Algorithm for Land (SEBAL) (W. G. Bastiaanssen, M. Menenti,

R. Feddes, & A. Holtslag, 1998), Surface Energy Balance System (SEBS) (Su, 2002),

Mapping EvapoTranspiration at High Resolution with Internalized Calibration

(METRIC) (R. G. Allen, Tasumi, & Trezza, 2007), Atmosphere-Land Exchange Inverse

(ALEXI) (Martha C Anderson, Norman, Mecikalski, Otkin, & Kustas, 2007), and

Simplified Surface Energy Balance (SSEB) (Senay, Budde, Verdin, & Melesse, 2007).

The foundation of the SEBAL model was developed in the mid-1990 for the purpose of

estimating ET over agricultural areas using satellite surface energy fluxes (W. G.

Bastiaanssen et al., 1998). The METRIC model uses the innovative SEBAL method for

estimating sensible heat flux by using the near surface to air temperature gradient (dT) for

each pixel within an image based on a regression relationship between the dT and

radiometric surface temperature of two anchor pixels. The anchor pixels represent the

conditions of an agricultural field with full vegetation cover and maximum crop ET (cold

condition) and a bare agricultural field with no vegetation cover (hot condition) (see

Appendix (Table A1)) (R. G. Allen, Tasumi, & Trezza, 2007; JH Kjaersgaard et al.,

2008). Entire details of how the METRIC model calculates LE, R_n, G, and H is described

in the next chapter in section 2.3.3.

One of the advantages of the METRIC model compared to previous surface

energy balance-based models for use in arid areas is that it utilizes reference

evapotranspiration (ET$_r$) for estimating actual evapotranspiration (ET$_a$) at the cold pixel

condition (R. G. Allen, Tasumi, & Trezza, 2007). Because ET$_r$ is based on ground-based

meteorological measurements, and because ET$_r$ is calibrated to account for atmospheric

conditions common in arid and semi-arid conditions, such as horizontal advection, the

METRIC model is particularly useful for ET$_a$ estimations under arid or semi-arid

conditions (R. G. Allen, Tasumi, & Trezza, 2007). In METRIC all weather data should be

subjected to a rigorous quality control prior to be used in any calculations as suggested by

R. G. Allen et al. (1998). Also, METRIC utilizes hourly ET$_r$ to auto calibrate the sensible

heat calculations for each overpass image. This internal calibration makes ET$_a$ estimates

more precise and robust (He et al., 2017). The METRIC model is also one of the most

appropriate models for estimating ET_a over agricultural fields during the growing season

(R. G. Allen, Tasumi, Morse, et al., 2007). For these reasons the METRIC model was

used in this dissertation to development accurate ET_a maps and estimate crop water use at

regional and field scales.

1.3 Vegetation Indices

Remote sensing techniques can estimate crop coefficients (K_c) based on spectral

reflectance of vegetation indices such as the Normalized Difference Vegetation Index

(NDVI) (Glenn et al., 2011). K_c developed from NDVI determine ET_c better than a

tabulated K_c because it represents the actual crop growth conditions and capture the

spatial variability among different fields (Gontia & Tiwari, 2010; Kullberg, DeJonge, &

Chávez, 2017; Lei & Yang, 2012; Neale et al., 2005). However, under periods with little

vegetation the K_c developed from NDVI is less accurate. The NDVI is the difference

between near-infrared (NIR) and Red band reflectances divided by their sum (Rouse Jr,

Haas, Schell, & Deering, 1974). NDVI is calculated as follows:

$$NDVI = \frac{NIR - Red}{NIR + Red} \tag{3}$$

where NIR and Red are the near-infrared and red bands, respectively.

Also NDVI values are related with physiological processes that depend on light

absorption by the canopy including ET (Glenn et al., 2011). Neale, Bausch, and Heerman

(1989) related the crop canopy reflectance to K_c for corn, developing a successful

technique for estimating ET_a.

1.4   Objectives

The specific objectives of this dissertation were to:

- Compare METRIC model and atmometer methods for estimating actual evapotranspiration (chapter 2)
- Assess the relationship between leaf area index (LAI), surface temperature (T_s), and actual evapotranspiration (ET_a) estimated using the remote sensing-based METRIC model and in-situ measurements (chapter 3)
- Compare actual evapotranspiration estimated with energy balance and vegetation index methods (chapter 4)
- Estimate crop evapotranspiration (ET_c) using satellite remote sensing-based vegetation index (chapter 5)

1.5   Dissertation Organization

The dissertation is organized in six chapters. The first chapter presents a general introduction. The second chapter compares the METRIC model and atmometer for ET_a estimations, this study was carried out in three corn fields at three sites (Brookings, Volga, and Oak Lake) in eastern South Dakota. The third chapter assess the relationship between LAI, T_s, and ET_a estimated with METRIC model and *in situ* measurements, this research was carried out at a commercial field in eastern South Dakota. LAI and T_s were measured in situ with AccuPAR and infrared thermometer, respectively and ET_a was estimated using an atmometer and a K_c. The fourth chapter compares ET_a estimated with energy balance and estimated with vegetation index (NDVI), this study was carried out in five corn field during two growing seasons in Brookings, SD. The energy balance method

used four input parameters including Landsat image, weather data, a digital elevation map, and a land cover map, while NDVI method used two input parameters including Landsat image and weather data for ET_a estimations. The fifth chapter estimates ET_c using remote sensing-based vegetation index, this research was carried out in five silage corn fields during four growing seasons in northern México. The sixth chapter gives a general conclusions.

1.6   Dissertation Contributions

This dissertation contributes to:

- Improving the estimation of crop water demands at regional and field scale

- Determining proper irrigation scheduling

- Improving irrigation water management

- Better water resource planning

- Estimating crop water use using minimum input parameters

- Helping to conserve irrigation water

1.7   Importance and implications of the dissertation

As groundwater is depleted, food and fiber production are threatened. This dissertation is important because developed tools to help to minimize the groundwater depletion, based on accurate estimation of crop water use using satellite remote sensing techniques.

The implications of the research were:

- Daily ET maps generated in this research will be used for irrigation scheduling because it show when and how much water is required by the crop

- Policy makers and consultants will have accurate estimates of crop water use using satellite remote sensing methods developed in this research

- Producers will use crop coefficients generated in this dissertation to have better irrigation water management

- Farmers will implement the results of this research to reduce their seasonal water application amounts by 18% just by using actual ET instead of reference ET

- Atmometers will be used to measure reference ET in places where weather stations are unavailable or impractical

1.8   References

Allen, R., Irmak, A., Trezza, R., Hendrickx, J. M., Bastiaanssen, W., & Kjaersgaard, J. (2011). Satellite-based ET estimation in agriculture using SEBAL and METRIC. *Hydrological Processes, 25*(26), 4011-4027.

Allen, R., Trezza, R., Tasumi, M., & Kjaersgaard, J. (2014). METRIC: Mapping Evapotranspiration at High Resolution Using Internalized Calibration Applications Manual for Landsat Satellite Imagery*., V 3.0*, 279.

Allen, R. G., Pereira, L. S., Howell, T. A., & Jensen, M. E. (2011). Evapotranspiration information reporting: I. Factors governing measurement accuracy. *Agricultural Water Management, 98*(6), 899-920.

Allen, R. G., Pereira, L. S., Raes, D., & Smith, M. (1998). Crop evapotranspiration-Guidelines for computing crop water requirements-FAO Irrigation and drainage paper 56. *FAO, Rome, 300*(9), D05109.

Allen, R. G., Tasumi, M., Morse, A., Trezza, R., Wright, J. L., Bastiaanssen, W., . . . Robison, C. W. (2007). Satellite-based energy balance for mapping

evapotranspiration with internalized calibration (METRIC)—Applications. *Journal of Irrigation and Drainage Engineering, 133*(4), 395-406.

Allen, R. G., Tasumi, M., & Trezza, R. (2007). Satellite-based energy balance for mapping evapotranspiration with internalized calibration (METRIC)—Model. *Journal of Irrigation and Drainage Engineering, 133*(4), 380-394.

Anderson, M. C., Norman, J. M., Mecikalski, J. R., Otkin, J. A., & Kustas, W. P. (2007). A climatological study of evapotranspiration and moisture stress across the continental United States based on thermal remote sensing: 1. Model formulation. *Journal of Geophysical Research: Atmospheres, 112*(D10).

Bastiaanssen, W. G., Menenti, M., Feddes, R., & Holtslag, A. (1998). A remote sensing surface energy balance algorithm for land (SEBAL). 1. Formulation. *Journal of Hydrology, 212*, 198-212.

Glenn, E. P., Neale, C. M., Hunsaker, D. J., & Nagler, P. L. (2011). Vegetation index-based crop coefficients to estimate evapotranspiration by remote sensing in agricultural and natural ecosystems. *Hydrological Processes, 25*(26), 4050-4062.

Gontia, N. K., & Tiwari, K. N. (2010). Estimation of crop coefficient and evapotranspiration of wheat (Triticum aestivum) in an irrigation command using remote sensing and GIS. *Water resources management, 24*(7), 1399-1414.

Gowda, P. H., Chavez, J. L., Colaizzi, P. D., Evett, S. R., Howell, T. A., & Tolk, J. A. (2008). ET mapping for agricultural water management: present status and challenges. *Irrigation Science, 26*(3), 223-237.

He, R., Jin, Y., Kandelous, M. M., Zaccaria, D., Sanden, B. L., Snyder, R. L., Jiang, J., & Hopmans, J. W. (2017). Evapotranspiration Estimate over an Almond Orchard Using Landsat Satellite Observations. *Remote Sensing, 9*(5), 436.

Irmak, A. (Ed.) (2011). *Evapotranspiration - Remote Sensing and Modeling*. Janeza Trdine 9, 51000 Rijeka, Croatia.

Kjaersgaard, J., Allen, R., Aggett, G., Schneider, C., Hattendorf, M., Irmak, A., . . . Robison, C. (2008). *Computation of Landsat based evapotranspiration maps along the South Platte and North Platte Rivers.* Paper presented at the World Environmental and Water Resources Congress 2008: Ahupua'A.

Kjaersgaard, J., Allen, R., & Irmak, A. (2011). Improved methods for estimating monthly and growing season ET using METRIC applied to moderate resolution satellite imagery. *Hydrological Processes, 25*(26), 4028-4036.

Knipper, K., Hogue, T., Scott, R., & Franz, K. (2017). Evapotranspiration Estimates Derived Using Multi-Platform Remote Sensing in a Semiarid Region. *Remote Sensing, 9*(3), 184.

Kullberg, E. G., DeJonge, K. C., & Chávez, J. L. (2017). Evaluation of thermal remote sensing indices to estimate crop evapotranspiration coefficients. *Agricultural Water Management, 179*, 64-73.

Lei, H., & Yang, D. (2012). Combining the Crop Coefficient of Winter Wheat and Summer Maize with a Remotely Sensed Vegetation Index for Estimating Evapotranspiration in the North China Plain. *Journal of Hydrologic Engineering, 19*(1), 243-251.

Maeda, E. E., Wiberg, D. A., & Pellikka, P. K. (2011). Estimating reference evapotranspiration using remote sensing and empirical models in a region with limited ground data availability in Kenya. *Applied Geography, 31*(1), 251-258.

Neale, C. M., Bausch, W. C., & Heerman, D. (1989). Development of reflectance-based crop coefficients for corn. *Trans. ASAE, 32*(6), 1891-1899.

Neale, C. M., Jayanthi, H., & Wright, J. L. (2005). Irrigation water management using high resolution airborne remote sensing. *Irrigation and Drainage Systems, 19*(3), 321-336.

Rouse Jr, J. W., Haas, R., Schell, J., & Deering, D. (1974). Monitoring vegetation systems in the Great Plains with ERTS.

Senay, G. B., Budde, M., Verdin, J. P., & Melesse, A. M. (2007). A coupled remote sensing and simplified surface energy balance approach to estimate actual evapotranspiration from irrigated fields. *Sensors, 7*(6), 979-1000.

Shoko, C., Dube, T., Sibanda, M., & Adelabu, S. (2015). Applying the Surface Energy Balance System (SEBS) remote sensing model to estimate spatial variations in evapotranspiration in Southern Zimbabwe. *Transactions of the Royal Society of South Africa, 70*(1), 47-55.

Su, Z. (2002). The Surface Energy Balance System (SEBS) for estimation of turbulent heat fluxes. *Hydrology and Earth System Sciences Discussions, 6*(1), 85-100.

Tasumi, M. (2003). *Progress in operational estimation of regional evapotranspiration using satellite imagery*.

Trezza, R., Allen, R. G., & Tasumi, M. (2013). Estimation of actual evapotranspiration along the Middle Rio Grande of New Mexico using MODIS and landsat imagery with the METRIC model. *Remote Sensing, 5*(10), 5397-5423.

USDA-SCS. (1993). Chapter 2. *Irrigation water requirements.* In Part 623 National Engineering Handbook. Washington, D.C.: USDA Soil Conservation Service.

Xu, T., Liu, S., Xu, L., Chen, Y., Jia, Z., Xu, Z., & Nielson, J. (2015). Temporal upscaling and reconstruction of thermal remotely sensed instantaneous evapotranspiration. *Remote Sensing, 7*(3), 3400-3425.

CHAPTER 2: Comparative Analysis of METRIC Model and Atmometer Methods for Estimating Actual Evapotranspiration

2.1 Abstract

Accurate estimation of crop evapotranspiration (ET) is a key factor in agricultural water management including irrigated agriculture. The objective of this study was to compare ET estimated from the satellite-based remote sensing METRIC model to *in situ* atmometer readings. Atmometer readings were recorded from three sites in eastern South Dakota every morning between 8:15 and 8:30 AM for the duration of the 2016 growing season. Seven corresponding clear sky images from Landsat 7 and Landsat 8 (Path 29, Row 29) were processed and used for comparison. Three corn fields in three sites were used to compare actual evapotranspiration (ET_a). The results showed a good relationship between ET_a estimated by the METRIC model (ET_a-METRIC) and ET_a estimated with atmometer (ET_a-atm) ($r^2 = 0.87$, Index of agreement of 0.84, and RMSE = 0.65 mm day^{-1}). However, ET_a-atm values were consistently lower than ET_a-METRIC values. The differences in daily ET_a between the two methods increase with high wind speed values (>4 m s^{-1}). Results from this study are useful for improving irrigation water management at local and field scales.

2.2 Introduction

With increasing demands placed on freshwater resources worldwide, it is necessary to accurately estimate crop water consumption efficiently. Uses for crop water use information is needed for a range of applications, including improving agricultural water management, irrigation and crop selection, water resource planning, water rights management, and water regulations (R. Allen, A. Irmak, R. Trezza, J. M. Hendrickx, et al., 2011; Martha C. Anderson, Allen, Morse, & Kustas, 2012; Marvin E Jensen & Allen, 2016). Irrigated agriculture produces 40% of global food and fiber supply from 20% of the world's croplands (Thenkabail, Hanjra, Dheeravath, & Gumma, 2010). In arid areas, up to 90% of all water withdrawals may be for irrigation purposes (Bos, Kselik, Allen, & Molden, 2008). With increasing population and water uses a scarce water supply is put under additional pressure and other water users relying on the same water supply may experience insufficient water allocations. At the same time, a reduction of irrigation water supply may result in loss of production and, ultimately, threatened food security. There is an opportunity, however, to optimize the management of water in agricultural production systems, and the accurate estimation of evapotranspiration (ET) is critical in that regard.

ET is the loss of water from the land surface to the atmosphere through two processes, *viz.* evaporation (E) from soil and water surfaces and transpiration (T) from vegetative surfaces (R. G. Allen, Tasumi, Morse, et al., 2007; Gowda, Chavez, et al., 2008). ET rates are affected by weather conditions such as solar radiation, air temperature, wind speed and air vapor pressure deficit, and plant and soil characteristics conditions (R. G. Allen et al., 1998; George, Reddy, Raghuwanshi, & Wallender, 2002). Different methods, direct and indirect exist to estimate ET. Direct methods include

weighing lysimeters and soil water balance estimations while indirect methods include

pan evaporation, atmometer, Bowen Ratio Energy Balance System (BREBS), Eddy

covariance (EC), scintillometer, sap flow, and remote sensing (R. G. Allen et al., 2011).

An attractive property of satellite-based remote sensing ET estimates using Landsat

imagery is its coverage on a field by field basis at a regional scale (R. Allen, A. Irmak, R.

Trezza, J. M. Hendrickx, et al., 2011; R. G. Allen, Tasumi, & Trezza, 2007; J

Kjaersgaard et al., 2011).

Several models have been developed to estimate ET using remote sensing. One of

them is the Mapping EvapoTranspiration at High Resolution using Internalized

Calibration (METRIC) Model. METRIC utilizes the innovative Surface Energy Balance

Algorithm for Land (SEBAL) method for estimating sensible heat flux. METRIC uses

the near surface to air temperature gradient (dT) for each pixel within an image based on

a regression relationship between the dT and radiometric surface temperature of two

anchor pixels. The anchor pixels represent the conditions of an agricultural field with full

vegetation cover and maximum crop ET (cold condition) and a bare agricultural field

with no vegetation cover (hot condition)(R. G. Allen, Tasumi, & Trezza, 2007; JH

Kjaersgaard et al., 2008).

One of the advantages of the METRIC model compared to previous surface energy

balance-based models for use in arid areas is that it utilizes reference evapotranspiration

(ET_r) for estimating actual evapotranspiration (ET_a) at the cold pixel condition (R. G.

Allen, Tasumi, & Trezza, 2007). Because ET_r is based on ground-based meteorological

measurements, and because ET_r is calibrated to account for atmospheric conditions

common in arid and semi-arid conditions, such as horizontal advection, the METRIC

model is particularly useful for ET_a estimations under arid or semi-arid conditions (R. G. Allen, Tasumi, & Trezza, 2007).

Previous studies have compared METRIC model outputs to other methods of ET_a estimation such as weighing lysimeter (R. G. Allen, Tasumi, & Trezza, 2007), soil water balance (Chavez, Gowda, Howell, Marek, & New, 2007), Bowen Ratio Energy Balance System (BREBS) (Carrasco-Benavides et al., 2014; Hankerson, Kjaersgaard, & Hay, 2012; Healey et al., 2011; Singh & Irmak, 2009), Eddy Correlation (EC) (e. g., (Folhes, Rennó, & Soares, 2009; Gordillo Salinas, Flores Magdaleno, Tijerina Chávez, & Arteaga Ramírez, 2014; Liebert, Huntington, Morton, Sueki, & Acharya, 2016; Zhang, Anderson, & Wang, 2015), Large Aperture Scintillometer (LAS) (Mkhwanazi, Chávez, & Rambikur, 2012) and the METRIC-MODIS method (Trezza et al., 2013). These studies showed from moderate to strong relationships between observed and METRIC-estimated ET_a, indicating that the METRIC model is a useful tool for estimating accurate ET_a at local and field scales. In addition, the METRIC model has been compared with other models such as water balance model (Santos, Lorite, Tasumi, Allen, & Fereres, 2008), trapezoid interpolation model (TIM) (Choi, Kim, Park, & Kim, 2011; Choi et al., 2009), two-source energy balance model (TSEB) (French, Hunsaker, & Thorp, 2015; Gonzalez-Dugo et al., 2009), SIMDualKc model (Paço et al., 2014), and the Landsat-MODIS fusion model (Bhattarai, Quackenbush, Dougherty, & Marzen, 2015). However, comparison of METRIC model outputs to an atmometer for ET_a estimation has not yet been attempted, indicating that a knowledge gap exist in developing a method to estimate crop water requirements using both the remote sensing-based METRIC model and the atmometer method.

An atmometer is a device that measures the amount of water evaporated from wet porous surface to the atmosphere (Broner & Law, 1991) Atmometers are simple and inexpensive devices, that consists of a ceramic evaporation plate (Bellani plate) covered by a green canvas, mounted on top of a cylindrical water reservoir, to provide a visual interpretation of atmospheric demand for pulling water out of the vegetation and the soil (Alam & Trooien, 2001; Magliulo, d'Andria, & Rana, 2003). The standard model with number 54 green canvas is recommended for measuring alfalfa ET_r similar to the alfalfa-based Penman-Monteith ET_r, while number 30 green canvas is designed to simulate grass ET_r similar to the grass-based Penman-Monteith ET_o (Alam & Trooien, 2001; S. Irmak, Dukes, & Jacobs, 2005).

Research demonstrated that ET_r estimated with atmometers was moderate correlated (r^2 = ~0.70) with weighing lysimeters values (Casanova, Messing, Joel, & Cañete, 2009; Mendonça, Sousa, Bernardo, Dias, & Grippa, 2003), strongly correlated (r^2 = 0.90) to pan evaporation values (Kidron, 2005; Pelton, 1964), and strongly correlated (r^2 = 0.92) to agrometeorological data values (e.g., (Knox, Rodriguez-Diaz, & Hess, 2011; Lamine, BODIAN, & DIALLO, 2015; Peterson, Bremer, & Fry, 2015; A. Reyes-Gonzalez et al., 2016; Taghvaeian, Chávez, Bausch, DeJonge, & Trout, 2014).

The objective of this study was to compare ET_a estimated from satellite-based remote sensing METRIC model to ET_a estimated with atmometers in corn fields in eastern South Dakota.

2.3   Material and Methods

2.3.1   Study Area

The study was carried out at three sites in eastern South Dakota at Brookings (44° 19'N, 96° 46'W), Volga (44° 18'N, 96° 55'W), and Oak Lake (44° 30'N, 96° 31'W) at elevations 500, 497, and 574 m above sea level, respectively. Three corn fields near to each atmometer (nine total fields) were selected and considered to estimate ET_a (Figure 2.1). The population density was approximately 78,000 plants ha^{-1} in all fields. Corn fields in Brookings and Volga had 0-2% slope, while the Oak Lake had 2-6% slope (NRCS Web Soil Survey, 2016 http://websoilsurvey.nrcs.usda.gov). All fields used in this study are in corn - soybean crop rotation system. The average annual precipitation is 533 mm, of which ¾ typically falls during the growing season April through October. The mean annual maximum temperature is 12.4 °C, minimum 0.89 °C, and mean 6.63 °C. The climate of the study area is classified as moist subhumid according to the Thornthwaite climate classification system (Keim, 2010).
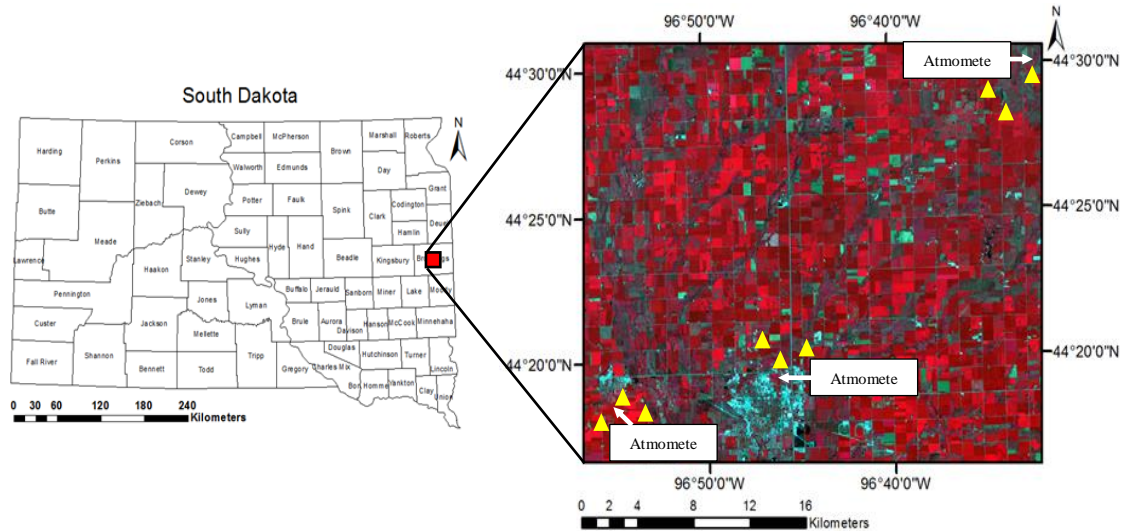
Figure 2.1 South Dakota with county boundaries. The red rectangle shows the study area in eastern South Dakota (left). Landsat 8 with false color composite (bands 4, 3, 2) indicates the atmometer locations and the nine yellow triangles show corn field sites (right).

2.3.2   Landsat Images

We used seven clear-sky images from Landsat 7 Enhanced Thematic Mapper Plus (ETM+) and Landsat 8 Operational Land Imager (OLI) and Thermal Infrared Sensor (TIRS) (Path 29, Row 29), Table 2.1. The images were downloaded from the United States Geological Survey (USGS) EROS Datacenter (http://glovis.usgs.gov). The images were selected based on the temporal coverage and cloud-free conditions. Images with cloud located >10 km from all study sites were considered acceptable. The images were processed using the METRIC model running in ERDAS Imagine Software environment (J Kjaersgaard & Allen, 2010). The time of satellite overpass of both Landsats ranged from 11:11 to 11:14 AM., local time (Table 2.1). Landsat 7 and 8 have a pixel resolution of 30 m by 30 m in the shortwave bands and 60 m by 60 m and 100 m by 100 m in the thermal band, respectively.

The wedge-shaped gaps appearing within the Landsat 7 images as a result of the SLC-off issue were removed using the Imagine built-in focal analysis tool. During the process, the gap are filled iterative based on information from nearby pixels. The gap filling is completed prior to image processing (http://landsat.usgs.gov/gap-filling-landsat-7-slc-single-scenes-using-erdas-imagine). An example of the process is shown in Figure 2.2.
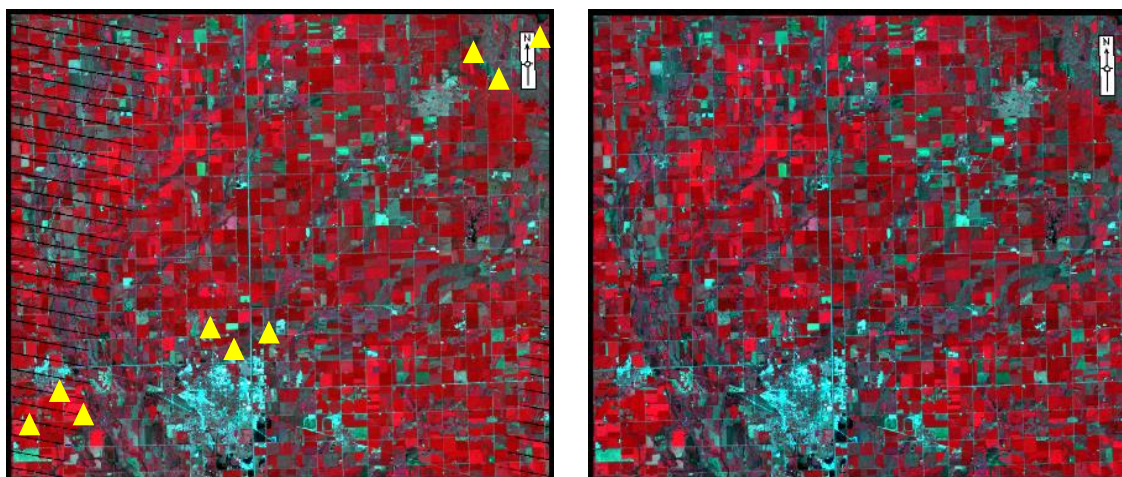
Figure 2.2 Stripes removed from Landsat 7 image. Original image with nine yellow triangles that indicate corn field sites (left) and final image without stripes, where SLC-off image filled after employing the focal analysis tool two times (right).

Table 2.1 Day of year (DOY), selected acquisition dates, Landsat satellite, path/row, and overpass time during corn growing season 2016, used for ET_a estimations.

DOY	Acquisition Dates	Satellite	Path/Row	Overpass time (local)
154	06/02/16	Landsat 8	29/29	11:11:03 AM
178	06/26/16	Landsat 7	29/29	11:13:56 AM
194	07/12/16	Landsat 7	29/29	11:13:55 AM
202	07/20/16	Landsat 8	29/29	11:11:21 AM
218	08/05/16	Landsat 8	29/29	11:11:24 AM
234	08/21/16	Landsat 8	29/29	11:11:30 AM
258	09/14/16	Landsat 7	29/29	11:14:05 AM

2.3.3 METRIC Model

ET$_a$ estimations using the METRIC model approach as described by R. G. Allen,

Tasumi, and Trezza (2007) and R. Allen, A. Irmak, R. Trezza, J. M. Hendrickx, et al.

(2011).

METRIC model is a remote sensing image processing model that computes

instantaneous ET values as a residual of the surface energy balance equation (R. Allen,

A. Irmak, R. Trezza, J. M. Hendrickx, et al., 2011; R. G. Allen, Tasumi, Morse, et al.,

2007; Bastiaanssen et al., 2005; Tasumi, Allen, Trezza, & Wright, 2005):

$$LE = R_n - G - H \tag{1}$$

where LE is the latent heat flux (W m^{-2}), or ET (mm day^{-1}), R_n is the net radiation

(W m^{-2}), G is the soil heat flux (W m^{-2}), and H is the sensible heat flux (W m^{-2}).

Net radiation (R_n) is calculated using surface reflectance and surface temperature

(T$_s$) derived by satellite imagery. R_n is the difference between incoming shortwave

radiation and outgoing longwave radiation compute as:

$$R_n = R_{S\downarrow} - \alpha R_{S\downarrow} + R_{L\downarrow} - R_{L\uparrow} - (1 - \varepsilon_o) R_{L\downarrow} \tag{2}$$

where $R_{S\downarrow}$ is the incoming shortware radiation (W m^{-2}) (solar radiation), α surface

albedo (dimensionless), $R_{L\downarrow}$ is the incoming longware radiation (W m^{-2}), $R_{L\uparrow}$ is the

outgoing longware radiation (W m^{-2}), and ε_o is the surface thermal emissivity

(dimensionless).

Soil heat flux (G) is the magnitude of the heat flux stored or released into the soil.

G was computed using the following equations described by Tasumi (2003).

$$\frac{G}{Rn} = 0.05 + 0.18 \, e^{-0.521 \, \text{LAI}} \qquad\qquad \text{LAI} \geq 0.5 \tag{3}$$

$$\frac{G}{Rn} = 1.80 \, (T_s - 273.16)/R_n + 0.084 \qquad\qquad \text{LAI} < 0.5 \tag{4}$$

Sensible heat flux (H) was determined using the aerodynamic based heat transfer equation as follows:

$$H = \rho_{air} \, C_p \, \frac{dT}{r_{ah}} \tag{5}$$

where ρ_{air} is the air density (kg m^{-3}), C_p is the air specific heat (1004 J kg^{-1} K^{-1}), dT is the temperature difference between two heights z_1 (0.1 m) and z_2 (2 m), and r_{ah} is the aerodynamic resistance to heat transfer (s m^{-1}).

For the H estimations, the METRIC model uses the CIMEC (Calibration using Inverse Modeling of Extreme Conditions) procedure described by W. Bastiaanssen, M. Menenti, R. Feddes, and A. Holtslag (1998) and R. G. Allen, Tasumi, and Trezza (2007) to calibrate the near surface to air temperature difference for each pixel within an image based on a regression relationship between the dT and T$_s$ of two anchor pixels (hot and cold). The advantage of the CIMEC approach within the METRIC model reduces possible impacts of biases in estimation of aerodynamic stability correction and surface roughness (R. G. Allen, Tasumi, & Trezza, 2007).

In this study, hot and cold pixels were selected for each image in agricultural fields near to the weather stations (<15 km). The hot pixel was selected in a bare agricultural field with no vegetation cover, based on high temperature values (~308 °K (33.85 °C)), albedo (~0.17), low biomass (LAI) (~0.85), and low NDVI (~0.3), while the cold pixel was selected in an agricultural field with full vegetation cover, based in low temperature values (~298 °K (24.85 °C)), albedo (~0.21), high biomass (LAI) (~5.6), and high NDVI (~0.82).

Based on LE values, the instantaneous values of ET was computed for each pixel as:

$$ET_{inst} = 3600 \; \frac{LE}{\lambda \rho w} \tag{6}$$

where ET_{inst} is the hourly instantaneous ET (mm h^{-1}), 3600 is used to convert to

hours, LE is the latent heat flux (W m^{-2}) consumed by ET, ρw is the density of water

(1000 kg m^{-3}), and λ is the latent heat of evaporation (j kg^{-1}), which is computed as:

$$\lambda = (2.501 - 0.00236(T_s - 273.15) \times 10^6) \tag{7}$$

The reference ET fraction (ET$_r$F) or crop coefficient (K$_c$) was calculated based on

ET$_{ins}$ for each pixel and ET$_r$ was obtained from locally weather data.

$$ET_r F = \frac{ET_{inst}}{ET_r} \tag{8}$$

Daily values of ET (ET$_{24}$) (mm day^{-1}) for each pixel was calculated as follows:

$$ET_{24} = ET_r F \; \times \; ET_r 24 \tag{9}$$

where $ET_r F$ is the reference ET fraction, $ET_r 24$ is the cumulative alfalfa reference

for the day (mm day^{-1}), and ET_{24} is the actual evapotranspiration for the entire 24-hour

period (mm day^{-1}).

Daily ET was estimated by the assumption that the ET$_r$F$_{ins}$ at satellite overpass

time is the same as the ET over the 24-hour average (R. G. Allen et al., 1998).

Monthly and seasonal ET$_a$ are calculated by interpolating daily values of ET$_r$F

between images and multiplying by ET$_r$ for each day and then integrated over the specific

month (R. G. Allen, Tasumi, & Trezza, 2007). The interpolation values of ET$_r$F are made

using a linear interpolation or a curvilinear interpolation function such as a spline

function (Wright, 1982). According to R. G. Allen, Tasumi, and Trezza (2007) one

cloud-free satellite image per month is enough to develop ET$_r$F curves for seasonal ET$_a$

estimations.

2.3.4 Meteorological Data

Hourly weather data was used for the internal calibration of the METRIC model. The weather observations were taken from the automatic Brookings, Volga, and Oak Lake stations. All weather stations are located in Brookings County, SD. The weather stations at Brookings and Oak Lake sites are surrounded by grass, whereas the weather station at Volga is surrounded by corn fields.

The ET$_r$ values were calculated using weather dataset using the Penman-Monteith equation (R. G. Allen et al., 1998; ASCE-EWRI, 2005) as follows:

$$ET_{ref} = \frac{0.408\,\Delta(R_n - G) + \gamma \frac{C_n}{T+273} u_2(e_s - e_a)}{\Delta + \gamma(1 + C_d u_2)} \tag{10}$$

where ET_{ref} is the alfalfa reference (mm day^{-1}), Δ is the slope pressure versus air temperature curve (kPa °C^{-1}), R_n is the net radiation at the crop surface (MJ m^{-2} day^{-1}), G is the soil heat flux at the soil surface (MJ m^{-2} day^{-1}), T is the mean air temperature at 1.5 to 2.5 m height (°C), u_2 is the mean daily wind speed at 2 m height (m s^{-1}), e_s is the saturation vapor pressure of the air (kPa), e_a is the actual vapor pressure of the air (kPa), γ is the psychrometric constant (0.0671 kPa °C^{-1}), $e_s - e_a$ is the vapor pressure deficit (kPa), C_n is the numerator constant (1600 K mm s^3 Mg^{-1} day^{-1}), C_d is the denominator constant (0.38 s m^{-1}) for alfalfa reference, and 0.408 is the coefficient constant (m^2 mm MJ^{-1}).

All weather data, were subjected to quality control (QC) prior to being used in any calculations as suggested by R. G. Allen et al. (1998) and ASCE-EWRI (2005). Hourly QC included the following weather variables such as solar radiation, air temperature (maximum and minimum), wind speed, and air vapor pressure deficit.

Therefore, accurate estimations of ET_a depends of the quality weather data. Some outputs of quality control are shown in the Appendix (Figures A1 and A2).

2.3.5   Atmometers

Three atmometers were used to measure daily ET_r. One automated atmometer Model E (ETgage Company, Loveland, Colorado, USA) was placed adjacent to the Oak Lake weather station. The automated atmometer Model E was connected to the automated Oak Lake weather station controlled by a CR1000 datalogger (Cambell Scientific, CSI, Logan, UT, USA), where the evaporated data were recorded every 5 minutes. Two manual atmometers were located adjacent to the Brookings and to the Volga weather station, respectively. Manual atmometers were manually recorded every morning between 8:00 and 8:30 AM at the Brookings and Volga sites, respectively. The evaporated water from the green canvas in manual atmometers was measured as the difference between the observed water levels on consecutive days (Gavilán & Castillo-Llanque, 2009).

All atmometers were covered with a number 54 green canvas that mimics evaporation rates of alfalfa reference crop. The atmometers were installed on a vertical wooden post using metal brackets and with the top of the ceramic evaporation surface 1.0 m above the ground surface. The atmometers were surrounded by grass at the Brookings and Oak Lake sites, while at the Volga site the atmometer was surrounded by rainfed corn fields (<5 m) in all directions. Due to rodent damage to the canvas, the wooden post at Volga site was replaced by a metal rod in early August (DOY 217) as shown in Figure 2.3 which prevented further damage and resulting loss of ET_r data.

The atmometer observation period was from May 17, 2016 (DOY 138) to September 18, 2016 (DOY 262), during this period the atmometers were refilled two times with distilled water. Distilled water was used in the atmometer reservoir to prevent accumulation of solutes in and on the top of the plate that can decrease the porosity of the plate and affect the evaporation rates (S. Irmak et al., 2005).
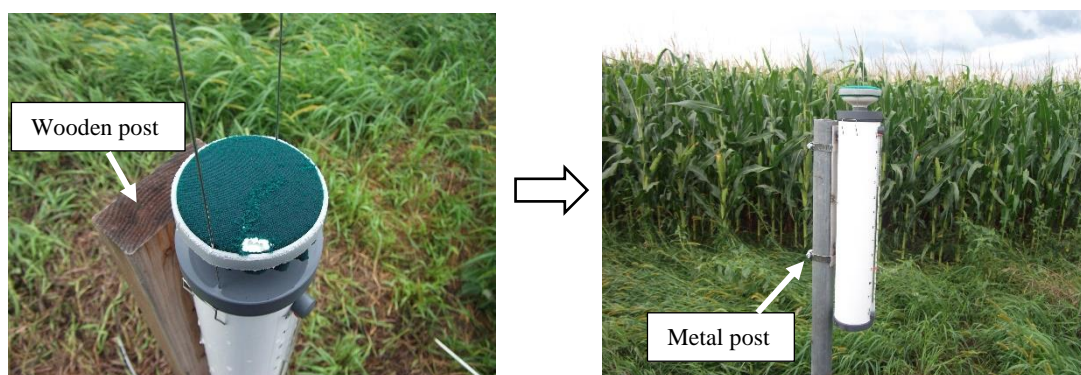
Figure 2.3 Atmometer mounted in wooden post damaged by mice (left) and mounted on a metal post (right) at Volga site.

2.3.6 Development of Crop Coefficient (K_c) Curves

K_c curves were developed for each corn field at three sites based on the alfalfa reference crop coefficient using Manual 70 (Appendix E) method (Marvin E Jensen & Allen, 2016). This method uses percent of time from planting to effective cover and days after effective cover to harvest for Kc calculations. In our study, the effective cover for corn fields occurred around 55 days after emergence (DAE) based on field observations. Thus the effective cover was used such as a reference point to calculate local Kc values. Local K_c values for different corn growth stages were calculated and adjusted using DAE. According to S. Irmak, Odhiambo, Specht, and Djaman (2013) the DAE is more

accurate because it ignores the period prior to emergence and is more closely related with

to the corn growing period, from emergence until physiological maturity.

The K_c curves generated in this study for different corn fields (Figure 2.6) were

multiplied by the ET_r obtained from atmometers to estimate ET_a (ET_a-atm) and compare

it with ET_a estimated with the METRIC model (ET_a-METRIC).

2.3.7 Statistical Analysis between ET$_a$-METRIC and ET$_a$-atm.

Statistical comparison between ET_a-METRIC and ET_a-atm was established using

a simple linear regression. For the simple regression the model was $y = a + bx$, where y

is ET_a-atm and x is ET_a-METRIC. Other statistical evaluations such as mean bias error

(MBE) (Eq. 11), root mean square error (RMSE) (Eq. 12), coefficient of determination

(r^2) (Eq. 13), and Willmott index of agreement "d" (Eq. 14) were used to determine

agreement between ET_a-atm and ET_a-METRIC (Willmott, 1981).

$$MBE = \frac{1}{n} \sum_{i=1}^{n}(x_i - y_i) \tag{11}$$

$$RMSE = \sqrt{\frac{1}{n} \sum_{i=1}^{n}(x_i - y_i)^2} \tag{12}$$

$$r^2 = \frac{\sum_{i=1}^{n}(x_i - \bar{x})(x_i - \bar{y})}{\sqrt{\sum_{i=1}^{n}(x_i - \bar{x})^2 \sum_{i=1}^{n}(y_i - \bar{y})^2}} \tag{13}$$

$$d = 1 - \frac{\sum_{i=1}^{n}(x_i - y_i)^2}{\sum_{i=1}^{n}(|x_i - \bar{x}| + |y_i - \bar{x}|)^2} \tag{14}$$

where n is the observation number, x_i is the estimated value with the METRIC

model, y_i is estimated value using atmometer, and the bars above the variables indicate

averages.

2.4   Results and Discussion

2.4.1   Precipitation and Reference Evapotranspiration (ET$_r$)

The cumulative precipitation values for the growing period were 450 mm, 497 mm, and 380 mm for Brookings, Volga, and Oak Lake, respectively. In 2016 the cumulative precipitation for the three sites were greater than the average rain (~360 mm) that typically falls during the growing season (April-October). The precipitation events had good distribution during the corn growing season due to the major events occurred in development stage (vegetation stage (V5) (June, 17) and tassel stage (VT) (July 10) (Figure 2.3). In the tassel stage corn is sensitive to water stress.

Daily values of ET$_r$ from atmometers (ET$_r$-atm) varied from 0.5 to 10, 0.5 to 9.5 and 0.5 to 7.6 mm day^{-1} for Brookings, Volga, and Oak Lake, respectively (Figure 2.4). The ET$_r$ from Penman-Monteith equation (ET$_r$-PM) varied from 1.3 to 9.1 mm day^{-1} for Brookings, 1.0 to 10.4 mm day^{-1} for Volga, and 1.3 to 9.6 mm day^{-1} for Oak Lake (Figure 2.4). The highest ET$_r$-atm values recorded in the three sites were in early June (day of the year (DOY) 161) and the lowest were in early September (DOY 249). The highest ET$_r$-PM values registered in the three sites were in early June (DOY 157) and the lowest values were in middle of September (DOY 259). Even so, moderate correlations between ET$_r$-PM values and ET$_r$-atm values in the three sites were found with r^2 of 0.64, 0.59, and 0.67 for Brookings, Volga, and Oak Lake sites, respectively (Figure 2.5).
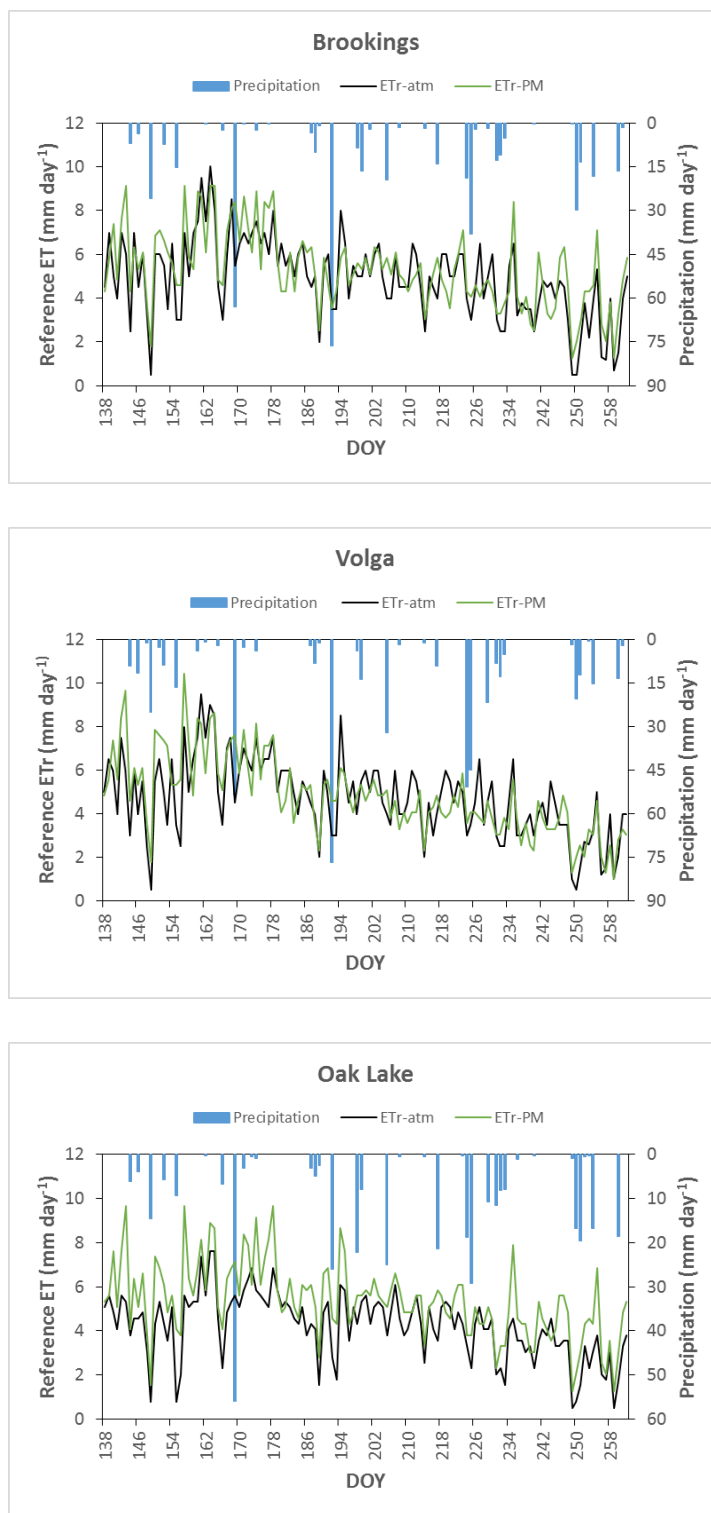
Figure 2.4 Daily ET$_r$ and precipitation for three different sites during the 2016 growing season in eastern South Dakota.
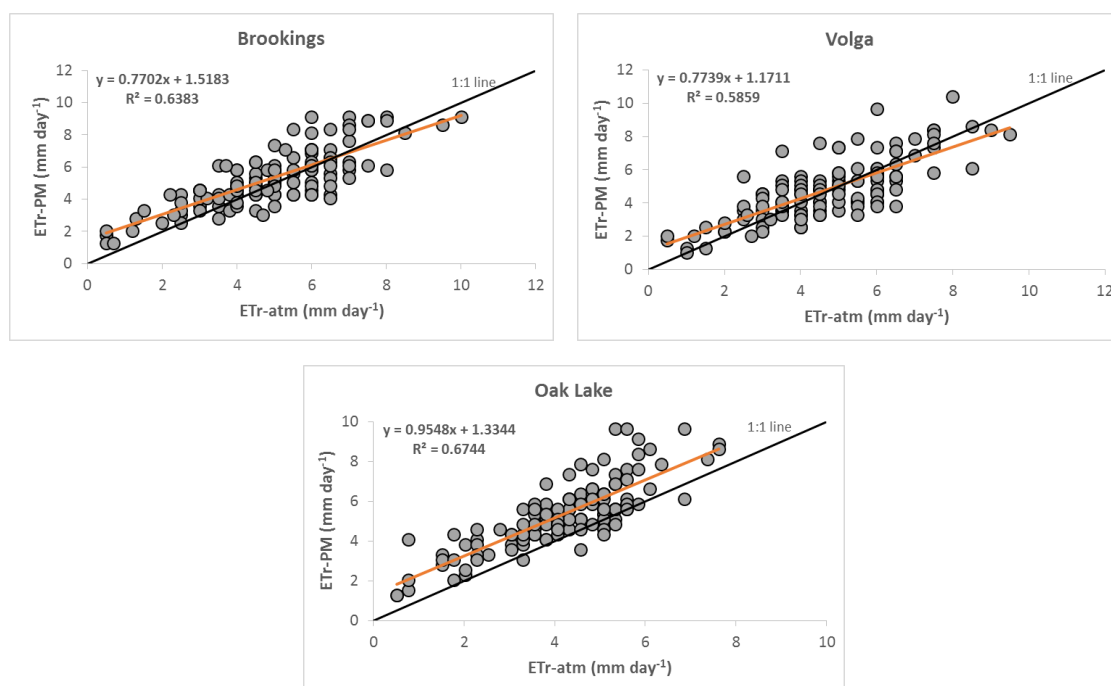
Figure 2.5 Relationship between ET_r-PM values and ET_r-atm values at the Brookings, Volga, and Oak Lake sites throughout the corn growing season 2016.

2.4.2 Development of Crop Coefficient (K_c) Curves

The trends of K_c for each corn field at three different sites during the growing season are shown in Figure 2.6. The K_c curves showed similar tendencies for all corn fields, where K_c values increased from initial stage (vegetation stage (V3)) to mid-season stage (VT). In this period the K_c values increase as a function of time between 10% of crop cover to 100% of effective cover. In the mid-season the K_c remains constant (K_c = 1.0), while in the late season the K_c values gradually decreased indicating the crop senescence. At the end of the season (reproductive stage (R6)) the K_c values are low again (K_c = ~0.5)

The K_c curves depend of vegetation index, soil water content, weather conditions, crop variety, and growing degree days (R. G. Allen et al., 1998; Djaman & Irmak, 2012;

S. Irmak et al., 2013; Reyes-González, Trooien, Kjaersgaard, Hay, & Reta-Sánchez, 2016). In this study, K_c curves for corn fields presented little variability because of rainfall events, emergence days, and air temperature were almost homogenous in our study area.

The maximum K_c values observed in this study were similar to the Kc_r (from alfalfa-reference) values reported by Djaman and Irmak (2012), who reported maximum Kc_r values from 50 to 70 DAE in corn with rainfed treatment. Also, Wright (1982) found maximum Kc_r values at the 100% of effective full cover for a corn field. However, our K_c values are different from those reported by other researchers A Irmak and Irmak (2008) and Singh and Irmak (2009). They found the peak Kc_r values (~1.0) from late July to early August (~70 DAE) for corn fields planted in south central Nebraska.
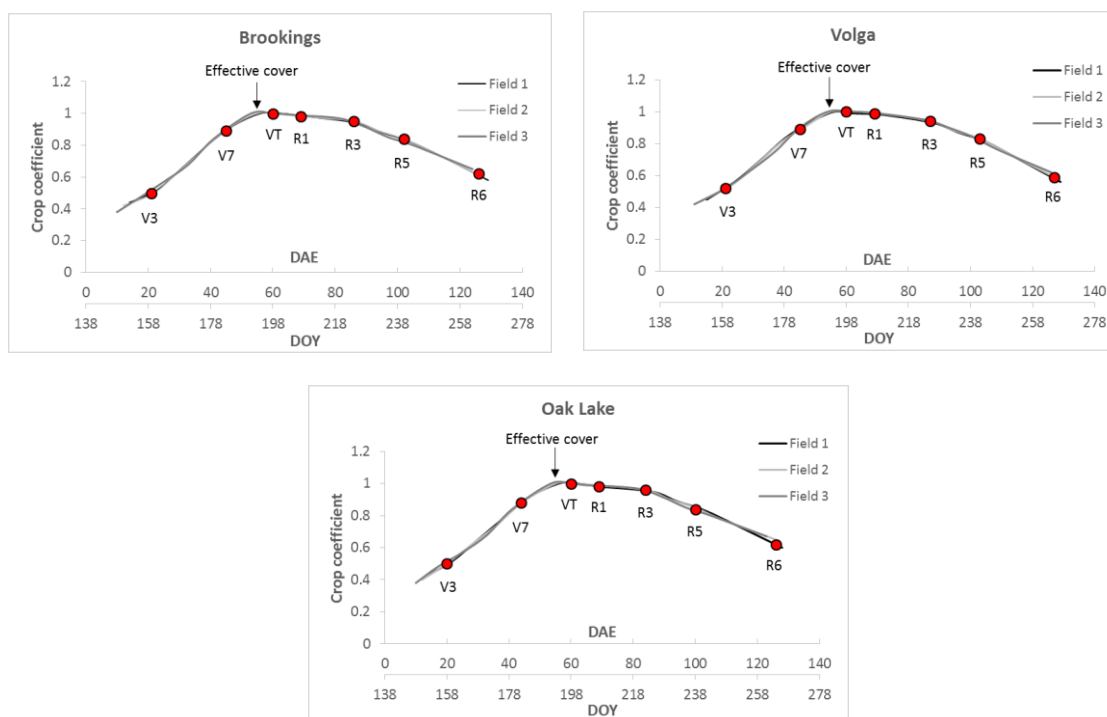
Figure 2.6 Crop coefficient curves based on the alfalfa-reference crop coefficient in three fields at the Brookings, Volga, and Oak Lake sites. The red circles indicates images dates.

2.4.3   ET$_a$ Maps and variation of ET$_a$ throughout the growing season

Spatial and temporal distribution of ET$_a$ maps during the growing season were generated by the METRIC model for Brookings, Volga, and Oak Lake (data no showed). However, Figure 2.7 shows two ET$_a$ maps for Brookings site, one ET$_a$ map displays high ET$_a$-METRIC values in a corn field at mid-season (DOY 194) and another ET$_a$ map shows low ET$_a$-METRIC values at the end of the season (DOY 258).

Figure 2.8 shows the variation of ET$_a$-METRIC values throughout the growing season at three sites. ET$_a$-METRIC values for Brookings ranged from 2.2 to 8.2 mm day^{-1}, for Volga ranged from 2.6 to 8.0 mm day^{-1}, and for Oak Lake ranged from 2.2 to 8.8 mm day^{-1}. In general the ET$_a$-METRIC values for corn were low in early stage when the corn height was around 0.22 m and 30% canopy cover, were high in mid-season when corn height was ~2.3 m and 100% canopy cover and then decrease in the late season when corn showed 60% of canopy cover. Early October all corn fields presented yellow leaves indicating that the growing season is almost finished. Early November all corn fields were harvested.

The ET$_a$ maps developed by the METRIC model in this study were similar to other ET maps generated by the METRIC model and reported by Chavez et al. (2007), Santos et al. (2008), Folhes et al. (2009), Droogers, Immerzeel, and Lorite (2010), Healey et al. (2011), Carrillo-Rojas, Silva, Córdova, Célleri, and Bendix (2016), where they reported the spatial and temporal distribution of daily ET$_a$ for different crops including corn. In other situations, Chavez et al. (2007) reported maximum ET$_a$ values (14.1 mm day^{-1}) due to high wind speed values (7.0 m s^{-1}) at the time of satellite overpass in corn field in Texas High Plains, USA.
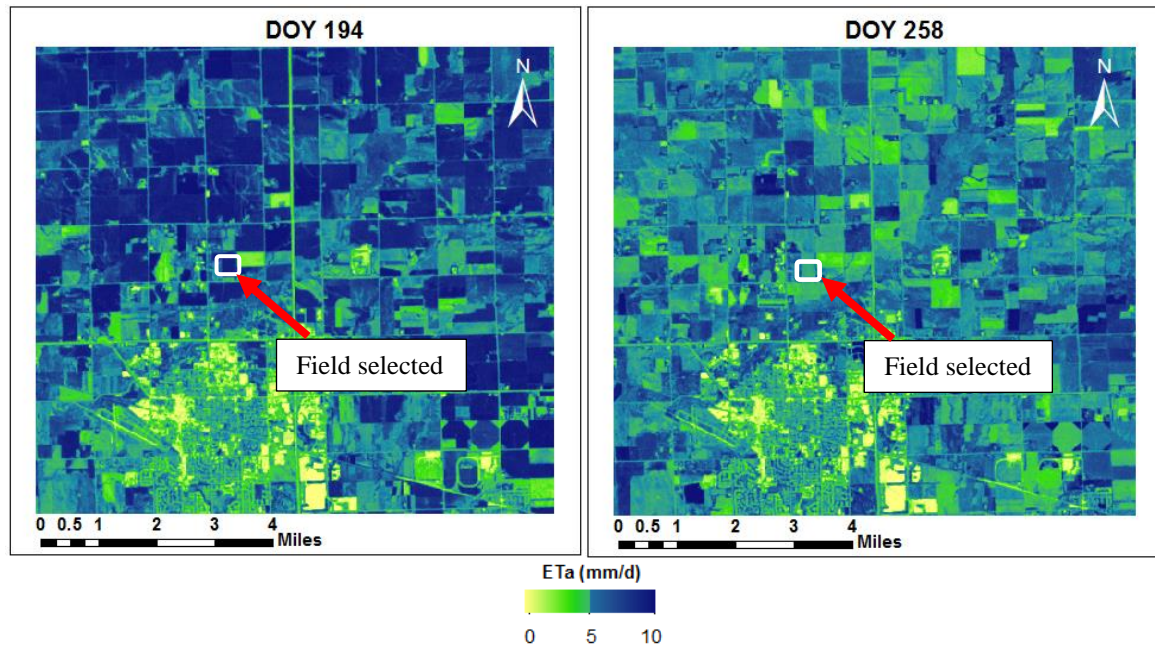
Figure 2.7 ET$_a$ maps developed by the METRIC model. White small rectangle show the corn field selected on DOY 194 and DOY 258. These dates showed high and low ET$_a$-METRIC values throughout the growing season 2016 at the Brookings site.
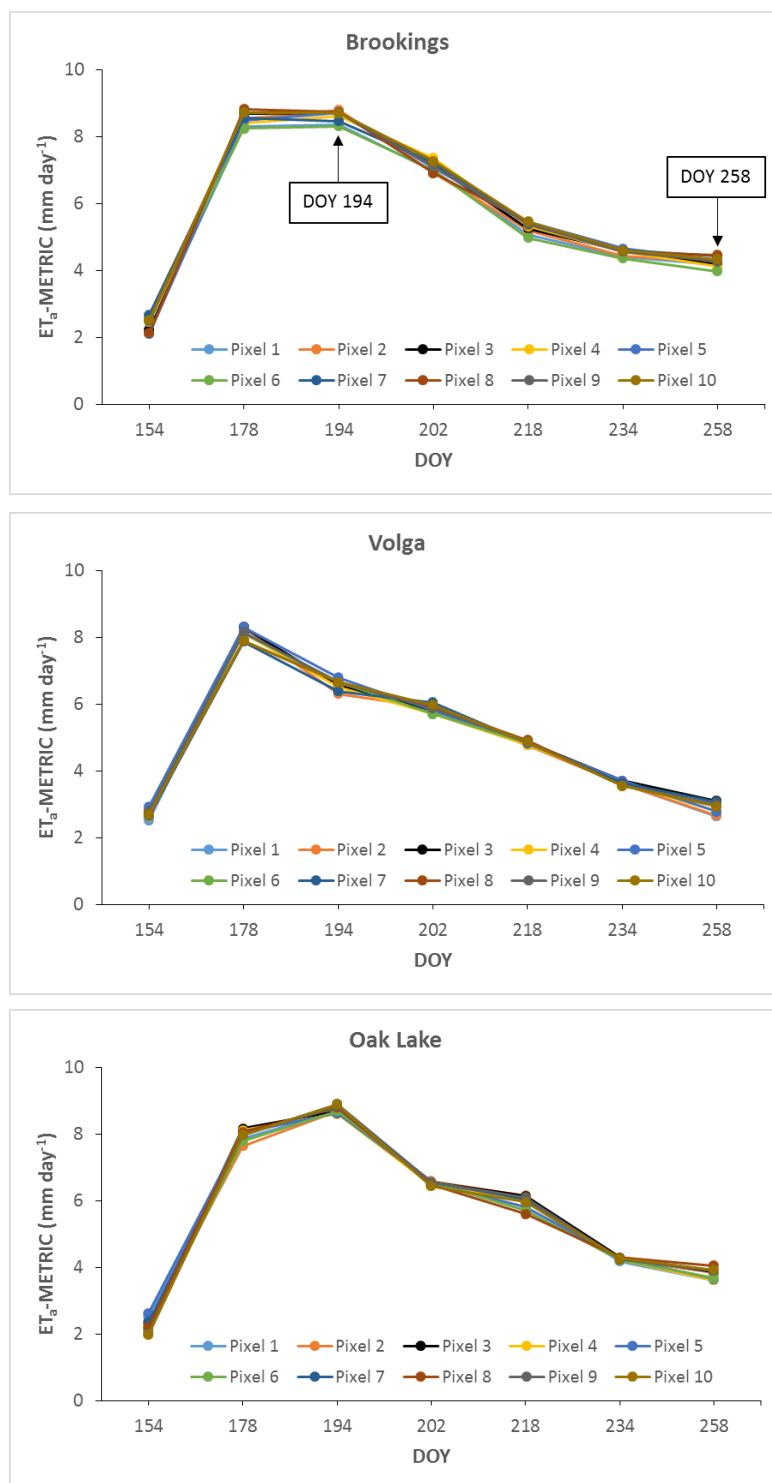
Figure 2.8 Evolution of ET$_a$-METRIC values at three sites in eastern South Dakota. Ten randomly pixels were selected within a field in each site. The values from those same pixels were observed throughout the growing season.

2.4.4 ET$_a$ Correlations between the METRIC Model and Atmometer

In the METRIC model ET$_a$ was taken from ten randomly selected pixels in three corn fields at three locations for each satellite image, while for the atmometer method the ET$_a$ was the result of multiplying ET$_r$ (from atmometer) by K$_c$ values generated in this study for each corn field.

The linear relationship between ET$_a$-METRIC values and ET$_a$-atm values in three fields at three sites are shown in Figure 2.9. Brookings and Volga sites demonstrated good distribution of points around the 1:1 line, whereas Oak Lake shows that the points were distributed below the 1:1 line, this means that ET$_a$-METRIC values overestimated ET$_a$-atm values except on DOY 154. Even so, a strong relationships were observed for Brookings and Oak Lake, and a good relationship was observed for Volga (Table 2.2). In addition, the sum for all corn fields, the ET$_a$-METRIC values and the ET$_a$-atm values correlated well (Table 2.3).

In general the difference between ET$_a$-METRIC (5.36 mm day^{-1}) and ET$_a$-atm (4.95 mm day^{-1}) at three sites was approximately 8%. The coefficient of determination (r^2) and index of agreement ("d") were 0.87 and 0.84 respectively. The corresponding MBE was 0.41 mm day^{-1} and RMSE was 0.65 mm day^{-1} (Table 2.3). According to RMSE value, this can be acceptable assuming an average daily ET$_a$-METRIC value of 5.36 mm day^{-1} and average daily ET$_a$-atm value of 4.95 mm day^{-1}.

Similar results in r^2 (~0.86) were reported by Healey et al. (2011), Morton et al. (2013), Gordillo Salinas et al. (2014), French et al. (2015), Liebert et al. (2016), who compared ET$_a$ estimated with the METRIC model and ET$_a$ measured with Bowen Ratio Energy Balance System (BREBS) and Eddy Covariance (EC) methods. Similar results (r^2

= ~0.85) were found in ET_r measured with atmometers by other researchers (Alam & Trooien, 2001; Gleason, Andales, Bauder, & Chávez, 2013), although different ET_r results (low r^2 = ~0.70) where reported by F. Chen and Robinson (2009) and Lamine et al. (2015). All these authors compared ET_r measured using atmometer covered with a No 54 green canvas (alfalfa-reference) with ET_r estimated using agrometeorological data under different weather conditions.
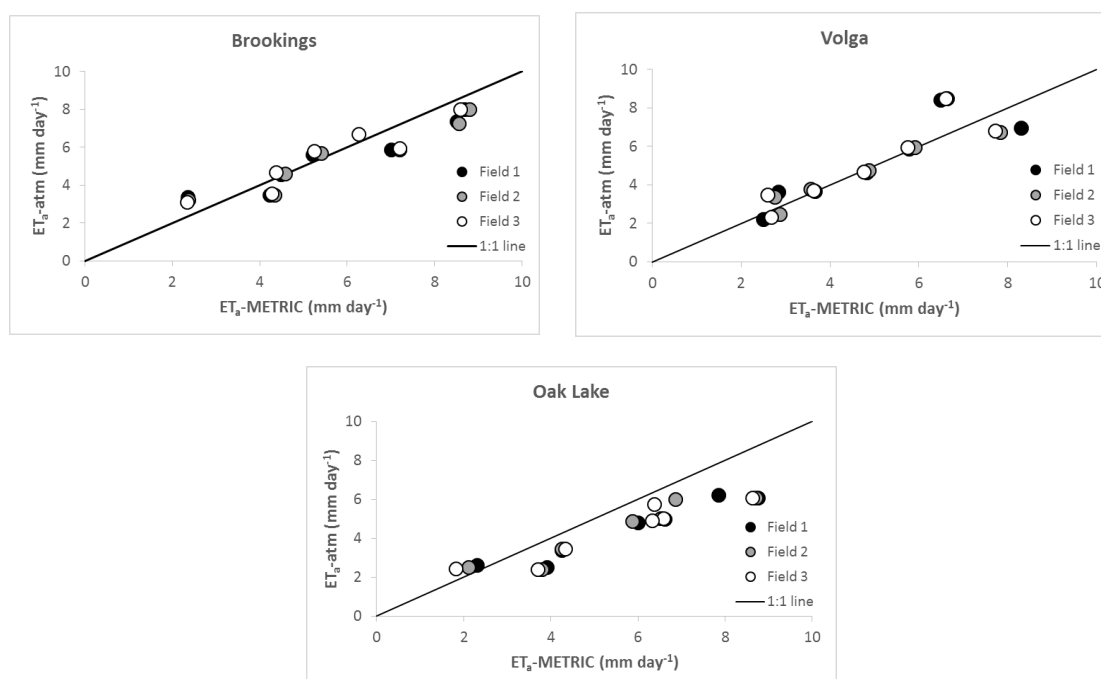
Figure 2.9 Relationship between ET_a-METRIC and ET_a-atm at three sites and nine corn fields in eastern South Dakota for the growing season 2016. The black line represents the 1:1 line.

Table 2.2 Regression coefficients between ET_a-METRIC values and ET_a-atm values for three corn fields at three sites.

Corn	Brookings			Volga			Oak Lake		
	Slope	Interc.	r^2	Slope	Interc.	r^2	Slope	Interc.	r^2
Field 1	0.73	1.28	0.92	0.90	0.61	0.79	0.65	0.73	0.93
Field 2	0.72	1.20	0.91	0.97	0.32	0.81	0.66	0.75	0.88
Field 3	0.78	1.14	0.87	0.98	0.33	0.82	0.64	0.86	0.88

Table 2.3 Statistics comparing between ET_a-METRIC and ET_a-atm at the Brookings, Volga, and Oka Lake sites.

Site	ET_a-METRIC (mm day^{-1})	ET_a-atm (mm day^{-1})	MBE (mm day^{-1})	RMSE (mm day^{-1})	r^2	d
Brookings	5.71	5.44	0.27	0.56	0.89	0.91
Volga	4.88	5.07	-0.19	0.91	0.81	0.89
Oak Lake	5.50	4.35	1.15	0.48	0.90	0.73
Average	5.36	4.95	0.41	0.65	0.87	0.84

2.4.5   ET$_a$ Differences between the METRIC Model and Atmometer

The difference between the daily ET_a estimated with the METRIC model (ET_a-METRIC) and ET_a estimated by atmometer (ET_a-atm) is presented in Figure 2.10. Negative values indicated that the ET_a-METRIC estimates are lower than ET_a-atm, while positive values indicated that the ET_a-METRIC estimates exceeds ET_a-atm.

In Brookings, the daily ET_a difference ranged from -0.95 to 1.32 mm day^{-1}, found in field 1 (DOY 154) (V3) and field 2 (DOY 202) (R1) respectively. The more negative values were presented early in the growing season (DOY 154) (V3) due to high K_c value (0.51) used with atmometer method compared to the low K_c value (0.38) used in the METRIC model method. In addition, on DOY 178 (V7) the corn field 3 shows negative value (-0.4 mm day^{-1}), this is attributed to hailstorm, which occurred on DOY 169 (V5) nine days before that satellite image overpass. The high positive values (DOY 178, 194, and 202) were related to high wind speed values (>4 m s^{-1}) at the time of satellite overpass (Figure 2.11). On DOY 218, 234, and 258 the difference between ET_a-METRIC and ET_a-atm were small (~0.5 mm day^{-1}).

At the Volga site, the daily ET_a difference varied between -1.93 and 1.33 mm day^{-1}. These values were found in field 1 for DOY 194 (VT) and for DOY 178 (V7)

respectively. The higher positive values were during the development stage (DOY 178) (V7) when the corn was 1 m tall. The lower negative values were during the mid-season (DOY 194) (VT) when the crop was 2 m tall. This discrepancy was due to not only to the wind speed values but also to ET_r recorded in atmometer on DOY 194 (VT). The ET_r recorded in this date was one of the highest values registered during the corn growing season (Figure 2.4, Volga). After DOY 202 (R1) the difference between ET_a-METRIC and ET_a-atm were minimal (<0.6 mm day^{-1}), because of the average wind speed values were less than 0.8 m s^{-1} (Table 2.4) and ET_r-PM were around of 10% lower than the ET_r-atm. It is important to mention that at the Volga site the weather station was surrounded by corn fields of 2 m tall and the wind speed is reduced by the corn height. So, when low wind speed is used to estimate the ET_r using the P-M equation, the resulting ET_r are too low. For this reason the wind speed did not affect the ET_a difference between ET_a-METRIC and ET_a-atm from mid-season to late-season period.

At the Oak Lake site, the daily ET_a difference ranged from -0.62 to 2.61 mm day^{-1}, reported for field 3 (DOY 154) (V3) and for field 1 (DOY 194) (VT), respectively. The negative values were found on DOY 154 (V3) for the three fields, this is attributed to the ET_a-atm was calculated using a K_c equal to 0.5, while ET_a-METRIC used a K_c (ET_rF) equal to 0.35, indicating an overestimation of 30% with ET_a-atm method. The higher positive (overestimated) values were observed in DOY 194 (VT) (2.6 mm day^{-1}). At the Oak Lake site, the ET_a-METRIC values tends to overestimate the ET_a-atm values in almost all corn growing season. This noticeable difference is due to the high wind speed values registered throughout the growing season (Figure 2.11, Table 2.4). These high values of wind speed may be attributed to the elevation of the weather station (574 m

above sea level), which is 13% higher than Brookings and Volga elevations. Also, at the

Oak Lake site the weather station and automated atmometer were located in smooth hill.

On the other hand, we observed different ET_a values on DOY 178 (V7) between corn

fields. This difference is attributed to hailstorm, which effect the canopy cover in the

fields 2 and 3 respectively (Figure 2.10, Oak Lake).

In general the daily ET_a differences were attributed to high wind speed values (>4

m s^{-1}) at time of satellite overpass (Figure 2.11). The ET_a-atm values were lower than

values observed in ET_a-METRIC. Hence, as the wind speed increases, the ET_a difference

increases. Similar results were found by Choi et al. (2011), who reported ET difference

between -2.2 and 2.5 mm day^{-1} for different land cover types using METRIC model and

Trapezoid Interpolation Model (TIM). They found high discrepancy in ET due to low

values of elevation, also they reported that as elevation increase the TIM model slightly

overestimate the METRIC ET. On the contrary, low ET difference (~1.0 mm day^{-1}) was

reported by Chavez et al. (2007) who compare ET estimated by METRIC and ET

derivate from soil water balance in irrigation corn in Texas. Also, Healey et al. (2011)

and Hankerson et al. (2012) reported ET difference ranged from -1.0 to 1.0 mm day^{-1}

between the METRIC model and BREBS method in different crops.
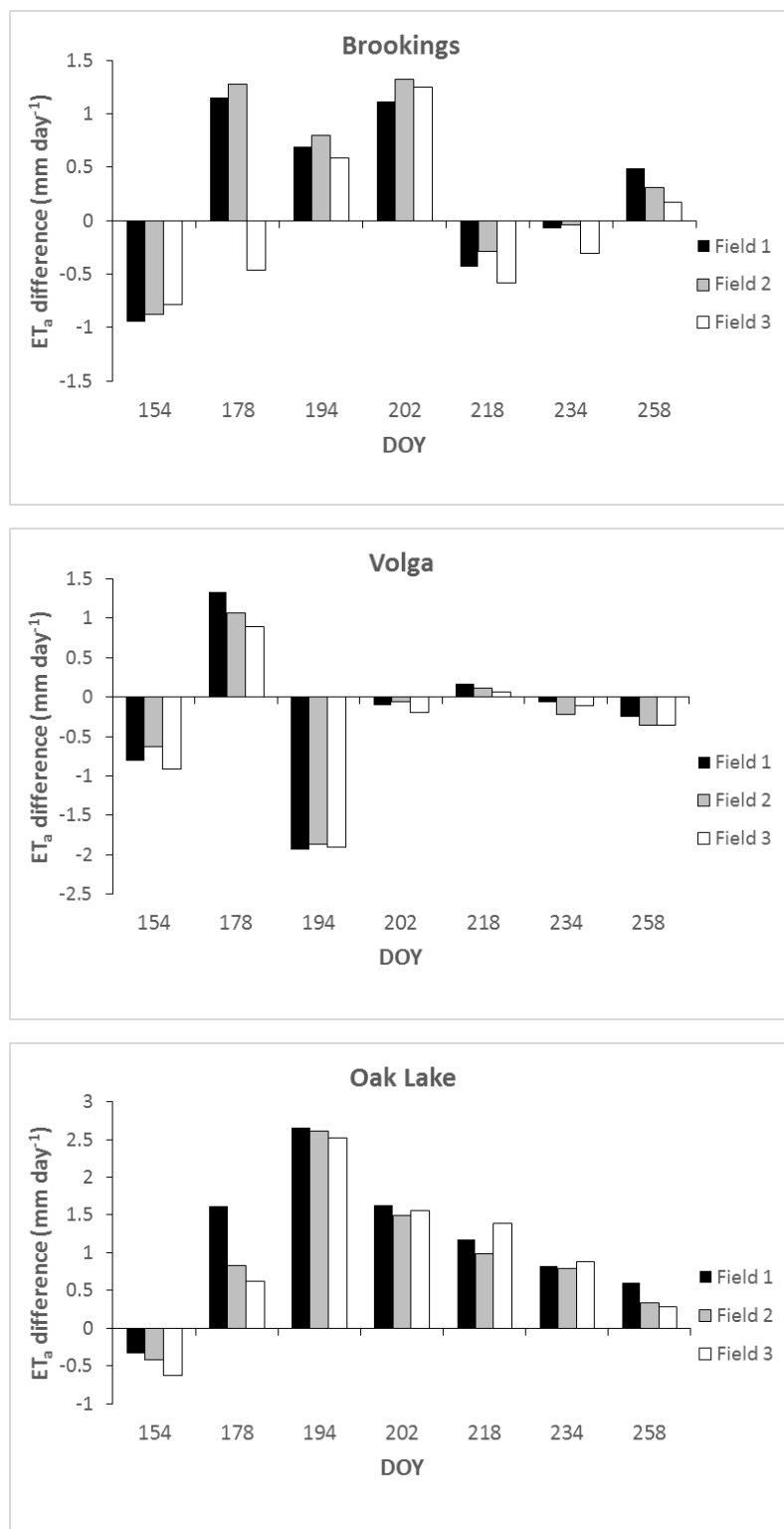
Figure 2.10 Daily ET_a difference between ET_a-METRIC and ET_a-atm at three different sites throughout the corn growing season 2016.

2.4.6 Hourly Wind Speed at Three Sites

Hourly average wind speed (m s^{-1}) for each overpass date at the Brookings, Volga, and Oak Lake sites are shown in Figure 2.11. The wind speed recorded at Volga is similar to Brookings and Oak Lake early in the season, but then is quite a bit lower later during the growing season. This is because Volga weather station is too close to the corn fields, and the wind speed is reduced by the corn crop. On the contrary, at the Oak Lake site higher average wind speed values were found, especially at time of satellite overpass (Figure 2.11). Also, the Oak Lake weather station recorded the maximum wind speed values throughout the season as shown in Table 2.4.

Based on the results from our study, ET$_r$ values from atmometer need to be adjust during the windy days. The adjustment factors (average ratio of ET$_r$-atm to ET$_r$-METRIC) for Brookings, Volga, and Oak Lake were 0.83, 0.87, and 0.68 respectively. These adjustment factors can be used to adjust the ET$_r$-atm values to get close estimates to the ET$_r$-PM values on windy days (>4 m s^{-1}). These adjustment factors are necessary to correct ET$_r$-atm values to obtain accurate ET$_a$ estimations.

In Maui Island, USA, for example, R. Anderson, Wang, Tirado-Corbala, Zhang, and Ayars (2015) and Zhang et al. (2015) reported high variation in evapotranspiration due to high wind speeds values in sugarcane fields. Similar to our results were reported by Westerhoff (2015) who found that as the wind speed increases the ET$_a$ values slightly increases. In addition, Gleason et al. (2013) reported ET underestimation with high wind speed conditions. Mokhtari, Ahmad, Hoveidi, and Busu (2013) reported that as the wind speed increase the ET$_a$ decrease, also they concluded that the METRIC-based ET is highly sensitive to surface temperature, but less sensitive to wind speed values.
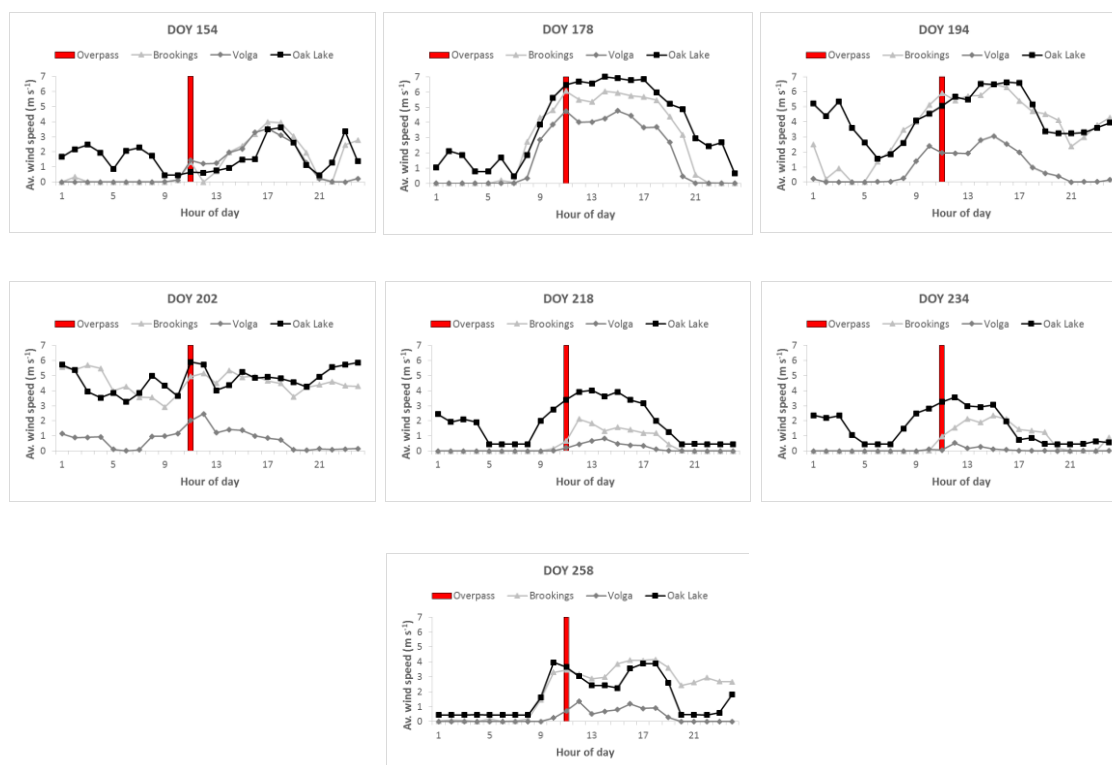
Figure 2.11 Hourly average wind speed values at three sites in eastern South Dakota. The red columns denote the time of satellite overpass (~11:12 AM).

Table 2.4 Daily average and maximum wind speed recorded during satellite overpass at Brookings, Volga, and Oak Lake sites.

	Daily wind speed (m s^{-1})					
	Average			Maximum		
DOY	Brooking	Volga	Oak Lake	Brooking	Volga	Oak Lake
154	1.19	0.93	1.64	3.99	3.54	3.62
178	2.75	1.83	3.85	6.06	4.76	7.21
194	3.64	0.94	4.34	6.49	3.05	6.62
202	4.52	0.79	4.72	5.69	2.47	5.90
218	0.50	0.15	1.91	2.12	0.82	4.01
234	0.67	0.06	1.60	2.34	0.53	3.56
258	2.13	0.32	1.70	4.15	1.35	3.97

2.5   Conclusions

Results of our study showed a good relationship between ET_a-METRIC and ET_a-atm with an r^2 of 0.87, "d" of 0.84, and RMSE of 0.65 mm day^{-1}. In general, the ET_a-atm values were lower than ET_a-METRIC values. The total difference or error between ET_a-METRIC (5.12 mm day^{-1}) and ET_a-atm (4.74 mm day^{-1}) at three sites was approximately 8%.

The daily difference between ET_a-METRIC and ET_a-atm for Brookings site ranged from -0.95 to 1.32 mm day^{-1}, for Volga from -1.93 to 1.33 mm day^{-1}, and for Oak Lake ranged from -0.62 to 2.61 mm day^{-1}. Negative values indicated that the ET_a-METRIC estimates are lower than ET_a-atm, while positive values indicated that the ET_a-METRIC estimates exceeds ET_a-atm. The higher positive values were related with high wind speed values. In general, daily ET_a differences is attributed to high wind speed values (>4 m s^{-1}) at the time of satellite image overpass. Hence, as the wind speed increases, the ET_a difference increases. However, based on our results, ET_r values from atmometer need to be adjust during the windy days. The adjustment factors were 0.83, 0.87, and 0.68 for Brookings, Volga, and Oak Lake sites, respectively. These adjustment factors can be used to adjust the ET_r-atm to get close estimates to the ET_r-PM values for windy days (>4 m s^{-1}).

In conclusion the results of this study can be used by policy makers, researchers, and producers for estimating actual evapotranspiration and improve irrigation water management at local and field scales, using both satellite-based remote sensing METRIC model method and atmometer method, respectively.

2.6   References

Alam, M., & Trooien, T. (2001). Estimating reference evapotranspiration with an atmometer. *Applied Engineering in Agriculture, 17*(2), 153-158.

Allen, R., Irmak, A., Trezza, R., Hendrickx, J. M., Bastiaanssen, W., & Kjaersgaard, J. (2011). Satellite-based ET estimation in agriculture using SEBAL and METRIC. *Hydrological Processes, 25*(26), 4011-4027.

Allen, R. G., Pereira, L. S., Howell, T. A., & Jensen, M. E. (2011). Evapotranspiration information reporting: I. Factors governing measurement accuracy. *Agricultural Water Management, 98*(6), 899-920.

Allen, R. G., Pereira, L. S., Raes, D., & Smith, M. (1998). Crop evapotranspiration-Guidelines for computing crop water requirements-FAO Irrigation and drainage paper 56. *FAO, Rome, 300*(9), D05109.

Allen, R. G., Tasumi, M., Morse, A., Trezza, R., Wright, J. L., Bastiaanssen, W., . . . Robison, C. W. (2007). Satellite-based energy balance for mapping evapotranspiration with internalized calibration (METRIC)—Applications. *Journal of Irrigation and Drainage Engineering, 133*(4), 395-406.

Allen, R. G., Tasumi, M., & Trezza, R. (2007). Satellite-based energy balance for mapping evapotranspiration with internalized calibration (METRIC)—Model. *Journal of Irrigation and Drainage Engineering, 133*(4), 380-394.

Anderson, M. C., Allen, R. G., Morse, A., & Kustas, W. P. (2012). Use of Landsat thermal imagery in monitoring evapotranspiration and managing water resources. *Remote*

Sensing of Environment, 122, 50-65. doi:http://dx.doi.org/10.1016/j.rse.2011.08.025

Anderson, R., Wang, D., Tirado-Corbala, R., Zhang, H., & Ayars, J. (2015). Divergence of actual and reference evapotranspiration observations for irrigated sugarcane with windy tropical conditions. *Hydrology and Earth System Sciences, 19*(1), 583-599.

ASCE-EWRI. (2005). *The ASCE standardized reference evapotranspiration equation; ASCE-EWRI Standardization of Reference Evapotranspiration Task Committee Report; ASCE: Reston, VA, USA*.

Bastiaanssen, W., Menenti, M., Feddes, R., & Holtslag, A. (1998). A remote sensing surface energy balance algorithm for land (SEBAL). 1. Formulation. *Journal of Hydrology, 212*, 198-212.

Bastiaanssen, W., Noordman, E., Pelgrum, H., Davids, G., Thoreson, B., & Allen, R. (2005). SEBAL model with remotely sensed data to improve water-resources management under actual field conditions. *Journal of Irrigation and Drainage Engineering, 131*(1), 85-93.

Bhattarai, N., Quackenbush, L. J., Dougherty, M., & Marzen, L. J. (2015). A simple Landsat–MODIS fusion approach for monitoring seasonal evapotranspiration at 30 m spatial resolution. *International journal of remote sensing, 36*(1), 115-143.

Bos, M. G., Kselik, R. A., Allen, R. G., & Molden, D. (2008). *Water requirements for irrigation and the environment*: Springer Science & Business Media.

Broner, I., & Law, R. (1991). Evaluation of a modified atmometer for estimating reference ET. *Irrigation Science, 12*(1), 21-26.

Carrasco-Benavides, M., Ortega-Farías, S., Lagos, L. O., Kleissl, J., Morales-Salinas, L., & Kilic, A. (2014). Parameterization of the Satellite-Based Model (METRIC) for the estimation of instantaneous surface energy balance components over a drip-irrigated vineyard. *Remote Sensing, 6*(11), 11342-11371.

Carrillo-Rojas, G., Silva, B., Córdova, M., Célleri, R., & Bendix, J. (2016). Dynamic mapping of evapotranspiration using an energy balance-based model over an Andean Páramo Catchment of Southern Ecuador. *Remote Sensing, 8*(2), 160.

Casanova, M., Messing, I., Joel, A., & Cañete, A. (2009). Methods to estimate lettuce evapotranspiration in greenhouse conditions in the central zone of Chile.

Chavez, J. L., Gowda, P. H., Howell, T. A., Marek, T. H., & New, L. L. (2007). *Evapotranspiration mapping using METRICTM for a region with highly advective conditions.* Paper presented at the 2007 ASABE Annual International Meeting, Technical Papers.

Chen, F., & Robinson, P. J. (2009). Estimating reference crop evapotranspiration with ETgages. *Journal of Irrigation and Drainage Engineering, 135*(3), 335-342.

Choi, M., Kim, T. W., Park, M., & Kim, S. J. (2011). Evapotranspiration estimation using the Landsat-5 Thematic Mapper image over the Gyungan watershed in Korea. *International journal of remote sensing, 32*(15), 4327-4341.

Choi, M., Kustas, W. P., Anderson, M. C., Allen, R. G., Li, F., & Kjaersgaard, J. H. (2009). An intercomparison of three remote sensing-based surface energy balance algorithms over a corn and soybean production region (Iowa, US) during SMACEX. *Agricultural and Forest Meteorology, 149*(12), 2082-2097.

Djaman, K., & Irmak, S. (2012). Actual crop evapotranspiration and alfalfa-and grass-reference crop coefficients of maize under full and limited irrigation and rainfed conditions. *Journal of Irrigation and Drainage Engineering, 139*(6), 433-446.

Droogers, P., Immerzeel, W., & Lorite, I. (2010). Estimating actual irrigation application by remotely sensed evapotranspiration observations. *Agricultural Water Management, 97*(9), 1351-1359.

Folhes, M. T., Rennó, C. D., & Soares, J. V. (2009). Remote sensing for irrigation water management in the semi-arid Northeast of Brazil. *Agricultural Water Management, 96*(10), 1398-1408.

French, A. N., Hunsaker, D. J., & Thorp, K. R. (2015). Remote sensing of evapotranspiration over cotton using the TSEB and METRIC energy balance models. *Remote Sensing of Environment, 158*, 281-294.

Gavilán, P., & Castillo-Llanque, F. (2009). Estimating reference evapotranspiration with atmometers in a semiarid environment. *Agricultural Water Management, 96*(3), 465-472.

George, B. A., Reddy, B., Raghuwanshi, N., & Wallender, W. (2002). Decision support system for estimating reference evapotranspiration. *Journal of Irrigation and Drainage Engineering, 128*(1), 1-10.

Gleason, D., Andales, A., Bauder, T., & Chávez, J. (2013). Performance of atmometers in estimating reference evapotranspiration in a semi-arid environment. *Agricultural Water Management, 130*, 27-35.

Gonzalez-Dugo, M., Neale, C., Mateos, L., Kustas, W., Prueger, J., Anderson, M., & Li, F. (2009). A comparison of operational remote sensing-based models for estimating

crop evapotranspiration. *Agricultural and Forest Meteorology, 149*(11), 1843-1853.

Gordillo Salinas, V. M., Flores Magdaleno, H., Tijerina Chávez, L., & Arteaga Ramírez, R. (2014). Estimación de la evapotranspiración utilizando un balance de energía e imágenes satelitales. *Revista mexicana de ciencias agrícolas, 5*(1), 143-155.

Gowda, P. H., Chavez, J. L., Colaizzi, P. D., Evett, S. R., Howell, T. A., & Tolk, J. A. (2008). ET mapping for agricultural water management: present status and challenges. *Irrigation Science, 26*(3), 223-237. doi:10.1007/s00271-007-0088-6

Hankerson, B., Kjaersgaard, J., & Hay, C. (2012). Estimation of evapotranspiration from fields with and without cover crops using remote sensing and in situ methods. *Remote Sensing, 4*(12), 3796-3812.

Healey, N. C., Irmak, A., Arkebauer, T. J., Billesbach, D. P., Lenters, J. D., Hubbard, K. G., . . . Kjaersgaard, J. (2011). Remote sensing and in situ-based estimates of evapotranspiration for subirrigated meadow, dry valley, and upland dune ecosystems in the semi-arid sand hills of Nebraska, USA. *Irrigation and Drainage Systems, 25*(3), 151-178.

Irmak, A., & Irmak, S. (2008). Reference and crop evapotranspiration in South Central Nebraska. II: Measurement and estimation of actual evapotranspiration for corn. *Journal of Irrigation and Drainage Engineering, 134*(6), 700-715.

Irmak, S., Dukes, M., & Jacobs, J. (2005). Using modified Bellani plate evapotranspiration gauges to estimate short canopy reference evapotranspiration. *Journal of Irrigation and Drainage Engineering, 131*(2), 164-175.

Irmak, S., Odhiambo, L. O., Specht, J. E., & Djaman, K. (2013). Hourly and daily single and basal evapotranspiration crop coefficients as a function of growing degree days, days after emergence, leaf area index, fractional green canopy cover, and plant phenology for soybean. *Trans. ASABE, 56*(5), 1785-1803.

Jensen, M. E., & Allen, R. G. (2016). *Evaporation, Evapotranspiration, and Irrigation Water Requirements*.

Keim, B. D. (2010). The lasting scientific impact of the Thornthwaite water–balance model. *Geographical Review, 100*(3), 295-300.

Kidron, G. J. (2005). Measurements of evaporation with a novel mini atmometer in the Negev. *Weather, 60*(9), 268-272.

Kjaersgaard, J., & Allen, R. (2010). Remote sensing technology to produce consumptive water use maps for the Nebraska Panhandle. *Final completion report submitted to the University of Nebraska, 88*.

Kjaersgaard, J., Allen, R., Aggett, G., Schneider, C., Hattendorf, M., Irmak, A., . . . Robison, C. (2008). *Computation of Landsat based evapotranspiration maps along the South Platte and North Platte Rivers.* Paper presented at the World Environmental and Water Resources Congress 2008: Ahupua'A.

Kjaersgaard, J., Allen, R., & Irmak, A. (2011). Improved methods for estimating monthly and growing season ET using METRIC applied to moderate resolution satellite imagery. *Hydrological Processes, 25*(26), 4028-4036.

Knox, J., Rodriguez-Diaz, J., & Hess, T. (2011). Estimating evapotranspiration by using atmometers for irrigation scheduling in a humid environment. *Journal of Irrigation and Drainage Engineering, 137*(11), 685-691.

Lamine, D., BODIAN, A., & DIALLO, D. (2015). Use of atmometers to estimate reference evapotranspiration in Arkansas. *African Journal of Agricultural Research, 10*(48), 4376-4383.

Liebert, R., Huntington, J., Morton, C., Sueki, S., & Acharya, K. (2016). Reduced evapotranspiration from leaf beetle induced tamarisk defoliation in the Lower Virgin River using satellite-based energy balance. *Ecohydrology, 9*(1), 179-193.

Magliulo, V., d'Andria, R., & Rana, G. (2003). Use of the modified atmometer to estimate reference evapotranspiration in Mediterranean environments. *Agricultural Water Management, 63*(1), 1-14.

Mendonça, J. C., Sousa, E. d., Bernardo, S., Dias, G. P., & Grippa, S. (2003). Comparação entre métodos de estimativa da evapotranspiração de referência (ETo) na região Norte Fluminense, RJ. *Revista Brasileira de Engenharia Agrícola e Ambiental, 7*(2), 275-279.

Mkhwanazi, M., Chávez, J. L., & Rambikur, E. H. (2012). Comparison of large aperture scintillometer and satellite-based energy balance models in sensible heat flux and crop evapotranspiration determination. *International Journal of Remote Sensing Applications, 2*(1), 24-30.

Mokhtari, M., Ahmad, B., Hoveidi, H., & Busu, I. (2013). Sensitivity analysis of METRIC–based evapotranspiration algorithm. *International Journal of Environmental Research, 7*(2), 407-422.

Morton, C. G., Huntington, J. L., Pohll, G. M., Allen, R. G., McGwire, K. C., & Bassett, S. D. (2013). Assessing calibration uncertainty and automation for estimating

evapotranspiration from agricultural areas using METRIC. *JAWRA Journal of the American Water Resources Association, 49*(3), 549-562.

Paço, T. A., Pôças, I., Cunha, M., Silvestre, J. C., Santos, F. L., Paredes, P., & Pereira, L. S. (2014). Evapotranspiration and crop coefficients for a super intensive olive orchard. An application of SIMDualKc and METRIC models using ground and satellite observations. *Journal of Hydrology, 519*, 2067-2080.

Pelton, W. (1964). Evaporation from atmometers and pans. *Canadian Journal of Plant Science, 44*(5), 397-404.

Peterson, K., Bremer, D., & Fry, J. (2015). Evaluation of Atmometers within Urban Home Lawn Microclimates. *Crop Science, 55*(5), 2359-2367.

Reyes-Gonzalez, A., Trooien, T., Hay, C., & Kjaersgaard, J. (2016, April 7). *Comparison of reference evapotranspiration estimated by automated weather station and measured with an atmometer.* Paper presented at the 2016 Western South Dakota Hydrology Conference, Rushmore plaza civic center, Rapid city, SD.

Reyes-González, A., Trooien, T., Kjaersgaard, J., Hay, C., & Reta-Sánchez, D. G. (2016). *Development of Crop Coefficients Using Remote Sensing-Based Vegetation Index and Growing Degree Days.* Paper presented at the 2016 ASABE Annual International Meeting.

Santos, C., Lorite, I., Tasumi, M., Allen, R., & Fereres, E. (2008). Integrating satellite-based evapotranspiration with simulation models for irrigation management at the scheme level. *Irrigation Science, 26*(3), 277-288.

Singh, R. K., & Irmak, A. (2009). Estimation of crop coefficients using satellite remote sensing. *Journal of Irrigation and Drainage Engineering, 135*(5), 597-608.

Taghvaeian, S., Chávez, J. L., Bausch, W. C., DeJonge, K. C., & Trout, T. J. (2014). Minimizing instrumentation requirement for estimating crop water stress index and transpiration of maize. *Irrigation Science, 32*(1), 53-65.

Tasumi, M. (2003). *Progress in operational estimation of regional evapotranspiration using satellite imagery*.

Tasumi, M., Allen, R. G., Trezza, R., & Wright, J. L. (2005). Satellite-based energy balance to assess within-population variance of crop coefficient curves. *Journal of Irrigation and Drainage Engineering, 131*(1), 94-109.

Thenkabail, P. S., Hanjra, M. A., Dheeravath, V., & Gumma, M. (2010). A holistic view of global croplands and their water use for ensuring global food security in the 21st century through advanced remote sensing and non-remote sensing approaches. *Remote Sensing, 2*(1), 211-261.

Trezza, R., Allen, R. G., & Tasumi, M. (2013). Estimation of actual evapotranspiration along the Middle Rio Grande of New Mexico using MODIS and landsat imagery with the METRIC model. *Remote Sensing, 5*(10), 5397-5423.

Westerhoff, R. (2015). Using uncertainty of Penman and Penman–Monteith methods in combined satellite and ground-based evapotranspiration estimates. *Remote Sensing of Environment, 169*, 102-112.

Willmott, C. J. (1981). On the validation of models. *Physical geography, 2*(2), 184-194.

Wright, J. L. (1982). New evapotranspiration crop coefficients. *Proceedings of the American Society of Civil Engineers, Journal of the Irrigation and Drainage Division, 108*(IR2), 57-74.

Zhang, H., Anderson, R. G., & Wang, D. (2015). Satellite-based crop coefficient and regional water use estimates for Hawaiian sugarcane. *Field Crops Research, 180*, 143-154.

CHAPTER 3: Assessing the Relationship between Leaf Area Index, Surface Temperature, and Actual Evapotranspiration Estimated using the Remote Sensing-based METRIC model and *in-situ* Measurements

3.1 Abstract

The verification of remotely sensed estimates of surface variables including leaf area index (LAI), surface temperature (T_s), and actual evapotranspiration (ET_a) is essential for any remote-sensing study. The objective of this study was to assess the relationship between LAI, T_s, and ET_a estimated using the remote sensing-based METRIC model and *in-situ* measurements collected at the satellite overpass time. The study was carried out at a commercial corn field in eastern South Dakota. Six clear sky images from Landsat 7 and Landsat 8 (Path 29, Row 29) were processed and used for the assessment. LAI, T_s, and ET_a were estimated using the METRIC model and measured *in situ*. LAI and T_s were measured with AccuPAR and infrared thermometers respectively and ET_a was estimated using an atmometer and crop coefficient values developed for this study. The results revealed good agreement between the variables measured *in situ* and estimated by the METRIC model. LAI showed $r^2 = 0.76$, and RMSE $= 0.59$ m^2 m^{-2}, the T_s comparison had an agreement of $r^2 = 0.87$ and RMSE 1.24 °C and ET_a presented $r^2 = 0.89$ and RMSE $= 0.71$ mm day^{-1}.

3.2 Introduction

The verification of remotely sensed estimates of surface variables is essential for any remote-sensing study (Jones & Vaughan, 2010; Qu, Zhu, Han, Wang, & Ma, 2014). A robust assessment of variables such as leaf area index (LAI), surface temperature (T_s),

and actual evapotranspiration (ET_a) collected *in situ* are needed for determining the accuracy of the information derived from remote sensing technologies.

Leaf area index (LAI) is a dimensionless measure of the one-sided area of canopy foliage (m^2) per unit ground surface area (m^2) (Asner, Scurlock, & A Hicke, 2003). Direct and indirect in situ methods can be used to determine LAI (Bréda, 2003; Garrigues et al., 2008; Weiss, Baret, Smith, Jonckheere, & Coppin, 2004). Direct methods involves harvesting the foliage for analysis and are labor intensive, time consuming, and destructive. Indirect methods are faster and non-destructive. The AccuPAR sensor (Decagon, Pullman, WA, USA) is an indirect method that estimates LAI from measurements of light above and below the canopy (Stewart et al., 2003; Tewolde, Sistani, Rowe, Adeli, & Tsegaye, 2005; Wilhelm, Ruwe, & Schlemmer, 2000). Image-based remote sensing are used to estimate LAI using empirical relationships between LAI and spectral vegetation indices (VIs) (S. Gao, Niu, Huang, & Hou, 2013; Gowda et al., 2015) at the scale of the input imagery (e.g., 30 m for Landsat imagery). The result is spatially distributed estimates of LAI are generated in less time and with less cost. The relationships between LAI and VIs derived from satellite-estimated information has been evaluated by Colombo, Bellingeri, Fasolini, and Marino (2003), S. Gao et al. (2013) Nguy-Robertson et al. (2012), Zipper and Loheide II (2014), while other studies compared the relationship between ground-based LAI and remote sensing based LAI estimates (Hosseini, McNairn, Merzouki, & Pacheco, 2015; Liang et al., 2015; Qu et al., 2014; Tang et al., 2011). However comparison between LAI measured *in situ* with AccuPAR and LAI estimated using the METRIC model has not been done in eastern South Dakota. LAI values derived from remote sensing vary in space and time (Liang et

al., 2015). Because of those variation, is essential to validate remote sensing based LAI

values with ground-based LAI measurement data.

Canopy surface temperature (T_s) is a useful method to monitor and quantify water

stress in plants (Colaizzi, Evett, O'Shaughnessy, & Howell, 2012; Han, Zhang, DeJonge,

Comas, & Trout, 2016). The T_s increases when solar radiation is absorbed and decreases

when that radiation energy is used to evaporate water (plant transpiration) rather than

heat the plant surfaces (DeJonge, Taghvaeian, Trout, & Comas, 2015). Under water

deficit conditions, as the stomata resistance increase and transpiration decreases, the

foliage gets warmer (Bijanzadeh, 2012; Colaizzi et al., 2012; Sandholt, Rasmussen, &

Andersen, 2002). The difference between air temperature (T_a) and T_s have been used to

quantify crop water stress and several crop water stress indices based in T_s have been

developed (for example CWSI, (Idso, Jackson, Pinter, Reginato, & Hatfield, 1981).

Numerous researchers have utilized infrared thermometer (IRTs) to measure T_s. IRTs

manually handled (S. Irmak, Haman, & Bastug, 2000; López-López, Ramírez, Sánchez-

Cohen, Bustamante, & González-Lauck, 2011; Taghvaeian, Chávez, Altenhofen, Trout,

& DeJonge, 2013) and IRTs mounted on center pivot irrigation systems (O'Shaughnessy

& Evett, 2010; Peters & Evett, 2008). Other researchers have utilized multispectral and

infrared thermal image cameras mounted on unmanned aerial vehicles (UAV) (Bellvert,

Zarco-Tejada, Girona, & Fereres, 2014; Berni, Zarco-Tejada, Suárez, & Fereres, 2009;

Ortega-Farías et al., 2016; Sepúlveda-Reyes et al., 2016) and mounted on truck-cranes

(Alchanatis et al., 2010; Cohen et al., 2015). Estimation of T_s based satellite remote

sensing have been reported at large scale (km^2) and field scale (m^2) by M. Anderson and

Kustas (2008), Gowda et al. (2015), and Senay, Friedrichs, Singh, and Velpuri (2016),

respectively. However, there is no evidence of comparisons between ground–based T_s measurements and satellite-based remote sensing T_s estimates in corn field. Thus, assessment of T_s values derived from the METRIC model with *in situ* measurements still not well examined in eastern South Dakota.

Evapotranspiration (ET) is the loss of water from the land surface to the atmosphere through two processes, *viz.* evaporation (E) from soil and water surfaces and transpiration (T) from vegetative surfaces (R. G. Allen, Tasumi, & Trezza, 2007; Gowda, Chavez, et al., 2008). ET has been estimated using satellite-based remote sensing at regional and field scales (R. G. Allen, Tasumi, Morse, et al., 2007; J Kjaersgaard et al., 2011). Estimations of ET using satellite imagery is economical, efficient and non-destructive. Numerous models have been developed to estimate actual ET (ET_a) using remote sensing techniques. One of them is the Mapping EvapoTranspiration at high Resolution using Internalized Calibration (METRIC) model. Studies reported good relationships between the METRIC model and methods for ET_a estimation such as weighing lysimeter (R. G. Allen, Tasumi, Morse, et al., 2007), soil water balance (Chavez et al., 2007), Bowen Ratio Energy Balance Systems (BREBS) (Carrasco-Benavides et al., 2014; Hankerson et al., 2012), Eddy Covariance (EC) (Liebert et al., 2016; Zhang et al., 2015), and Large Aperture Scintillometer (LAS) (Mkhwanazi et al., 2012). However, little is known about relationship between the METRIC model and atmometer for ET estimation. An atmometer is an instrument that measures the amount of water evaporated to the atmosphere from wet porous surface (Broner & Law, 1991) An atmometer is a simple and economical device, and provides a visual interpretation of reference ET (ET_r) data and is very useful for practical applications of on-farm water

management (Alam & Trooien, 2001). There is a need to estimate the representativeness of atmometer readings located at a location where a user would place it (e.g., near the edge of a field) to the ET of the field it is adjacent to.

The objectives of this study were to 1) assess the relationship between actual ET (ET_a) estimated by atmometer and estimate to spatially distributed ET estimates generated using the METRIC model and 2) assess the relationship between leaf area index and surface temperature, estimated by remote sensing-based METRIC model and *in-situ* measurements at the same time of satellite image overpass over a corn field in eastern South Dakota.

3.3 Material and Methods

3.3.1 Study Area

The study was carried out at a commercial corn field in eastern South Dakota (Figure 3.1). The corn field is located at 43° 56' N latitude and 96° 45' W longitude, and 495 m above sea level. The corn row direction was from north to south, the row spacing was 0.76 m and 6 plants per linear meter. The final population density was 78, 000 plants ha^{-1}. The sources of fertilizer were beef manure or inorganic fertilizer supplied at the beginning of the growing season to achieve a yield goal of 180 bu. acre^{-1}. Beef manure was applied only at East (E) location. The field is in a corn - soybean rotation, which represent the most common cropping system in eastern South Dakota. The soil at the experimental site is silt loam with a field capacity (FC) of 0.31 m^3 m^{-3} and a permanent wilting point (PWP) of 0.15 m^3 m^{-3}. The particle size distribution is 18% sand, 56% silt, and 26% clay, with 1-3.5% organic matter content. The average annual precipitation at

the field site is 23 inches (584 mm), of which ¾ typically falls during the growing season from April to October. The mean daily maximum and minimum temperatures are 12.3 °C, and 0.3 °C, respectively, and the annual mean temperature is 6.3 °C. Five observation locations were georeferenced to collect *in situ* measurements (Figures 3.1 and 3.2, and Table 3.1). The *in situ* data were collected from 2 June (day of year (DOY) 154) to 14 September (DOY 258) during the 2016 growing season.
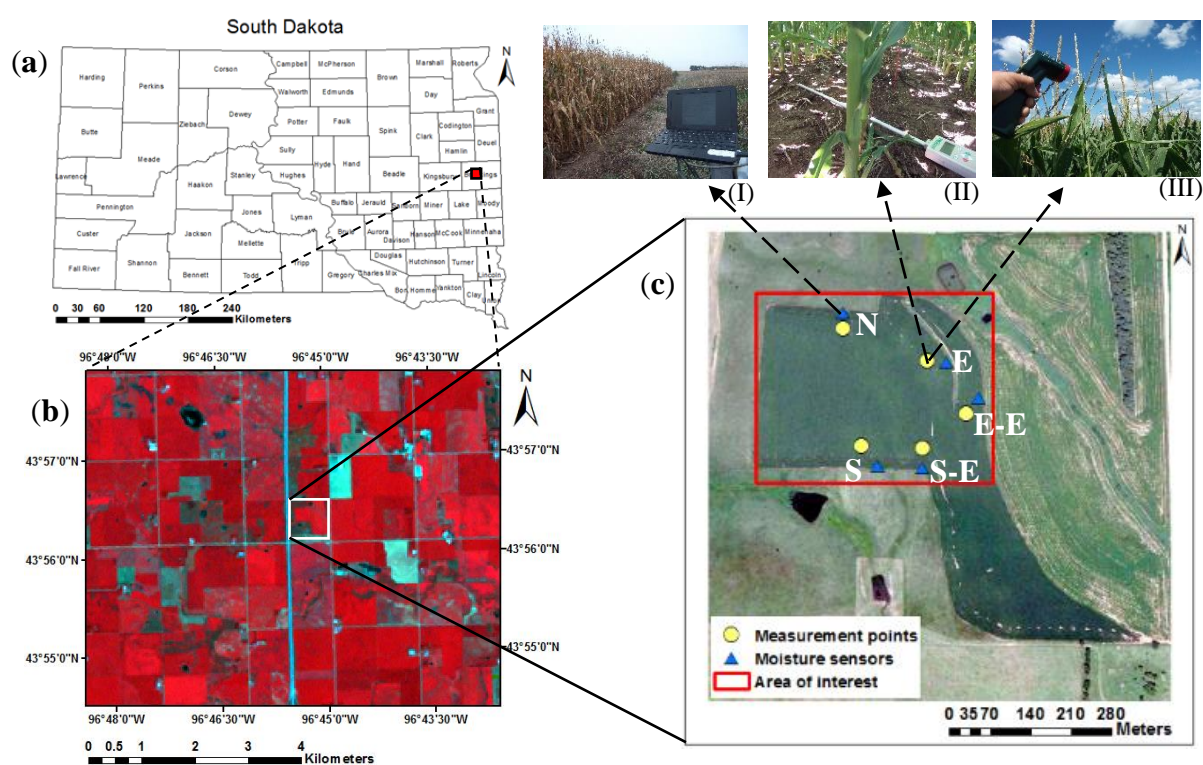
Figure 3.1 South Dakota with county boundaries, the red rectangle shows the study area in eastern South Dakota (a). Landsat 8 with false color composite (bands 4, 3, 2), the white rectangle indicates the experimental corn field (b), and the aerial photo with area of interest shows measurement points (yellow circles) and moisture sensors (blue triangles) at the five observation locations (S-E, S, N, E and E-E) (c).

Table 3.1 Observation locations, altitude, soil texture, field capacity (FC) and permanent wilting point (PWP).

Site	Latitude (N)	Longitude (W)	Altitude (m)	Soil texture	FC (m^3m^{-3})	PWP (m^3m^{-3})
South-east (S-E)	43° 56' 20.7"	96° 45' 11.6"	495	silt clay loam	0.33	0.19
South (S)	43° 56' 20.8"	96° 45' 15.7"	493	silt loam	0.31	0.15
North (N)	43° 56' 27.6"	96° 45' 19.5"	501	silt clay loam	0.33	0.19
East (E)	43° 56' 25.6"	96° 45' 11.5"	493	silt loam	0.31	0.15
East-east (E-E)	43° 56' 23.0"	96° 45' 10.0"	492	silt loam	0.31	0.15
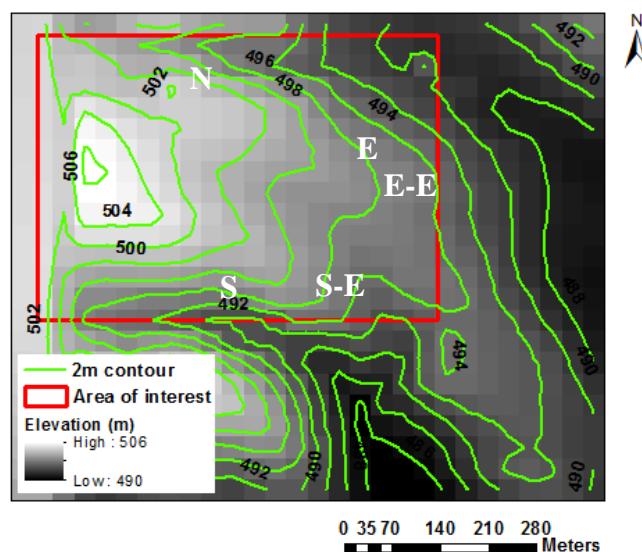
Figure 3.2 Elevation map of corn field with 2 m contour and area of interest (red rectangle) and five observation locations.

3.3.2   Landsat Images

Six clear sky images collected by Landsat 7 Enhanced Thematic Mapper Plus (ETM+) and Landsat 8 Operational Land Imager (OLI) and Thermal Infrared Sensor (TIRS) (Path 29, Row 29), Table 3.2 during 2016 was used for the analysis. The images were downloaded from the United States Geological Survey (USGS) EROS Datacenter

(http://glovis.usgs.gov). The images were selected based on temporal coverage and

cloud-free conditions. Images with cloud located >10 km from the area of interest were

considered acceptable. The images were processed using the METRIC model running in

ERDAS Imagine (R. Allen, A. Irmak, R. Trezza, J. M. Hendrickx, et al., 2011; R. G.

Allen, Tasumi, & Trezza, 2007; J Kjaersgaard & Allen, 2010).

Table 3.2 DOY, acquisition dates, satellite platform, path/row, and overpass time of the
imagery used for the 2016 growing season.

DOY	Acquisition Dates	Satellite	Path/Row	Overpass time (local)
178	06/26/16	Landsat 7	29/29	11:13:56 a.m.
194	07/12/16	Landsat 7	29/29	11:13:55 a.m.
202	07/20/16	Landsat 8	29/29	11:11:21 a.m.
218	08/05/16	Landsat 8	29/29	11:11:24 a.m.
234	08/21/16	Landsat 8	29/29	11:11:30 a.m.
258	09/14/16	Landsat 7	29/29	11:14:05 a.m.

3.3.3 METRIC Model

METRIC uses physically based equations to estimate leaf area index, surface

temperature and actual evapotranspiration described by R. G. Allen, Tasumi, and Trezza

(2007), R. Allen, A. Irmak, R. Trezza, J. M. Hendrickx, et al. (2011).

Leaf area index (LAI) was calculated using surface reflectance data and was

calculated as follows:

$$LAI = \frac{\ln[(0.69 - SAVI_{ID}/0.59)]}{0.91} \tag{1}$$

where soil adjusted vegetation index ($SAVI_{ID}$) is computed using bands 3 and 4

for Landsat 7 and bands 4 and 5 for Landsat 8.

For Landsat 7 $SAVI_{ID}$ is calculated as follows:

$$SAVI_{ID} = \frac{(1+L)(NIR_{band\ 4} - Red_{band\ 3})}{L + (NIR_{band\ 4} + Red_{band\ 3})} \tag{2}$$

For Landsat 8 $SAVI_{ID}$ is calculated as follows:

$$SAVI_{ID} = \frac{(1+L)(NIR_{band\ 5} - Red_{band\ 4})}{L + (NIR_{band\ 5} + Red_{band\ 4})} \tag{3}$$

where L is a constant $(L = 0.1)$ (Tasumi, 2003).

Surface temperature (Ts) is computed using the following equation:

$$T_S = \frac{K_2}{\ln\left(\frac{\varepsilon_{NB}\ K_1}{R_c}+1\right)} \tag{4}$$

where ε_{NB} is narrow band emissivity corresponding to the satellite thermal sensor wave length band. R_c is the corrected thermal radiance from the surface. K_1 and K_2 are constants, $K_1 = 666.1$ and $K_2 = 1282.7$ for Landsat 7 (Band 6) and $K_1 = 480.9$ and $K_2 = 1201.1$ for Landsat 8 (Band 10).

Actual evapotranspiration (ETa) was estimated using METRIC model approach as described by R. G. Allen, Tasumi, and Trezza (2007), R. Allen, A. Irmak, R. Trezza, J. M. Hendrickx, et al. (2011).

3.3.4 Meteorological Data

Weather dataset were taken from the Brookings automated weather station operated by the South Dakota Climate Office. The Brookings station is located at 44° 19' N, 96° 46' W and 500 m above sea level. The Brookings weather station is located approximately 40 km from the study site. The reference ET (ETr) was calculated using the Penman-Monteith equation (R. G. Allen et al., 1998; ASCE-EWRI, 2005). All weather dataset, were subjected to quality control (QC) prior to being used in any calculations as suggested by R. G. Allen et al. (1998) and ASCE-EWRI (2005). Hourly QC included solar radiation, air temperature, wind speed, and air vapor pressure deficit.

3.3.5   In Situ Measurements

3.3.5.1   Leaf area index with AccuPAR

Leaf area index (LAI) was measured using AccuPAR model Lp-80 PAR/LAI Ceptometer (Decagon Devices, Inc. Pullman, WA, USA). The AccuPAR calculates LAI based on the above and below canopy photosynthetically active radiation (PAR) measurements. The LAI measurements were collected starting 2 June (DOY 154) (vegetation stage (V3)) to 14 September (DOY 258) (reproductive stage (R6)) 2016. The probe was positioned at a 45° angle across the center row to measure PAR interception along the probe as shown in Figure 3.1 (II). PAR interception was measured at five geolocated locations, each location (30 m x 30 m) with five points and five replications per point above and below the corn canopy. The readings were taken between 11:00 AM. and 12:00 noon every eight days on clear days to minimize diffuse radiation from sky and clouds (Stewart et al., 2003). The LAI values *in situ* with AccuPAR corresponding pixels were compared with the LAI values of corresponding METRIC pixels. The *in situ* measurement of LAI obtained during the time of satellite overpass was used to assess the LAI by the METRIC model at the same pixel and the same time throughout the season. At the same time, the corn height was measured in the same dates of LAI measurements. The plant height was taken by measuring the distance between the soil surface and the tip of the longest leaf or tassel using a measuring tape. Ten plants were chosen randomly (within pixel) for plant height measurements at each location site. The location site has the same area as a pixel (30 m x 30 m).

3.3.5.2 Surface Temperature Measured with Infrared Thermometer

Surface temperature (T_s) was measured with infrared thermometer model 42530 (Extech instruments Inc. Boston, MA, USA). T_s was measured every eight days from 26 June (V6, DOY 178) when the corn height was ~1.0 m, LAI = 4.5 m^2 m^{-2}, and canopy cover 80% to 14 September (R6, DOY 258). T_s measurements were taken in cloud free and no windy days. The infrared thermometer was held approximately 0.2 m above the corn canopy at about a 15° angle below the horizontal as shown in Figure 3.1 (III). The infrared thermometer had an 8:1 field of view (8 ft. away the area measured is 1 ft. in diameter). At each location site, ten readings were taken, five readings pointing north and five pointing south perpendicular to the row directions, and then averaged. When the corn height was around 2.0 m, T_s measurements were taken using a bench to reach the desired height and were taken almost at the same time of satellite overpasses (~11:12: AM.). The T_s measurements of five location sites were taken at the same period of time as the LAI readings (11:00 AM. and 12:00 noon).

3.3.5.3 Actual Evapotranspiration estimated with an Atmometer

Actual evapotranspiration (ET_a) was the result of multiplying reference ET (ET_r) from atmometer located in Brookings SD by a crop coefficient (K_c). The K_c values were calculated based on the alfalfa-reference crop coefficient from the ASCE Manual 70 (Appendix E) method (Marvin E Jensen & Allen, 2016). This method uses percent of time from planting to effective cover and days after effective cover to harvest for calculating K_c values. For our study, effective cover occurred at 55 days after emergence (DAE) when the ground cover was 100% (V12). Thus the effective cover was used as a reference point to calculate local K_c values of corn crop.

3.3.5.4 Soil Moisture measured with Soil Moisture Sensors

Soil water content was measured at three depths within the profile (0.1, 0.5, and 1.0 m) using 5TM soil moisture sensors (Decagon Devices, Inc. Pullman, WA, USA). The soil moisture sensors measure the volumetric water content (VWC) between 0% and 100% with an accuracy of ~1.0% (5TM manual Decagon Devices, Inc.). The sensors were connected to Em50 dataloggers (Decagon Devices, Inc. Pullman, WA, USA) and measurements were recorded every 30 minutes during the corn growing season. The information recorded was downloaded every eight days using ECH$_2$O utility software (Decagon Devices, Inc. Pullman, WA, USA) (Figure 3.1 (I)). The soil moisture sensors were installed on May 30, 2014, blue triangles in Figure 1.1 (c).

3.3.6 Statistical Analysis between METRIC Model and in situ Measurements

Linear relationships between LAI, T$_s$, and ET$_a$ estimated using the METRIC model and *in situ* measurements were established. Other statistical evaluations such as coefficient of determination (r^2) (Eq. 5), mean bias error (MBE) (Eq. 6), and root mean square error (RMSE) (Eq. 7) were computed to assess the performance of the METRIC model.

$$r^2 = \frac{\sum_{i=1}^{n}(x_i - \bar{x})(x_i - \bar{y})}{\sqrt{\sum_{i=1}^{n}(x_i - \bar{x})^2 \sum_{i=1}^{n}(y_i - \bar{y})^2}} \tag{5}$$

$$MBE = \frac{1}{n}\sum_{i=1}^{n}(x_i - y_i) \tag{6}$$

$$RMSE = \sqrt{\frac{1}{n}\sum_{i=1}^{n}(x_i - y_i)^2} \tag{7}$$

where n is the number of observations, x_i is the estimated value with the METRIC model, y_i is the measured value *in situ*, and the bars above the variables indicate averages.

3.4   Results and discussion

3.4.1   Precipitation and Soil Water Content

The total precipitation during the period of study was 365.75 mm (21 May to 22 September 2016). The precipitation data were collected and recorded using a tipping bucket rain gauge (TE525, Texas Instrument, Houston, Texas) located near to the S observation site. The rainfall data were reported every 30 minutes to be the same recorded as the soil moisture sensors data (30 min.).

Seasonal trends of soil water content (average depth) at the five locations and precipitation observed throughout the growing season are shown in Figure 3.3. The movements of the graph shows that the soil water content increase after major rain events and decreases as the crop extract water from the root zone. All plot sites showed similar soil moisture trend during the growing season. The soil water content was at or near field capacity early stages (VE) and then decreased towards the end of the season (R6). Rainfall was well distributed during the growing season providing adequate amount of water for the crop. Although low moisture levels were observed at South-East and North locations at time of satellite overpass, low water content may be attributed to higher the higher landscape position of these two location sites (Table 3.1 and Figure 3.2). The satellite overpass dates are indicated with black bars (Figure3.3).
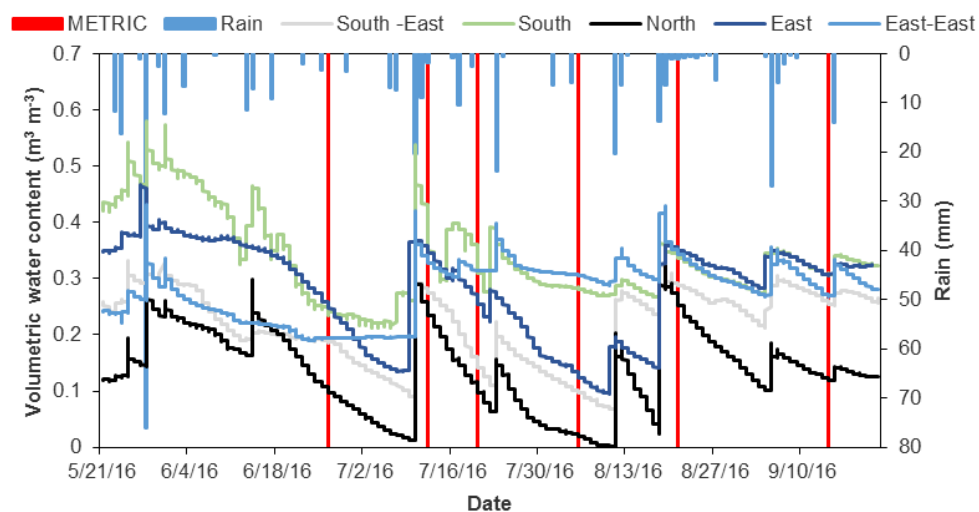
Figure 3.3 Seasonal trends of soil water content (average depths) at the five observation locations. The blue bars indicate precipitation throughout the corn growing season and the red bars denoted remote sensing overpass dates (METRIC).

3.4.2 LAI Maps, Relationship and Comparison of LAI between the METRIC model and AccuPAR

Spatial LAI maps (30 m resolution) of the entire corn field were generated as an output using the METRIC model. The LAI maps captured corn growth stages extending from the middle of the corn vegetative phase (V6, DOY 178) to late season (R6, DOY 258). Example of the resulting maps are presented in Figure 3.4, with an example of high LAI values near the peak of leaf area (R1, DOY 202) and lower LAI values as the crop senesces (R6, DOY 258). The LAI maps developed in this study were similar to LAI maps derived from remote sensing applications by J. M. Chen et al. (2002), Colombo et al. (2003), Martínez, García-Haro, and Camacho-de Coca (2009), Liang et al. (2015), who reported LAI maps for one overpass date in corn fields. However, Qu et al. (2014) reported seasonal LAI maps ranged between 1.0 and 6.0 m^2 m^{-2}, where LAI values increased from 1.0 m^2 m^{-2} (DOY 151) to 6.0 m^2 m^{-2} (DOY 192) and then decrease at 2.0

m^2 m^{-2} (DOY 263) at the end of the season, the corn was planted and observed during the

2012 growing season in the Heihe watershed of northwest China.
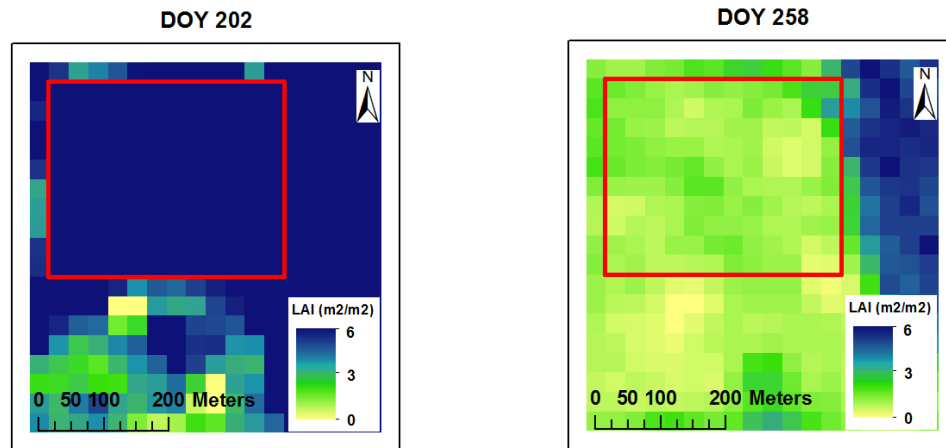
Figure 3.4 Spatial and temporal LAI maps developed from the METRIC model for two overpass dates (DOY 202 and DOY 258). The red rectangle indicates the area of interest within the corn field.

The *in situ* measurements of LAI obtained during the time of satellite overpass

was compared to the LAI estimates by the METRIC model. The progression and

comparison of calculated and measured LAI values at the five observations locations

during the 2016 growing season are shown in Figure 3.5 and Table 3.3. In the METRIC

model the maximum LAI reached (6.0 m^2 m^{-2}) was found in the mid-season stage (R1,

DOY 202) and then drop at 2.2 m^2 m^{-2} at the end of the growing season (R6, DOY 258).

In *in situ* measurements at the beginning of the season the crop presented LAI values

around 0.27 m^2 m^{-2} on DOY 154 (V3) and then gradually increased from 0.67 m^2 m^{-2} in

development stage (V4) to 7.0 m^2 m^{-2} in mid-season stage, which occurred in the silk and

kernel formation period (VT-R4, DOY 194 - 226), and then the LAI values decreased at

3.5 m^2 m^{-2} in the late season, which occurred in the physical maturity period (R6, DOY

258). The standard deviation (vertical bars) of LAI values collected *in situ* with AccuPAR during the corn growing season are presented in Figure 3.5.

The lowest LAI values observed at the North and South-East locations during the season may be attributed to the limited soil moisture due to those locations are located at a higher elevation (Table 3.1 and Figure 3.2). Limited moisture values affects crop canopy development which led to low LAI values (Igbadun, Salim, Tarimo, & Mahoo, 2008). Low moisture values also affected the corn height (Figure 3.6). The METRIC LAI values were slightly smaller than AccuPAR LAI values, this was attributed mainly to different LAI scales, for the METRIC model the range was from 0 to 6 m^2 m^{-2}, while in the AccuPAR the range was 0 to 7 m^2 m^{-2}. METRIC model estimates the average LAI for all plants with a 30 m by 30 m grid, whereas the AccuPAR measures the PAR interception of few plants within a pixel (30 x 30 m). However, both methods have errors in METRIC model for example LAI is capped at 6 m^2 m^{-2}, the LAI is derived from SAVI and thus not a direct measurement (Eq. 1). Exist different factors that over or underestimate LAI values when measure with AccuPAR, for example row spacing, crop height, time of measurement and placement of the meter (Tewolde et al., 2005). In our study, choosing the correct placement of the sensor bar and choosing the time of day (same at satellite overpass) were used for effective use of the AccuPAR to measure LAI values. In general LAI values measured *in situ* with AccuPAR were greater than the LAI values estimated with the METRIC model by about 12% (Table 3.3).
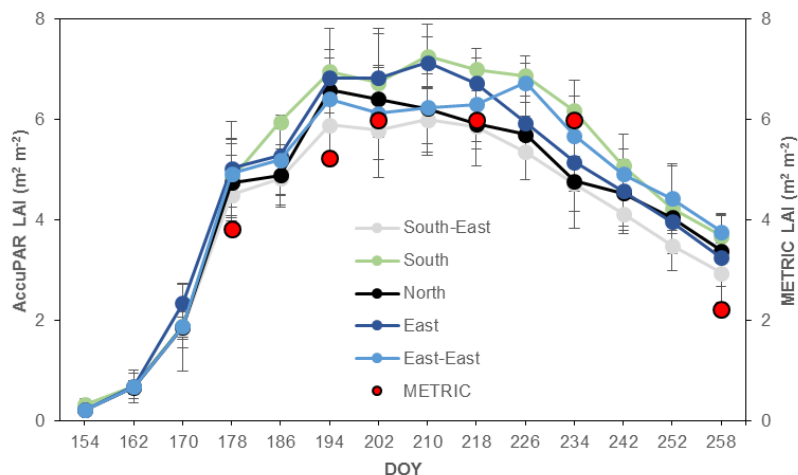
Figure 3.5 Seasonal progression and comparison of LAI estimated with the METRIC model (average of the five locations in each date) (red circles) and measured with AccuPAR (five locations, each location with five points and five replications per location) throughout the season. Vertical bars represent standard deviations of LAI values measured *in situ* with AccuPAR.
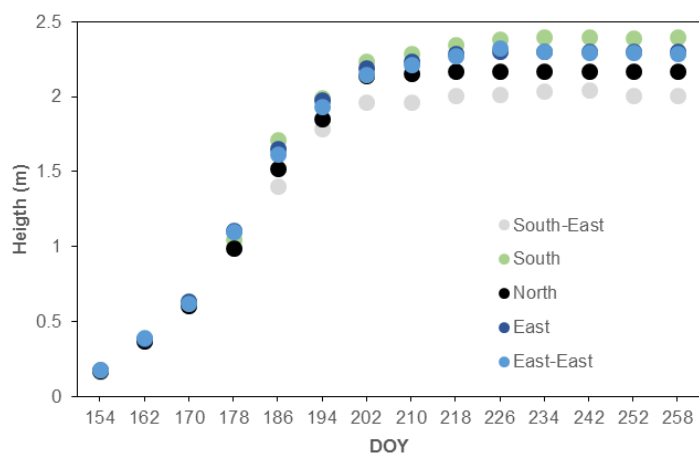
Figure 3.6 Season progression of corn height at five observation locations throughout the 2016 growing season.

Table 3.3 Comparison of LAI values estimated with the METRIC (MT) model and measured with AccuPAR (AP) at five locations during the 2016 growing season, for assessing the LAI by the METRIC model.

	LAI (m² m⁻²)									
DOY	**South-East**		**South**		**North**		**East**		**East-East**	
	MT	AP	MT	AP	MT	AP	MT	AP	MT	AP
178	3.6	4.5	4.0	4.8	3.8	4.7	4.1	5.0	3.8	4.9
194	4.6	5.9	6.0	7.0	4.7	6.6	5.5	6.8	5.3	6.4
202	6.0	5.8	6.0	6.7	6.0	6.4	6.0	6.8	6.0	6.1
218	6.0	5.9	6.0	7.0	6.0	5.9	6.0	6.7	6.0	6.3
234	6.0	4.7	6.0	6.2	6.0	5.7	6.0	5.2	6.0	5.7
258	1.3	3.0	2.6	3.7	2.4	3.4	2.3	3.3	2.5	3.8

The relationship between LAI calculated with the METRIC model and LAI measured *in situ* with AccuPAR is showed in Figure 3.7. A good linear correlation was found between *in situ* measured and estimated LAI, with a coefficient of determination (r^2) of 0.76, MBE of 0.61 m^2 m^{-2} and RMSE of 0.59 m^2 m^{-2}. The large scatter at LAI (6.0 m^2 m^{-2}) is because the METRIC model is capped at LAI = 6 m^2 m^{-2}, while in the AccuPAR LAI values ranged from 4.72 to 7.0 m^2 m^{-2}. Higher coefficient of determination values (0.89) were found by Liang et al. (2015). They compared LAI measured in ground-based with LICOR LAI-2000 Plant Canopy Analyzer versus LAI estimated from several vegetation indices using satellite remote sensing in different crops including corn.
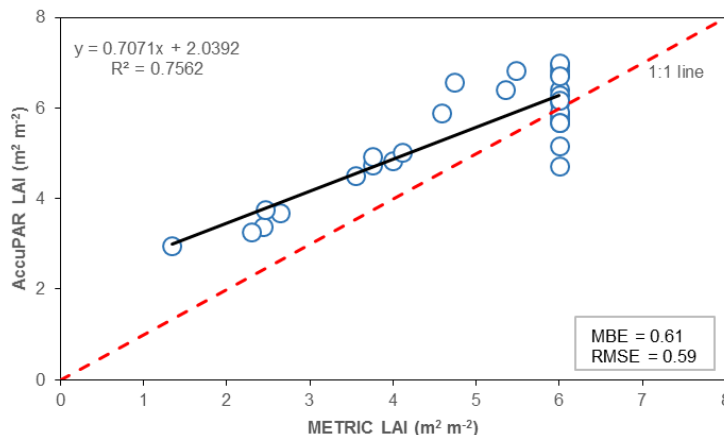
Figure 3.7 Relationship between LAI values estimated with the METRIC model and LAI values measured with AccuPAR in five observation locations during the 2016 corn growing season. The red dashed line represent the 1:1 line.

The relationship and seasonal progression between average crop height and LAI measured with AccuPAR is illustrated in Figure 3.8. A strong relationship ($r^2 = 0.95$) was found between corn plant height and LAI values until DOY 226 (R4) (Figure 3.6 (a)). Similar relationship value ($r^2 = 0.99$) was reported by Tasumi (2003), who made relationships between crop height and LAI for agricultural crops including corn crop in Kimberly, Idaho, and by S. Gao et al. (2013)) ($r^2 = 0.92$), who took from 5 to 10 representative corn plants to determine their mean height and correlated with the LAI values. For our study, the average crop height started with 0.17 m (DOY 154) (V3) before plateauing at 2.2 m around DOY 202 (R1) (Figure 3.8 (b)).

(**a**)   (**b**)
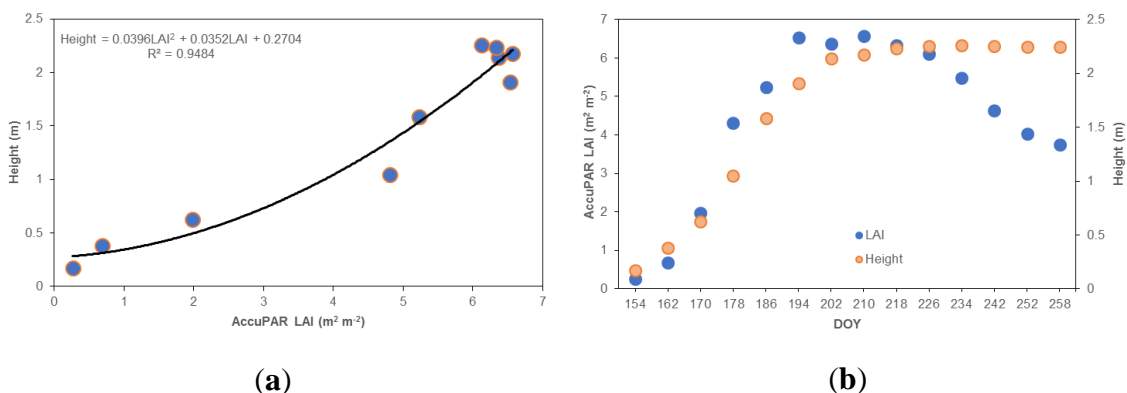
Figure 3.8 Relationship between average crop height and average LAI (a). Seasonal progression of crop height (ten reading average for each location) and LAI measured with AccuPAR (average of five locations, each location with five points and five replications per location) throughout the 2016 growing season (b).

3.4.3 T_s Maps, Relationship and Comparison of Surface Temperature between METRIC and Infrared Thermometer.

Surface temperature (T_s) maps were derived from the METRIC model using Landsat 7 and Landsat 8 with 60 m and 100 m spatial resolution in the thermal band respectively. T_s varied from low values (20.8°C) to high values (29.5 °C) for DOY 258 and for DOY 202, respectively during the growing season as shown in Figure 3.9 and Table 3.4. T_s is impacted by the water status of the plant, soil moisture content, and climatic conditions (Gallardo, 1992). Similar land surface temperature maps at field scale were developed by other researchers (Gowda et al., 2015; Senay et al., 2016), using satellite remote sensing.
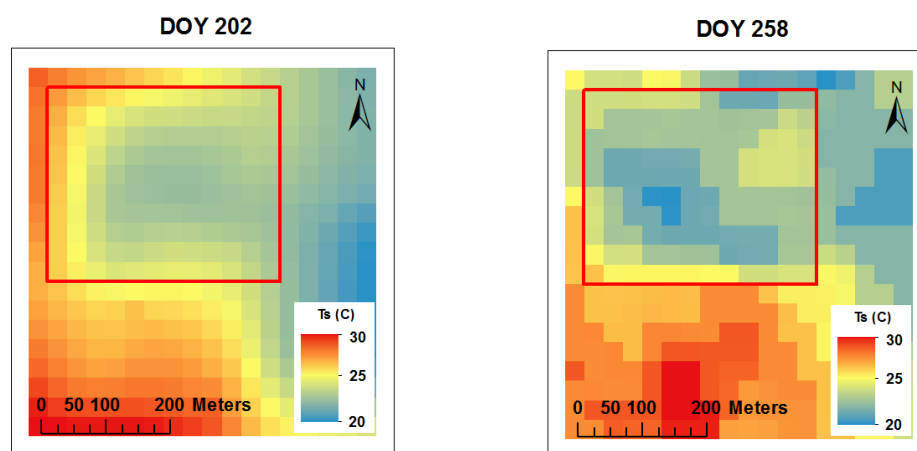
DOY 202

DOY 258

Figure 3.9 Maps of land surface temperature derived from the METRIC model acquired using Landsat 7 (DOY 258) and Landsat 8 (DOY 202) with 60 m and 100 m spatial resolution respectively, throughout the 2016 corn growing season. The red rectangle indicates the area of interest within corn field.

The variation of instantaneous T_s calculated with METRIC model and measured *in situ* with infrared thermometer in five locations are illustrated in Figure 3.10 and Table 3.4. A wide range of T_s was observed during the period of study (19 - 31 °C), where the coolest temperature (~19 °C) occurred at the end of the season (R6, DOY 258) and the warmer temperature (~31°C) occurred at the mid-season (R1, DOY 202) for both methods. Slightly higher T_s values were observed at the North and South-East locations, whereas the lowest temperatures values were observed at the South, East, and East-East locations. The highest T_s values registered at the North and South-East locations may be due to high altitude (Table 3.1) and lower moisture content in the root zone (Figure 3.3). In addition as the soil moisture decreases, the T_s increases, this result coincide with the results reported by other researchers e.g., (M. Anderson & Kustas, 2008; Bellvert et al., 2014; Cohen et al., 2015; Durigon & van Lier, 2013). They reported that the crop canopy temperature increases as soil water content decreases. Also M. Anderson and Kustas

(2008) and Durigon and van Lier (2013) reported that low water content in the root zone leads to stomatal closure, reduce transpiration and increase T_s.

During the growing season the METRIC T_s values were slightly higher than infrared thermometer T_s values for corresponding location, except on DOY 202. (Figure 3.10 and Table 3.4), however for the whole season the METRIC model were higher than the *in situ* values by 0.85 °C. The slightly difference between T_s estimated by the METRIC model and measured by infrared thermometer could be attributed to the measurements, which were carried out at different scales and different parts of the plant for example Landsat look down from nadir and sees canopy and some soil, while *in situ* measurements canopy only, and at a different angle than Landsat. Another could be attribute at the error in both methods. In the METRIC model the potential bias in T_s calculations are reduced by internal calibration technique CIMEC (calibration using inverse modeling at extreme conditions) (R. Allen, A. Irmak, R. Trezza, J. M. Hendrickx, et al., 2011; R. G. Allen, Kjaersgaard, Garcia, Tasumi, & Trezza, 2008). In i*n situ* measurements the bias were attributed to the time of readings (11:00 AM. to 12:00 noon) assuming that readings at 11:00 AM. are slightly colder than readings at noon, also some T_s reading were affected by the wind speed at the time of satellite overpass. Jones and Vaughan (2010) mentioned that instantaneous T_s measured in the field is very sensitive to climatic factors (e.g. cloud cover, wind speed, and solar radiation). In our study, instantaneous T_s was affected by wind speed and cloud cover from 1 to 2 °C and from 3 to 4 °C, respectively, lower than normal (no wind and no cloud conditions) T_s values. However, instantaneous T_s values affected by wind speed and cloud cover were excluded in our analysis.

In our study, standard deviation of canopy temperature (CTSD) values were lower than 2.0 °C among observation locations for each date throughout the season (Figure 3.10). Han et al. (2016) used the CTSD to classify corn water stress into three levels: severe stress when CTSD is greater than 3.0 °C, intermediate stress when CTSD is between 2.0 and 3.0 °C, and no stress when CTSD is less than 2.0 °C. On the other hand, Zia et al. (2011), Romano et al. (2011), and Taghvaeian et al. (2013), reported differences in canopy temperature between corn plants ranged of 2.2 – 3.0 °C for corn under different irrigation treatments.
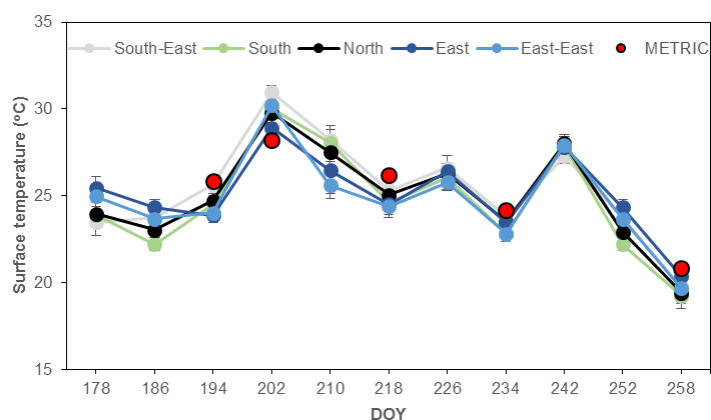
Figure 3.10 Seasonal and comparison of instantaneous T_s calculated with the METRIC model red circles (values at the time of satellite overpass date for corresponding location) and measured *in situ* with infrared thermometer (ten readings average in each location). Vertical bars represent standard deviations of T_s values measured with infrared thermometer.

Table 3.4 Comparison of T_s values between the METRIC (MT) model and infrared thermometer (IT) at five locations and five dates during the corn growing season.

	T_s (ºC)									
	South-East		South		North		East		East-East	
DOY	MT	IT	MT	IT	MT	IT	MT	IT	MT	IT
194	26.4	25.6	26.4	24.5	25.9	24.7	25.9	23.9	25.9	24.0
202	29.5	31.0	28.2	30.1	27.7	29.7	26.9	28.9	28.3	30.2
218	26.7	25.3	26.6	24.6	26.9	25.1	26.2	24.5	26.1	24.4
234	24.8	23.8	24.6	22.8	24.7	23.5	24.2	23.5	24.2	22.8
258	20.9	19.7	21.2	19.2	20.9	19.4	20.9	20.4	20.8	19.7

The relationship between T_s estimated with the METRIC model and T_s measured *in situ* with infrared thermometer is presented in Figure 3.11. Good correlation ($r^2 =$ 0.87), and acceptable values of MBE (0.85 °C) and RMSE (1.24 °C) were found. Similar RMSE values were reported by Neukam, Ahrends, Luig, Manderscheid, and Kage (2016), who reported RMSE less than 2.0 °C between simulated and measured canopy temperatures.
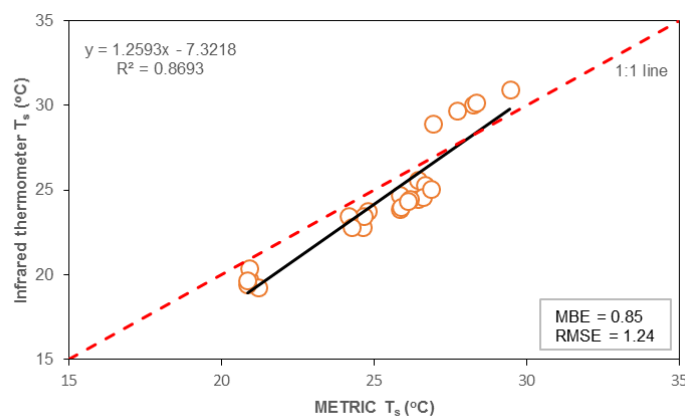
Figure 3.11 Linear correlation of T_s between the METRIC model and infrared thermometer of corn throughout growing season. The red dashed line represent the 1:1 line.

3.4.4 ET$_a$ Maps, Crop Coefficient, Relationship and Comparison of ET$_a$ between METRIC and Atmometer

Spatially distributed maps of ET$_a$ were calculated with the METRIC model for the corn field. The estimated ET$_a$ values ranged between 2.7 to 9.7 mm day^{-1} (Table 3.5). Two ET$_a$ maps for the mid-season (DOY 194) and late season (DOY 258) are shown in Figure 3.12. The maps show the highest (VT, DOY 194) and the lowest (R6, DOY 258) ET$_a$ values estimated with the METRIC model during the corn growing season. Generally, high ET rates are related to high crop water demands, which normally

occurred in the mid-season period (VT-R4, DOY 194 - 226), while low ET rates occurred in the late season (R6, DOY 258) when the crop is in the senescence stage. ET_a maps have been developed by remote sensing in hourly, daily, monthly and annually basis from individual field scale to global scale e.g., (Choi et al., 2011; Gowda, Chávez, Howell, Marek, & New, 2008; Ke, Im, Park, & Gong, 2016; Li, Zhao, & Deng, 2015; Liebert et al., 2016; Maeda et al., 2011; Santos et al., 2008; Senay et al., 2016; Simons et al., 2016; Weiß & Menzel, 2008; Zipper & Loheide II, 2014), where some of them used the METRIC model to generated ET_a maps.
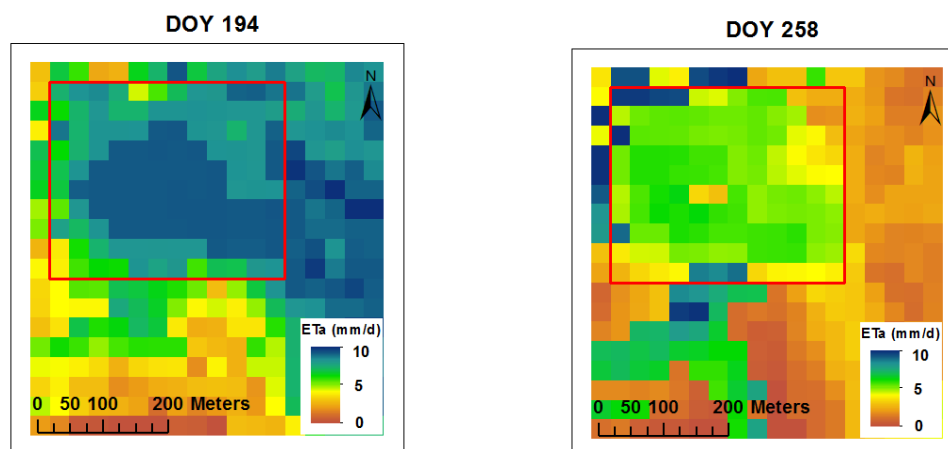
Figure 3.12 Daily ET_a maps developed by the METRIC model for mid-season (DOY 202) and late season (DOY 258) during the 2016 corn growing season. The red rectangle indicates the area of interest within corn field.

Table 3.5 ET_a values estimated by the METRIC model for five observation locations and six overpass dates during the corn growing season.

	METRIC ET_a (mm day^{-1})					
DOY	South-east	South	North	East	East-east	Average
178	7.98	8.06	7.68	8.45	8.22	8.08
194	9.40	9.41	8.87	9.72	9.45	9.37
202	7.16	7.08	7.10	7.14	7.26	7.15
218	4.63	4.63	4.56	4.82	4.92	4.71
234	3.91	3.96	3.93	4.23	4.23	4.05
258	2.69	2.87	2.75	2.60	2.67	2.72

Figure 3.13 shows the K_c curve developed for the corn field based on the alfalfa-reference crop coefficient (Marvin E Jensen & Allen, 2016). From the initial (V3, DOY 154) to mid-season stage (VT, DOY 194) the K_c values increase as a function of time between 30% of crop cover to 100% of effective cover, which occurred around 55 days after emergence. In late season the K_c values gradually decreased indicating the crop senescence. At the end of the season (R6, DOY 158) the K_c value is low again (K_c = ~0.6).
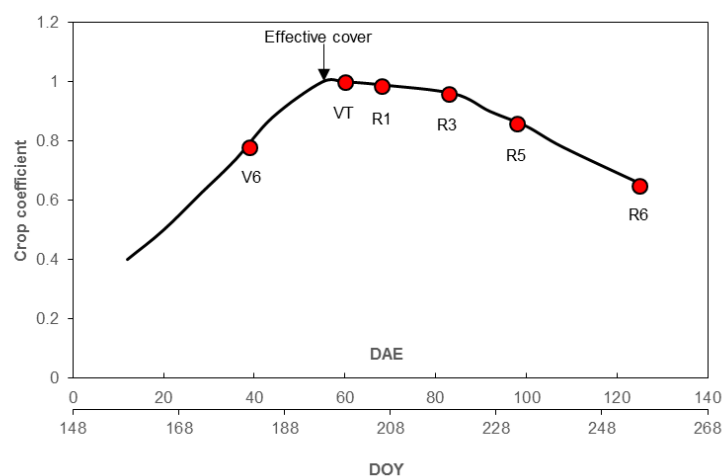
Figure 3.13 Crop coefficient curve based on the alfalfa-reference crop coefficient of corn field throughout the growing season. The red circles denote satellite overpass dates.

The comparison between ET_a estimated by the METRIC model and by the atmometer is illustrated in Figure 3.14. In general, the highest ET_a values were found on DOY 194 (VT) for the METRIC model was 9.7 mm day^{-1} and for atmometer was 8.0 mm day^{-1} and the smallest were observed on DOY 258 (R6) for the METRIC model was 2.7 mm day^{-1} and for atmometer was 2.3 mm day^{-1}. Those dates coincided with the biggest and the smallest ET_rF and K_c values for the METRIC model method and for the atmometer method, respectively.

Figure 3.14 shows that ET_a values estimated with the METRIC model were greater than ET_a values estimated by atmometer, however on DOY 218 and DOY 234 the ET_a values estimated with the METRIC model were lower than ET_a values estimated with atmometer, this was because the wind speed values at time of satellite overpass were low (~1.0 m s^{-1}) (Figure 3.16). The largest difference in ET_a between the METRIC model and atmometer was on DOY 194 (VT) with 1.4 mm day^{-1}, this was attributed to the high wind speed values at time of satellite overpass (5.9 m s^{-1}) (black line in Figure 3.16). According to S. Irmak et al. (2005) the atmometer readings are not altered by windy actions, however when high wind speed value is used to estimate ET_r using Penman-Monteith equation, the resulting ET_r values are high.

Results of daily ET_a estimations error for each image date between the METRIC model and the atmometer ranged between 4 to 17%. These error values are in agreement with R. G. Allen, Tasumi, and Trezza (2007) and Gowda, Chavez, et al. (2008), who reported that daily ET_a estimates from METRIC model has ET_a error from 10 to 20%. (Chavez et al., 2007), who compared daily ET_a values derived from the METRIC model and derived from soil water budget at four commercial fields, concluded that daily ET_a estimates error were below than 15%. Healey et al. (2011), they compared daily estimates of ET_a from the METRIC model and from (BREBS) at three locations, they found daily ET_a error around 20%. Gordillo Salinas et al. (2014) compared daily ET_a values calculated from the METRIC model and calculated from (EC) reported average daily ET_a error of 7%.
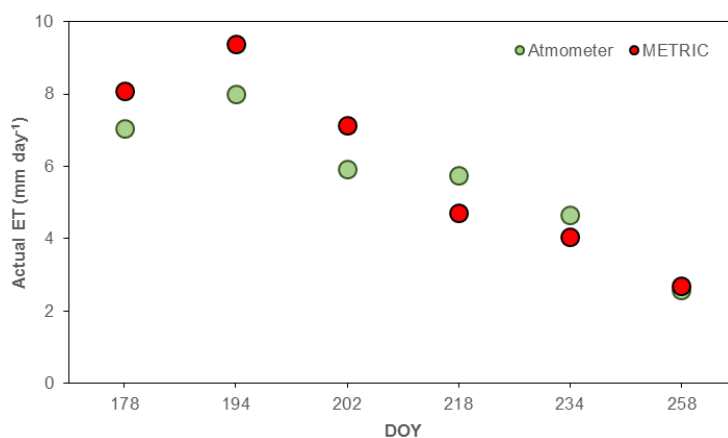
Figure 3.14 Progression and comparison between daily ET_a estimated by the METRIC model (average values of each overpass date) and estimated by atmometer and K_c during the corn growing season 2016.

The relationship of ET_a between the METRIC model and atmometer are presented in Figure 3.15. In the METRIC model ET_a values were taken from the ET_a maps, where nine average pixels of ET_a around each measure point were chosen by each observation location and then average. In the atmometer method the ET_a was the result of multiplied ET_r measured with atmometer by a K_c, which was developed based on alfalfa reference crop coefficient (Figure 3.11). The ET_a values derived from atmometer was for entire area of interest for each overpass date. The relationship revealed good agreement between ET_a estimations, with a coefficient of determination equal to 0.89, MBE and RMSE equal to 0.34 and 0.71 mm day^{-1}, respectively. Researchers have reported similar coefficients of determination (0.86) (French et al., 2015; Liebert et al., 2016), while higher coefficients (0.97) were found by Ayse Irmak et al. (2011), Mkhwanazi and Chávez (2012), Gordillo Salinas et al. (2014), and lower coefficients (0.79) were reported by Healey et al. (2011). All these authors estimated daily ET_a in agricultural crops using the METRIC model.
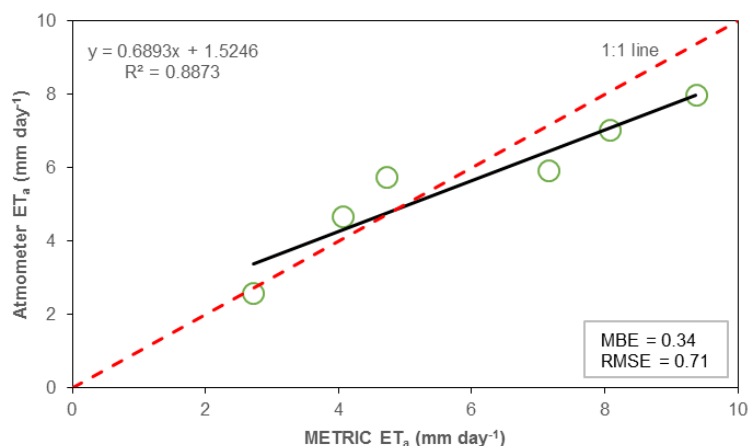
Figure 3.15 Relationship between ET_a estimated by the METRIC model and estimated by atmometer during the period of study. The red dashed line represent the 1:1 line.
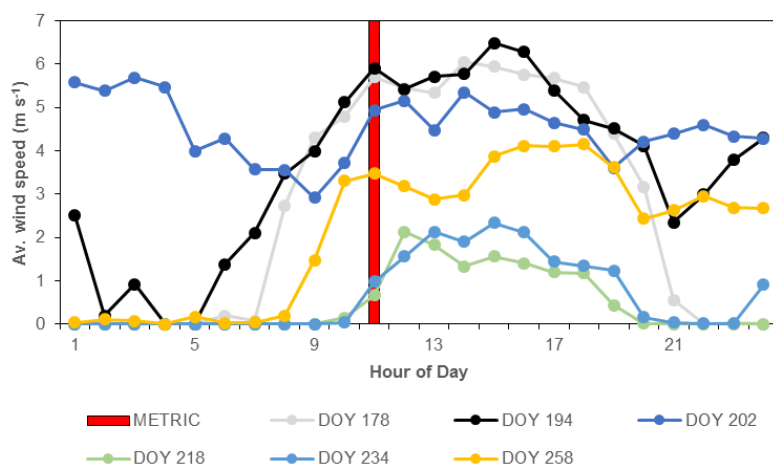
Figure 3.16 Hourly average wind speed values at the Brookings weather station. The red column represent the time of satellite overpass (METRIC) (~11:12 AM).

3.5 Conclusions

This paper assess the relationship between, leaf area index (LAI), surface temperature (T_s), and actual evapotranspiration (ET_a) estimated by remote sensing-based METRIC model and *in-situ* measurements at the same time of satellite overpass over a corn field in eastern South Dakota. In order to assess the METRIC model performance

the coefficient of determination (r2), mean bias error MBE), and root means square error (RMSE) were considered.

The *in situ* measurements of LAI obtained with AccuPAR during the time of satellite overpass was compared to the LAI estimates by the METRIC model. The output of LAI values from the METRIC model were slightly smaller (12%) than the LAI values derived from AccuPAR, this slightly difference was attributed to the different LAI scales. METRIC model estimated the average LAI for all plants with a 30 m by 30 m grid, while the AccuPAR measured the LAI only in few plants within a pixel (30 x 30 m). However, good linear correlation was found between *in situ* measured and estimated LAI, with a coefficient of determination (r^2) of 0.76 and RMSE of 0.59 m^2 m^{-2}.

Surface temperature maps were derived from the METRIC model using Landsat 7 and Landsat 8 with 60 and 100 m spatial resolution in the thermal bands respectively. For whole season the T_s estimated using the METRIC model was higher than the T_s measured *in situ* using infrared thermometer by 0.85 °C. The slightly difference was attributed to the measurements, which were carried out at different scales and different parts of the plant. A good correlation ($r^2 = 0.87$), and acceptable value of RMSE (1.24 °C) were found between estimated and measured T_s. The T_s measurements were affected by soil water content, wind speed, and cloud cover.

Result of comparisons between estimated ET_a during the 2016 corn growing season showed that ET_a values estimated with the METRIC model were greater than ET_a values estimated by atmometer. The largest difference in daily ET_a between the METRIC model and atmometer was 1.4 mm day^{-1}, this was attributed to the high wind speed values at time of satellite overpass. Daily ET_a estimations error for each image date

between the METRIC model and the atmometer ranged between 4 to 17%. The relationship revealed good agreement between ET_a estimations, with high coefficient of determination ($r^2 = 0.89$) and low RMSE (0.71 mm day^{-1}).

Finally, the landscape position of observation locations were affected by soil water content, which lead to low crop height, low LAI, and high T_s in both methods using remote sensing and *in situ* measurements.

3.6   References

Alam, M., & Trooien, T. (2001). Estimating reference evapotranspiration with an atmometer. *Applied Engineering in Agriculture, 17*(2), 153-158.

Alchanatis, V., Cohen, Y., Cohen, S., Moller, M., Sprinstin, M., Meron, M., . . . Sela, E. (2010). Evaluation of different approaches for estimating and mapping crop water status in cotton with thermal imaging. *Precision agriculture, 11*(1), 27-41.

Allen, R., Irmak, A., Trezza, R., Hendrickx, J. M., Bastiaanssen, W., & Kjaersgaard, J. (2011). Satellite-based ET estimation in agriculture using SEBAL and METRIC. *Hydrological Processes, 25*(26), 4011-4027.

Allen, R. G., Kjaersgaard, J., Garcia, M., Tasumi, M., & Trezza, R. (2008). *Fine-tuning components of inverse-calibrated, thermal-based remote sensing models for evapotranspiration.* Paper presented at the Proc. 17th Pecora Conference on the Future of Land Imaging, Denver, November.

Allen, R. G., Pereira, L. S., Raes, D., & Smith, M. (1998). Crop evapotranspiration-Guidelines for computing crop water requirements-FAO Irrigation and drainage paper 56. *FAO, Rome, 300*(9), D05109.

Allen, R. G., Tasumi, M., Morse, A., Trezza, R., Wright, J. L., Bastiaanssen, W., . . . Robison, C. W. (2007). Satellite-based energy balance for mapping evapotranspiration with internalized calibration (METRIC)—Applications. *Journal of Irrigation and Drainage Engineering, 133*(4), 395-406.

Allen, R. G., Tasumi, M., & Trezza, R. (2007). Satellite-based energy balance for mapping evapotranspiration with internalized calibration (METRIC)—Model. *Journal of Irrigation and Drainage Engineering, 133*(4), 380-394.

Anderson, M., & Kustas, W. (2008). Thermal remote sensing of drought and evapotranspiration. *Eos, Transactions American Geophysical Union, 89*(26), 233-234.

ASCE-EWRI. (2005). *The ASCE standardized reference evapotranspiration equation; ASCE-EWRI Standardization of Reference Evapotranspiration Task Committee Report; ASCE: Reston, VA, USA*.

Asner, G. P., Scurlock, J. M., & A Hicke, J. (2003). Global synthesis of leaf area index observations: implications for ecological and remote sensing studies. *Global Ecology and Biogeography, 12*(3), 191-205.

Bellvert, J., Zarco-Tejada, P. J., Girona, J., & Fereres, E. (2014). Mapping crop water stress index in a 'Pinot-noir' vineyard: comparing ground measurements with thermal remote sensing imagery from an unmanned aerial vehicle. *Precision agriculture, 15*(4), 361-376.

Berni, J. A., Zarco-Tejada, P. J., Suárez, L., & Fereres, E. (2009). Thermal and narrowband multispectral remote sensing for vegetation monitoring from an unmanned aerial vehicle. *IEEE Transactions on Geoscience and Remote Sensing, 47*(3), 722-738.

Bijanzadeh, E. (2012). Evaluation of crop water stress index, canopy temperature and grain yield of five Iranian wheat cultivars under late season drought stress. *Journal of Plant Physiology & Breeding, 2*(1), 23-33.

Bréda, N. J. (2003). Ground-based measurements of leaf area index: a review of methods, instruments and current controversies. *Journal of experimental botany, 54*(392), 2403-2417.

Broner, I., & Law, R. (1991). Evaluation of a modified atmometer for estimating reference ET. *Irrigation Science, 12*(1), 21-26.

Carrasco-Benavides, M., Ortega-Farías, S., Lagos, L. O., Kleissl, J., Morales-Salinas, L., & Kilic, A. (2014). Parameterization of the Satellite-Based Model (METRIC) for the estimation of instantaneous surface energy balance components over a drip-irrigated vineyard. *Remote Sensing, 6*(11), 11342-11371.

Chavez, J. L., Gowda, P. H., Howell, T. A., Marek, T. H., & New, L. L. (2007). *Evapotranspiration mapping using METRICTM for a region with highly advective conditions.* Paper presented at the 2007 ASABE Annual International Meeting, Technical Papers.

Chen, J. M., Pavlic, G., Brown, L., Cihlar, J., Leblanc, S., White, H., . . . Trofymow, J. (2002). Derivation and validation of Canada-wide coarse-resolution leaf area index maps using high-resolution satellite imagery and ground measurements. *Remote Sensing of Environment, 80*(1), 165-184.

Choi, M., Kim, T. W., Park, M., & Kim, S. J. (2011). Evapotranspiration estimation using the Landsat-5 Thematic Mapper image over the Gyungan watershed in Korea. *International journal of remote sensing, 32*(15), 4327-4341.

Cohen, Y., Alchanatis, V., Sela, E., Saranga, Y., Cohen, S., Meron, M., . . . Orolov, V. (2015). Crop water status estimation using thermography: Multi-year model development using ground-based thermal images. *Precision agriculture, 16*(3), 311-329.

Colaizzi, P. D., Evett, S. R., O'Shaughnessy, S. A., & Howell, T. A. (2012). *Using plant canopy temperature to improve irrigated crop management.* Paper presented at the Proc. 24th Annual Central Plains Irrigation Conf., 21-22 February 2012, Colby, USA.

Colombo, R., Bellingeri, D., Fasolini, D., & Marino, C. M. (2003). Retrieval of leaf area index in different vegetation types using high resolution satellite data. *Remote Sensing of Environment, 86*(1), 120-131.

DeJonge, K. C., Taghvaeian, S., Trout, T. J., & Comas, L. H. (2015). Comparison of canopy temperature-based water stress indices for maize. *Agricultural Water Management, 156*, 51-62.

Durigon, A., & van Lier, Q. d. J. (2013). Canopy temperature versus soil water pressure head for the prediction of crop water stress. *Agricultural Water Management, 127*, 1-6.

French, A. N., Hunsaker, D. J., & Thorp, K. R. (2015). Remote sensing of evapotranspiration over cotton using the TSEB and METRIC energy balance models. *Remote Sensing of Environment, 158*, 281-294.

Gallardo, I. T. (1992). *Using infrared canopy temperature and leaf water potential for irrigation scheduling in peppermint (Mentha piperita L.).*

Gao, S., Niu, Z., Huang, N., & Hou, X. (2013). Estimating the Leaf Area Index, height and biomass of maize using HJ-1 and RADARSAT-2. *International Journal of Applied Earth Observation and Geoinformation, 24*, 1-8.

Garrigues, S., Shabanov, N., Swanson, K., Morisette, J., Baret, F., & Myneni, R. (2008). Intercomparison and sensitivity analysis of Leaf Area Index retrievals from LAI-2000, AccuPAR, and digital hemispherical photography over croplands. *Agricultural and Forest Meteorology, 148*(8), 1193-1209.

Gordillo Salinas, V. M., Flores Magdaleno, H., Tijerina Chávez, L., & Arteaga Ramírez, R. (2014). Estimación de la evapotranspiración utilizando un balance de energía e imágenes satelitales. *Revista mexicana de ciencias agrícolas, 5*(1), 143-155.

Gowda, P. H., Chavez, J. L., Colaizzi, P. D., Evett, S. R., Howell, T. A., & Tolk, J. A. (2008). ET mapping for agricultural water management: present status and challenges. *Irrigation Science, 26*(3), 223-237.

Gowda, P. H., Chávez, J. L., Howell, T. A., Marek, T. H., & New, L. L. (2008). Surface energy balance based evapotranspiration mapping in the Texas high plains. *Sensors, 8*(8), 5186-5201.

Gowda, P. H., Howell, T. A., Chávez, J. L., Paul, G., Moorhead, J. E., Holman, D., . . . Colaizzi, P. D. (2015). *A decade of remote sensing and evapotranspiration research at USDA-ARS Conservation and Production Research Laboratory.* Paper presented at the ASABE Annual International Meeting.

Han, M., Zhang, H., DeJonge, K. C., Comas, L. H., & Trout, T. J. (2016). Estimating maize water stress by standard deviation of canopy temperature in thermal imagery. *Agricultural Water Management, 177*, 400-409.

Hankerson, B., Kjaersgaard, J., & Hay, C. (2012). Estimation of evapotranspiration from fields with and without cover crops using remote sensing and in situ methods. *Remote Sensing, 4*(12), 3796-3812.

Healey, N. C., Irmak, A., Arkebauer, T. J., Billesbach, D. P., Lenters, J. D., Hubbard, K. G., . . . Kjaersgaard, J. (2011). Remote sensing and in situ-based estimates of evapotranspiration for subirrigated meadow, dry valley, and upland dune ecosystems in the semi-arid sand hills of Nebraska, USA. *Irrigation and Drainage Systems, 25*(3), 151-178.

Hosseini, M., McNairn, H., Merzouki, A., & Pacheco, A. (2015). Estimation of Leaf Area Index (LAI) in corn and soybeans using multi-polarization C-and L-band radar data. *Remote Sensing of Environment, 170*, 77-89.

Idso, S., Jackson, R., Pinter, P., Reginato, R., & Hatfield, J. (1981). Normalizing the stress-degree-day parameter for environmental variability. *Agricultural Meteorology, 24*, 45-55.

Igbadun, H. E., Salim, B. A., Tarimo, A. K., & Mahoo, H. F. (2008). Effects of deficit irrigation scheduling on yields and soil water balance of irrigated maize. *Irrigation Science, 27*(1), 11-23.

Irmak, A., Ratcliffe, I., Ranade, P., Hubbard, K. G., Singh, R. K., Kamble, B., & Kjaersgaard, J. (2011). Estimation of land surface evapotranspiration with a satellite remote sensing procedure. *Great plains research*, 73-88.

Irmak, S., Dukes, M., & Jacobs, J. (2005). Using modified Bellani plate evapotranspiration gauges to estimate short canopy reference evapotranspiration. *Journal of Irrigation and Drainage Engineering, 131*(2), 164-175.

Irmak, S., Haman, D. Z., & Bastug, R. (2000). Determination of crop water stress index for irrigation timing and yield estimation of corn. *Agronomy Journal, 92*(6), 1221-1227.

Jensen, M. E., & Allen, R. G. (2016). *Evaporation, Evapotranspiration, and Irrigation Water Requirements*.

Jones, H. G., & Vaughan, R. A. (2010). *Remote sensing of vegetation: principles, techniques, and applications*: Oxford university press.

Ke, Y., Im, J., Park, S., & Gong, H. (2016). Downscaling of MODIS One kilometer evapotranspiration using Landsat-8 data and machine learning approaches. *Remote Sensing, 8*(3), 215.

Kjaersgaard, J., & Allen, R. (2010). Remote sensing technology to produce consumptive water use maps for the Nebraska Panhandle. *Final completion report submitted to the University of Nebraska, 88*.

Kjaersgaard, J., Allen, R., & Irmak, A. (2011). Improved methods for estimating monthly and growing season ET using METRIC applied to moderate resolution satellite imagery. *Hydrological Processes, 25*(26), 4028-4036.

Li, A., Zhao, W., & Deng, W. (2015). A Quantitative Inspection on Spatio-Temporal Variation of Remote Sensing-Based Estimates of Land Surface Evapotranspiration in South Asia. *Remote Sensing, 7*(4), 4726-4752.

Liang, L., Di, L., Zhang, L., Deng, M., Qin, Z., Zhao, S., & Lin, H. (2015). Estimation of crop LAI using hyperspectral vegetation indices and a hybrid inversion method. *Remote Sensing of Environment, 165*, 123-134.

Liebert, R., Huntington, J., Morton, C., Sueki, S., & Acharya, K. (2016). Reduced evapotranspiration from leaf beetle induced tamarisk defoliation in the Lower Virgin River using satellite-based energy balance. *Ecohydrology, 9*(1), 179-193.

López-López, R., Ramírez, R. A., Sánchez-Cohen, I., Bustamante, W. O., & González-Lauck, V. (2011). Evapotranspiration and Crop Water Stress Index in Mexican Husk Tomatoes (Physalis ixocarpa Brot). *Evapotranspiration–From Measurements to Agricultural and Environmental Applications*, 187.

Maeda, E. E., Wiberg, D. A., & Pellikka, P. K. (2011). Estimating reference evapotranspiration using remote sensing and empirical models in a region with limited ground data availability in Kenya. *Applied Geography, 31*(1), 251-258.

Martínez, B., García-Haro, F., & Camacho-de Coca, F. (2009). Derivation of high-resolution leaf area index maps in support of validation activities: Application to the cropland Barrax site. *Agricultural and Forest Meteorology, 149*(1), 130-145.

Mkhwanazi, M., & Chávez, J. L. (2012). Using METRIC to estimate surface energy fluxes over an alfalfa field in Eastern Colorado. *Hydrology Days, Colorado State University USA (Accessed on August 26th 2014 from: http:// hydrologydays. colostate. edu/ Papers_ 2012/ Mcebisi_ paper. pdf)*.

Mkhwanazi, M., Chávez, J. L., & Rambikur, E. H. (2012). Comparison of large aperture scintillometer and satellite-based energy balance models in sensible heat flux and crop evapotranspiration determination. *International Journal of Remote Sensing Applications, 2*(1), 24-30.

Neukam, D., Ahrends, H., Luig, A., Manderscheid, R., & Kage, H. (2016). Integrating wheat canopy temperatures in crop system models. *Agronomy, 6*(1), 7.

Nguy-Robertson, A., Gitelson, A., Peng, Y., Viña, A., Arkebauer, T., & Rundquist, D. (2012). Green leaf area index estimation in maize and soybean: combining vegetation indices to achieve maximal sensitivity. *Agronomy Journal, 104*(5), 1336-1347.

O'Shaughnessy, S., & Evett, S. R. (2010). Canopy temperature based system effectively schedules and controls center pivot irrigation of cotton. *Agricultural Water Management, 97*(9), 1310-1316.

Ortega-Farías, S., Ortega-Salazar, S., Poblete, T., Kilic, A., Allen, R., Poblete-Echeverría, C., . . . Sepúlveda, D. (2016). Estimation of energy balance components over a drip-irrigated olive orchard using thermal and multispectral cameras placed on a helicopter-based unmanned aerial vehicle (UAV). *Remote Sensing, 8*(8), 638.

Peters, R. T., & Evett, S. R. (2008). Automation of a center pivot using the temperature-time-threshold method of irrigation scheduling. *Journal of Irrigation and Drainage Engineering, 134*(3), 286-291.

Qu, Y., Zhu, Y., Han, W., Wang, J., & Ma, M. (2014). Crop leaf area index observations with a wireless sensor network and its potential for validating remote sensing products. *IEEE Journal of Selected Topics in Applied Earth Observations and Remote Sensing, 7*(2), 431-444.

Romano, G., Zia, S., Spreer, W., Sanchez, C., Cairns, J., Araus, J. L., & Müller, J. (2011). Use of thermography for high throughput phenotyping of tropical maize adaptation in water stress. *Computers and Electronics in Agriculture, 79*(1), 67-74.

Sandholt, I., Rasmussen, K., & Andersen, J. (2002). A simple interpretation of the surface temperature/vegetation index space for assessment of surface moisture status. *Remote Sensing of Environment, 79*(2), 213-224.

Santos, C., Lorite, I., Tasumi, M., Allen, R., & Fereres, E. (2008). Integrating satellite-based evapotranspiration with simulation models for irrigation management at the scheme level. *Irrigation Science, 26*(3), 277-288.

Senay, G. B., Friedrichs, M., Singh, R. K., & Velpuri, N. M. (2016). Evaluating Landsat 8 evapotranspiration for water use mapping in the Colorado River Basin. *Remote Sensing of Environment, 185*, 171-185.

Sepúlveda-Reyes, D., Ingram, B., Bardeen, M., Zúñiga, M., Ortega-Farías, S., & Poblete-Echeverría, C. (2016). Selecting Canopy Zones and Thresholding Approaches to Assess Grapevine Water Status by Using Aerial and Ground-Based Thermal Imaging. *Remote Sensing, 8*(10), 822.

Simons, G., Bastiaanssen, W., Ngô, L. A., Hain, C. R., Anderson, M., & Senay, G. (2016). Integrating Global Satellite-Derived Data Products as a Pre-Analysis for Hydrological Modelling Studies: A Case Study for the Red River Basin. *Remote Sensing, 8*(4), 279.

Stewart, D., Costa, C., Dwyer, L., Smith, D., Hamilton, R., & Ma, B. (2003). Canopy structure, light interception, and photosynthesis in maize. *Agronomy Journal, 95*(6), 1465-1474.

Taghvaeian, S., Chávez, J. L., Altenhofen, J., Trout, T., & DeJonge, K. (2013). Remote sensing for evaluating crop water stress at field scale using infrared thermography: potential and limitations. *Hydrology Days*, 73-83.

Tang, R., Li, Z.-L., Jia, Y., Li, C., Sun, X., Kustas, W. P., & Anderson, M. C. (2011). An intercomparison of three remote sensing-based energy balance models using Large Aperture Scintillometer measurements over a wheat–corn production region. *Remote Sensing of Environment, 115*(12), 3187-3202.

Tasumi, M. (2003). *Progress in operational estimation of regional evapotranspiration using satellite imagery*.

Tewolde, H., Sistani, K., Rowe, D., Adeli, A., & Tsegaye, T. (2005). Estimating cotton leaf area index nondestructively with a light sensor. *Agronomy Journal, 97*(4), 1158-1163.

Weiss, M., Baret, F., Smith, G., Jonckheere, I., & Coppin, P. (2004). Review of methods for in situ leaf area index (LAI) determination: Part II. Estimation of LAI, errors and sampling. *Agricultural and Forest Meteorology, 121*(1), 37-53.

Weiß, M., & Menzel, L. (2008). A global comparison of four potential evapotranspiration equations and their relevance to stream flow modelling in semi-arid environments. *Advances in Geosciences, 18*, 15-23.

Wilhelm, W., Ruwe, K., & Schlemmer, M. R. (2000). Comparison of three leaf area index meters in a corn canopy. *Crop Science, 40*(4), 1179-1183.

Zhang, H., Anderson, R. G., & Wang, D. (2015). Satellite-based crop coefficient and regional water use estimates for Hawaiian sugarcane. *Field Crops Research, 180*, 143-154.

Zia, S., Spohrer, K., Wenyong, D., Spreer, W., Romano, G., & Xiongkui, H. (2011). Monitoring physiological responses to water stress in two maize varieties by

infrared thermography. *International Journal of Agricultural and Biological Engineering, 4*(3), 7-15.

Zipper, S. C., & Loheide II, S. P. (2014). Using evapotranspiration to assess drought sensitivity on a subfield scale with HRMET, a high resolution surface energy balance model. *Agricultural and Forest Meteorology, 197*, 91-102.

CHAPTER 4: Comparison of Actual Evapotranspiration Estimated with Energy Balance and Vegetation Index Methods

4.1   Abstract

The estimation of actual crop evapotranspiration (ET_a) maps using complex equations and remotely sensed shortwave and thermal infrared imagery can be challenging and time consuming. Thus, there is a need to develop a simple and fast method to estimate ET_a maps using minimum input parameters for situations where limited input data is available or greater uncertainty in the resulting ET estimates are acceptable. We estimated ET_a using vegetation indices input parameters based on remote sensing techniques on maize fields during two growing seasons in eastern South Dakota, USA. Clear sky images from Landsat 7 and Landsat 8 were processed and used for the ET_a estimations. Two methods were used, namely 1) an energy balance method (EB method) utilizing Landsat imagery, weather data, a digital elevation map and a land cover map, and 2) a $K_{c\text{-NDVI}}$ method that use two input parameters: the Landsat image and weather data. Results showed that the ET_a values from the $K_{c\text{-NDVI}}$ method were lower than the ET_a values from the EB method by 18% for 2015 and 11% for 2016 growing seasons. During the period of study the accuracy of ET_a estimation decreased 17% with the $K_{c\text{-NDVI}}$ method. However, a strong relationship between the two methods during two seasons was found with r^2 of 0.97 and RMSE of 0.37 mm day^{-1}. Hence, the $K_{c\text{-NDVI}}$ method performed well for ET_a estimations during the two growing seasons, indicating that $K_{c\text{-NDVI}}$ method can be a robust and reliable method to estimate ET_a maps with minimum input parameters at focused regional and field scales for short time periods.

4.2   Introduction

The precise estimation of crop evapotranspiration (ET) plays an important role in irrigation water management such as in system planning and design, and irrigation scheduling (Garatuza-Payan & Watts, 2005). ET varies regionally and seasonally according to the weather data such as solar radiation, wind speed, air temperature, and air vapor pressure deficit and plant and soil conditions (R. G. Allen et al., 1998; George et al., 2002; Hanson, 1991).

In irrigated agriculture a widely used and recommended method for estimating crop water requirements or actual evapotranspiration (ET_a) is multiplying reference evapotranspiration (ET_r) with a crop coefficient (K_c) (R. G. Allen et al., 1998; ASCE-EWRI, 2005; Marvin Eli Jensen, Burman, & Allen, 1990) (Eq. 1).

$$ET_a = ET_r \times K_c \tag{1}$$

ET_r is estimated based on meteorological information from local weather stations, using the Penman-Monteith equation (R. G. Allen et al., 1998; ASCE-EWRI, 2005). The K_c is typically taken from literature values (R. G. Allen et al., 1998; 2005; Marvin E Jensen & Allen, 2016).

As an alternative to using K_c values from the literature, there are several methods for measuring ET directly to estimate K_c values over homogeneous surfaces. Methods include weighing lysimeter to measure water consumed through ET directly based on a mass balance, flux measurements using Bowen Ratio Energy Balance System (BREBS), Eddy Covariance technique (EC) or scintillometers that measure components of the surface energy balance to estimate crop ET (R. G. Allen et al., 2011; Gowda, Chavez, et al., 2008), or soil water balance methods. However, a limitation of these systems is that

they provide point or near point measurements that may not fully represent the ET from a larger population of fields other than where the measurement was conducted (Ayse Irmak et al., 2011; Santos et al., 2008). To overcome this problem of estimating ET from multiple fields, satellite-based remote sensing ET methods are becoming a popular methodology for estimating crop water use, providing ET estimates on a field-by-field basis at a regional scale (R. G. Allen, Tasumi, Morse, et al., 2007b; 2011a; J Kjaersgaard et al., 2011).

Several models have been developed to estimate actual evapotranspiration (ET_a) using remote sensing at different scales (Gowda, Chavez, et al., 2008). One of them is the Mapping EvapoTranspiration at High Resolution using Internalized Calibration (METRIC) Model (R. G. Allen, Tasumi, & Trezza, 2007a; 2011a; Tasumi et al., 2005). The METRIC model estimates ET as a residual of the surface energy balance equation (R. G. Allen, Tasumi, & Trezza, 2007) computed as:

$$LE = R_n - G - H \tag{2}$$

where LE is the latent heat flux (W m^{-2}) which are converted to ET (mm day^{-1}) using the latent heat of evaporation, R_n is the net radiation (W m^{-2}), G is the soil heat flux (W m^{-2}), and H is the sensible heat flux (W m^{-2}).

In the last decade the METRIC model has been used to estimate ET_a at field and regional scales in different crops including cotton (Chavez et al., 2007; French et al., 2015), wheat (Droogers et al., 2010; Santos et al., 2008), banana orchard (Folhes et al., 2009), soybean (Choi et al., 2009), corn (Ayse Irmak et al., 2011; Singh & Irmak, 2009), cover crops (Hankerson et al., 2012), alfalfa (Mkhwanazi & Chávez, 2012), pistacho (Mokhtari et al., 2013), vineyard (Carrasco-Benavides et al., 2014; Gordillo Salinas et al.,

2014), olive orchard (Paço et al., 2014), sugarcane (Zhang et al., 2015), and forest in the Amazon (Numata, Khand, Kjaersgaard, Cochrane, & Silva, 2017).

Use of remotely sensed vegetation indices such as the Normalized Difference Vegetation Index (NDVI), has been used to estimate K_c (Glenn et al., 2011; Rouse Jr et al., 1974) for ET_a estimation using Eq. 1. NDVI is a commonly used remote sensing product that provides an indication of the density and robustness of surface vegetation (Rafn, Contor, & Ames, 2008) and reflects the actual crop conditions (Garatuza-Payan & Watts, 2005; Glenn et al., 2011; Gontia & Tiwari, 2010). For well watered crops there is typically a linear relationship between NDVI and K_c. For more than 30 years local regression relationship between NDVI and K_c have been established for agricultural crops for ET_a estimations e.g., (Bausch, 1995; Campos, Neale, Calera, Balbontín, & González-Piqueras, 2010; Duchemin et al., 2006; Er-Raki, Rodriguez, Garatuza-Payan, Watts, & Chehbouni, 2013; Garatuza-Payan, Tamayo, Watts, & Rodríguez, 2003; Gontia & Tiwari, 2010; González-Dugo & Mateos, 2008; Hunsaker, Pinter Jr, Barnes, & Kimball, 2003; 2005; Jayanthi, Neale, & Wright, 2007; Neale et al., 1989; Pôças, Paço, Paredes, Cunha, & Pereira, 2015; Arturo Reyes-Gonzalez, Hay, Kjaersgaard, & Neale, 2015; 2016; Singh & Irmak, 2009; Tasumi et al., 2005; Trout, Johnson, & Gartung, 2008; Wright, 1982).

We used the two satellite-based approaches to estimate ET_a for irrigation applications namely 1) the energy balance method using METRIC and 2) the K_c vs NDVI method (R. G. Allen et al., 2011; Barbagallo, Consoli, & Russo, 2009; Neale et al., 2005; Yebra, Van Dijk, Leuning, Huete, & Guerschman, 2013). The energy balance method (EB method) is complex, computational involved and data intensive and require trained

personnel. In contrast, the K_c vs NDVI method, which will be referred to as $K_{c\text{-NDVI}}$ method henceforth is simpler, less data intensive and can be completed within a shorter timeframe, and at the same spatial resolution as the energy balance (R. G. Allen et al., 2011; Barbagallo et al., 2009; Morton et al., 2013; Rafn et al., 2008). The comparison between these methods for ET_a estimation has not been clearly determined in eastern South Dakota. The objective of this study was to compare the accuracy of $K_{c\text{-NDVI}}$ method to calculate ET_a compared to EB method calculated by the METRIC model over two growing seasons in eastern South Dakota.

4.3   Material and Methods

4.3.1   Study Area

The study was carried out in eastern South Dakota during the 2015 and 2016 growing seasons (Figure 1 (a)). The study area had an average latitude of 44° 19' N and longitude of 96° 46' W and elevation of 500 m above sea level. Five maize fields near to the Brookings weather station (< 15 km) in each growing season were used in the study (Figure 1 (c)). All fields were in a maize - soybean crop rotation system common to the region. The soils were silty clay loam with 0-2% slope (NRCS Web Soil Survey 2016). The maize was planted in late April and harvested in late October. The maize plant population density was around 78, 000 plants ha^{-1} and the fields were managed using common agricultural practices used in the region. The crop was not considered subjects to growth-limiting stress from pests, weed or nutrient deficiencies. The maize fields were around 64 hectares in size. Irrigation is uncommon in the study area and none of the study fields were irrigated. The normal average annual precipitation is 533 mm, of which

¾ typically falls during the growing season (April-October). The mean annual maximum temperature is 12.3 °C, minimum 0.3 °C, and mean 6.3 °C. The climate of the study area is classified as moist subhumid according to the Thornthwaite climate classification system (Keim, 2010).
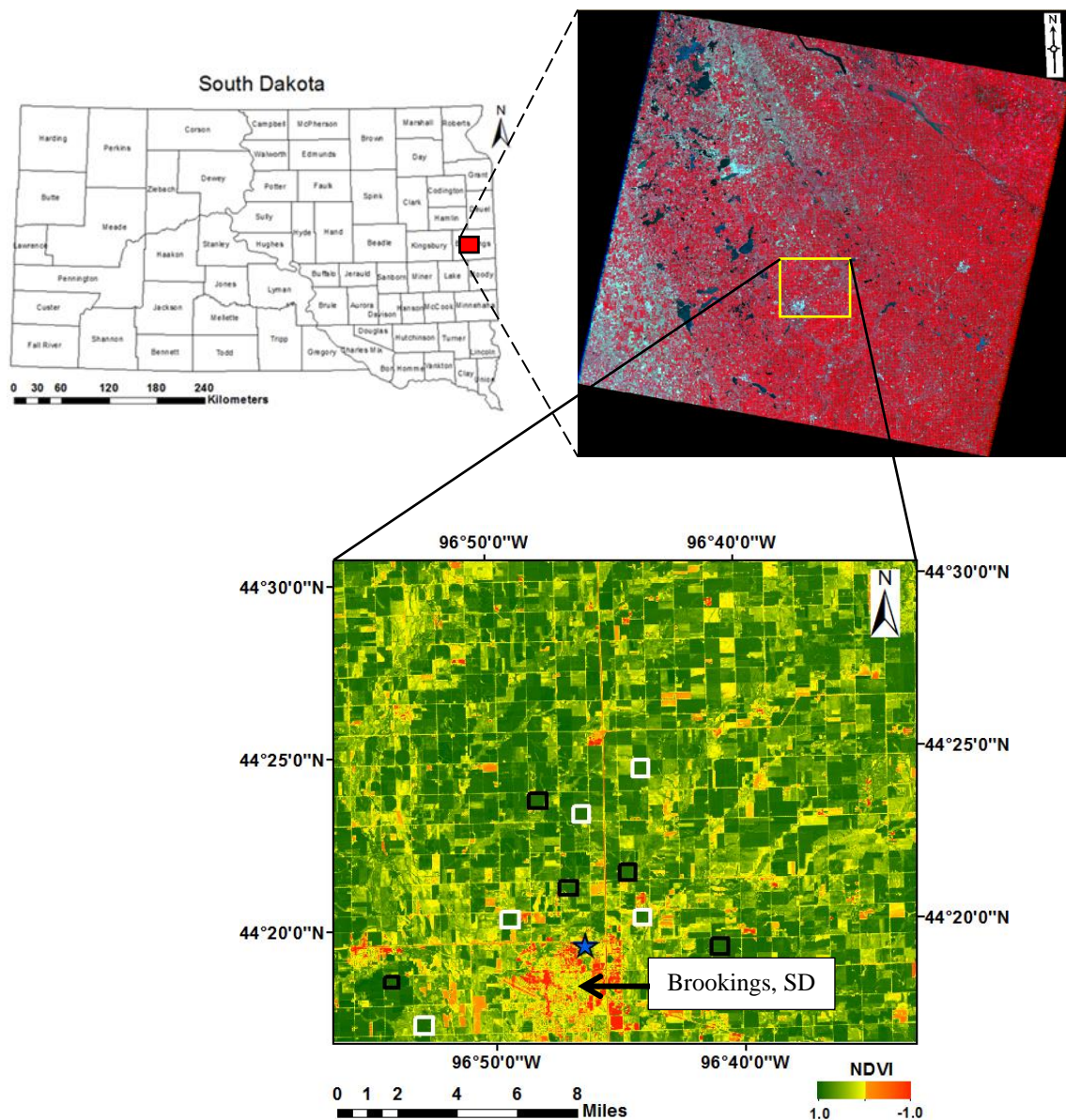
Figure 4.1 Map of South Dakota outline and counties with the red rectangle showing the study area (a). Landsat image shown with false color composite (bands 4, 3, 2) (path 29, row 29) with the yellow rectangle indicating the study area (b), and Landsat NDVI values map on July 18, 2015, the white and black rectangles indicating maize fields selected in 2015 and 2016, respectively and the blue star showing the weather station location (c).

4.3.2 Landsat Images

Clear sky images from Landsat 7 Enhanced Thematic Mapper Plus (ETM+) and Landsat 8 Operational Land Imager (OLI) and Thermal Infrared Sensor (TIRS) (Path 29, Row 29) were used for the ET_a estimations (Table 1). The images were downloaded from the United States Geological Survey (USGS) EROS Datacenter. The images were selected based on the temporal coverage and cloud-free conditions. Images with clouds present more than 10 km from the study area were considered acceptable for ET_a comparisons. The images were processed using the METRIC model running in the ERDAS Imagine software environment (J Kjaersgaard & Allen, 2010). Landsat 7 and 8 have a pixel resolution of 30 m by 30 m in the shortwave bands and 60 m by 60 m and 100 m by 100 m in the thermal band, respectively.

Table 4.1 The year, acquisition dates, Landsat satellite, path/row, image overpass time for the imagery used for the ET_a estimations.

Year	Acquisition Dates	Satellite	Path/Row	Overpass time (local)
2015	June 8	Landsat 7	29/29	11:10:58 AM
	July 10	Landsat 7	29/29	11:11:06 AM
	July 18	Landsat 8	29/29	11:10:57 AM
	August 3	Landsat 8	29/29	11:11:00 AM
	September 12	Landsat 7	29/29	11:11:18 AM
	September 20	Landsat 8	29/29	11:11:21 AM
2016	June 2	Landsat 8	29/29	11:11:03 AM
	June 26	Landsat 7	29/29	11:13:56 AM
	July 12	Landsat 7	29/29	11:13:55 AM
	July 20	Landsat 8	29/29	11:11:21 AM
	August 5	Landsat 8	29/29	11:11:24 AM
	August 21	Landsat 8	29/29	11:11:30 AM
	September 14	Landsat 7	29/29	11:14:05 AM

4.3.3 Pixel selection

During the study ten pixels for each field were selected and extracted from NDVI, K_c and ET_a maps. Those pixels were located within each maize field for each overpass date during two growing seasons. The same pixels were used throughout each growing season. The number of pixels (10) were assumed to be representative of the entire maize field.

4.3.4 METRIC Model and Input Parameters

METRIC model version 3.0 was used to estimate ET_a using the energy balance (EB) method. Please see (R. G. Allen, Tasumi, & Trezza, 2007a; 2011a; 2014) for a detailed discussion of the model calculations.

In the METRIC model four primary input parameters are used to estimate ET_a namely the Landsat image, digital elevation map, land cover map, and weather data (Figure 2). National elevation data (USGS NED N44 W097) and National land cover dataset (NLCD 2011_LC N42 W096) for the study area were downloaded from http://viewer.nationalmap.gov. The elevation data and land cover map were reprojected in meters to the same pixel size as the Landsat image (30 m x 30 m).

Hourly and daily weather observations (e.g. maximum and minimum air temperature, wind speed, relative humidity, solar radiation precipitation and ET_r) were taken from the automated agricultural weather station located by Brookings, South Dakota. All weather data were subjected to a rigorous quality control prior to be used in any calculations as suggested by R. G. Allen et al. (1998).

The ET$_r$ values were calculated using the Penman-Monteith (R. G. Allen et al., 1998; ASCE-EWRI, 2005)as follows:

$$ET_{ref} = \frac{0.408 \, \Delta (R_n - G) + \gamma \frac{C_n}{T+273} u_2 (e_s - e_a)}{\Delta + \gamma (1 + C_d u_2)} \tag{3}$$

where ET_{ref} is the alfalfa reference (mm day^{-1}), Δ is the slope pressure versus air temperature curve (kPa °C^{-1}), R_n is the net radiation at the crop surface (MJ m^{-2} day^{-1}), G is the soil heat flux at the soil surface (MJ m^{-2} day^{-1}), T is the mean air temperature at 1.5 to 2.5 m height (°C), u_2 is the mean daily wind speed at 2 m height (m s^{-1}), e_s is the saturation vapor pressure of the air (kPa), e_a is the actual vapor pressure of the air (kPa), γ is the psychrometric constant (0.0671 kPa °C^{-1}), $e_s - e_a$ is the vapor pressure deficit (kPa), C_n is the numerator constant (1600 K mm s^3 Mg^{-1} day^{-1}), C_d is the denominator constant (0.38 s m^{-1}) for alfalfa reference, and 0.408 is the coefficient constant (m^2 mm MJ^{-1}).

Figure 4.2 Examples of the input information needed for the ET_a estimation using METRIC, namely the Landsat image (a) here shown in false color, digital elevation map (b), land cover map (c), and weather data (d).

4.3.5 Flow chart of the METRIC model

A summary of the ET_a estimation with the METRIC model with the primary input parameters is showed in Figure 3.
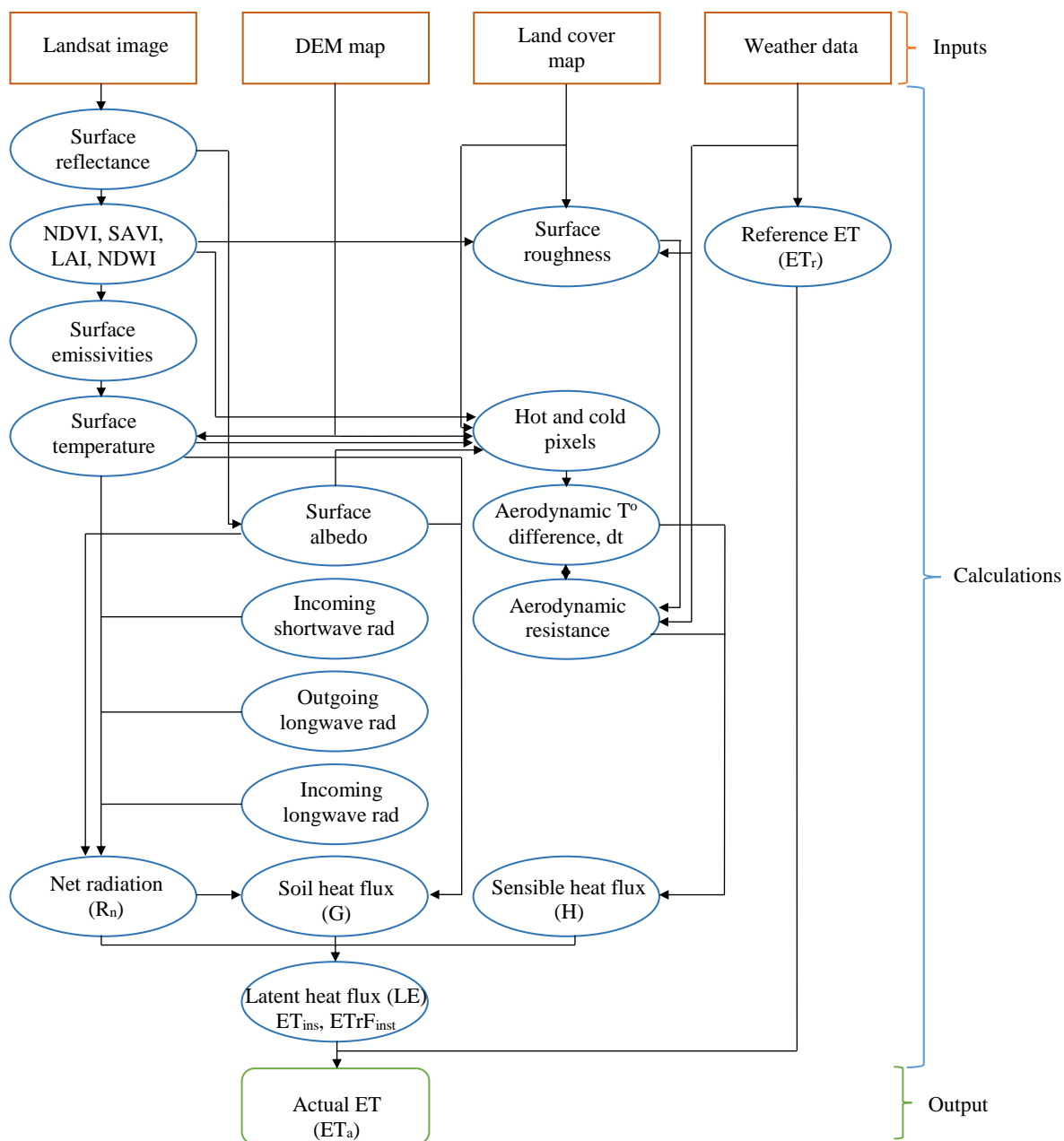
Figure 4.3 The flow chart of the METRIC using primary input parameters to estimate ET_a.

4.3.6 NDVI Calculations

The NDVI is defined as the difference between near-infrared (NIR) and red band reflectances divided by their sum (Rouse Jr et al., 1974). NDVI values range from -1.0 to

1.0, with water having negative values and dense vegetation having high positive values (Bannari, Morin, Bonn, & Huete, 1995; Bausch, 1993).

For Landsat 7 NDVI was calculated as:

$$NDVI = \frac{(NIR_{band\,4} - Red_{band\,3})}{(NIR_{band\,4} + Red_{band\,3})} \tag{4}$$

For Landsat 8 NDVI was calculated as:

$$NDVI = \frac{(NIR_{band\,5} - Red_{band\,4})}{(NIR_{band\,5} + Red_{band\,4})} \tag{5}$$

where NIR_{band} and Red_{band} are the corrected spectral radiance in the near-infrared and red bands, respectively.

4.3.7 Coefficient coefficients (K_c) curves for NDVI based method

The K_c values were calculated based on the alfalfa reference crop coefficient from ASCE Manual 70 (Appendix E) method (Marvin E Jensen & Allen, 2016) for 2015 and 2016 crop growing seasons. For K_c calculations this method divides the growing season into two periods, *viz.* percent of time from planting to effective cover and days after effective cover to harvest. The effective cover of maize for our study occurred in middle of July for 2015 and early July for 2016 based on field observations of the crop phenology.

4.3.8 Relationship between NDVI and K_c and K_c and ET_a maps

A relationship between NDVI derived from NDVI maps and K_c's values from ASCE Manual 70 (Appendix E) (Marvin E Jensen & Allen, 2016) corresponding to each overpass date was established. This relationship was used to develop a linear regression equation for both seasons. Those linear regression equations were used to generate K_c maps. The K_c values derived from the K_c maps were multiplied by ET_r to create ET_a

maps for both seasons using the K_{c-NDVI} method. Finally, the ET_a values from ET_a maps were compared with ET_a values obtained from the EB method for each overpass date and for each growing season.

4.3.9 Average ratio of ET_a K_{c-NDVI} to ET_a EB and their relationship

The average ratio of ET_a K_{c-NDVI} to ET_a EB was calculated to quantify the accuracy and performance of the K_{c-NDVI} method for ET_a estimations. A linear relationship between ET_a K_{c-NDVI} values and ET_a EB values was established for the 2015 and 2016 growing seasons.

4.3.10 Flow chart of ERDAS Imagine software (model maker)

A summary of ET_a estimation with ERDAS Imagine software using K_{c-NDVI} method with two input parameters is presented in Figure 4.4.
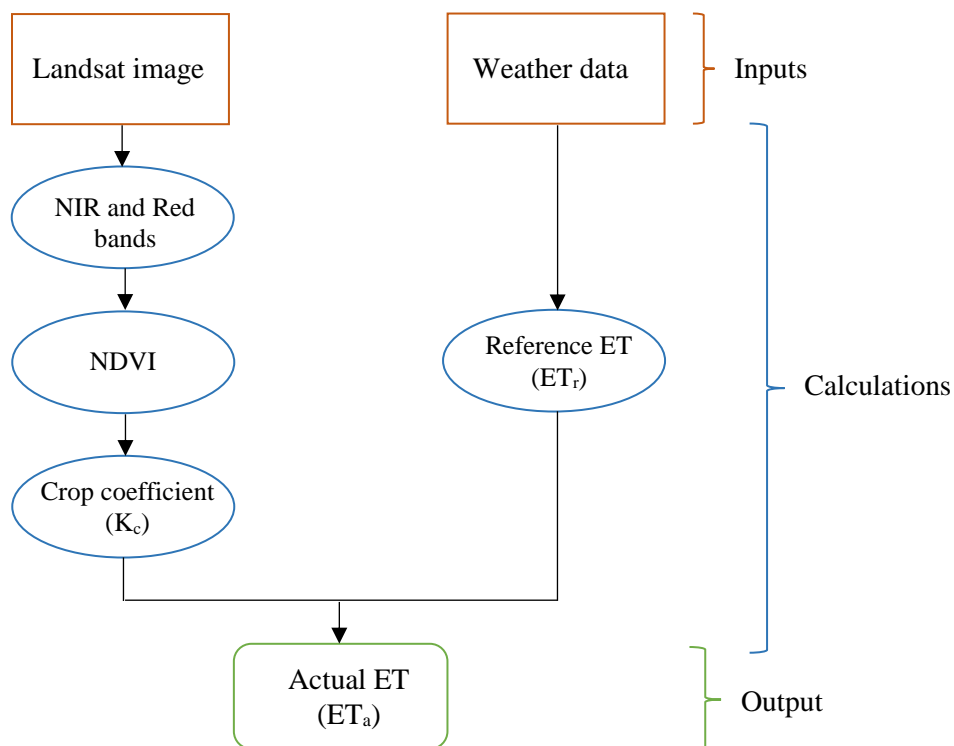
Figure 4.4 The flow chart of ERDAS Imagine software (model maker) using $K_{c\text{-NDVI}}$ method for ET_a estimation.

4.4   Results and discussion

4.4.1   Mean Temperature and Precipitation

The minimum daily mean temperature during the growing season was 2.12 °C for 2015 and 4.69 °C for 2016 both recorded during May and the maximum daily mean temperature were 26.34 and 27.91 °C for 2015 and for 2016, respectively, both recorded on July (Figure 5).

The total precipitation during the crop growing season for 2015 was 460 mm and for 2016 was 483 mm. The major precipitation events for 2015 occurred in the reproductive stages (R1, R2, and R3) July 25, August 6, and 18 respectively (Figure 4.5

(2015)), while in 2016 occurred in development stage (vegetation stage (V5) (June, 17) and tassel (VT) (July 10) (Figure 4.5 (2016)).
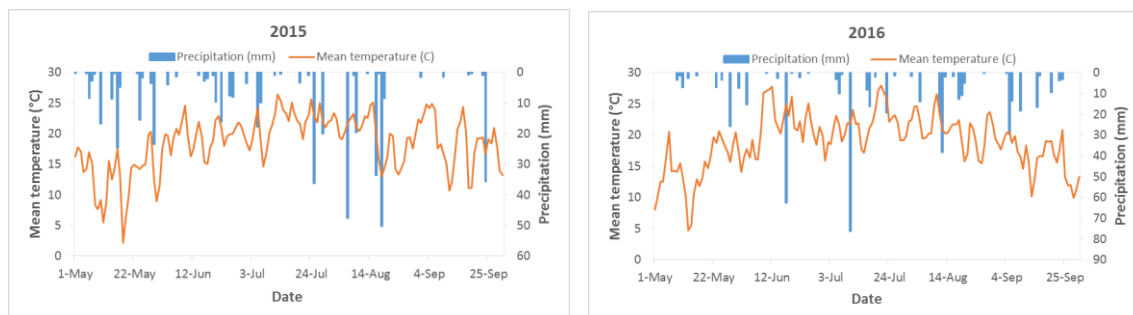
Figure 4.5 Mean daily temperature and precipitation data observed at the Brookings automated weather station for the 2015 and 2016 growing seasons.

4.4.2   NDVI generated with ERDAS Imagine software using K$_{c-NDVI}$ method

Figure 4.6 shows the seasonal evolution of NDVI of ten average selected pixels in each maize field and average K$_c$ for two growing seasons. In both seasons the NDVI values were very similar. For both years, NDVI increased from initial stage (±0.3) (V3) (June 4) to full cover (±0.83) (VT) (July 12), reached its maximum values and it remains constant over plateau characterizing the mid-season stage (VT through R3) and then slightly decrease at the end of the season (±0.65) (R6) (September 14). The maximum NDVI values reported in this study were similar to reported by Tasumi et al. (2005) and Singh and Irmak (2009) in rainfed corn, however highest NDVI values were reported by Kamble, Kilic, and Hubbard (2013) (0.89) and DeJonge, Mefford, and Chávez (2016) (0.91) in irrigated corn. Irrigation systems often have higher wetting frequencies than rainfed system, resulting in higher NDVI values (R. G. Allen, Tasumi, et al., 2005). Therefore, maximum NDVI values in irrigated corn were greater than NDVI values in rainfed corn.

Similar temporal evolution of NDVI of maize were reported by Neale et al.

(1989), Jackson et al. (2004), P.-Y. Chen, Fedosejevs, Tiscareno-Lopez, and Arnold

(2006), Thomason, Phillips, and Raymond (2007), de Souza, Mercante, Johann,

Lamparelli, and Uribe-Opazo (2015) and F. Gao et al. (2017). All these researchers found

low NDVI values (0.2) at the initial stage, maximum values (0.8) at mid-season stage and

medium values (0.6) at the end of season. In addition, in northern México A. Reyes-

Gonzalez, U., J.G., and Reta-Sánchez (2012) found similar evolution of NDVI values

estimated with remote sensing for forage corn during two years (unpublished). On the

other hand, Bausch (1993) and González-Dugo and Mateos (2008) reported that NDVI is

sensitive to soil background before full cover and leaf senescence at the end of growing

season. They made ground radiometric measurements of NDVI in agricultural crops

including corn.
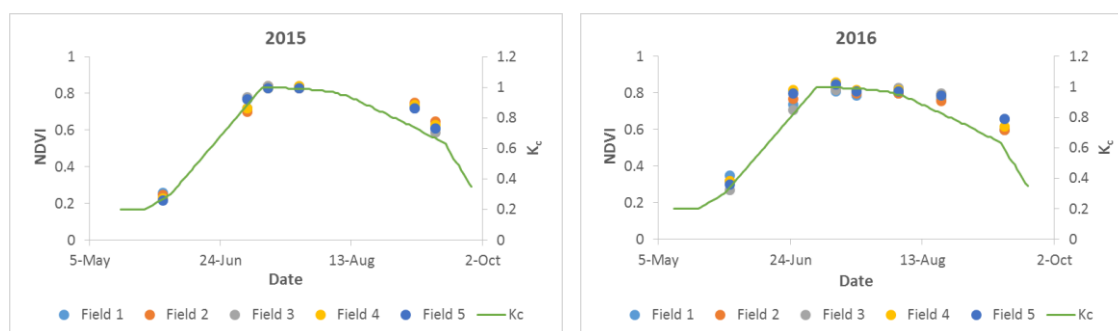
Figure 4.6 Temporal progression of NDVI and K_c curves at five maize fields for 2015 and 2016 growing seasons.

4.4.3   Relationship between NDVI and K_c

Linear relationships between NDVI and K_c values over six and seven satellite

overpass dates for 2015 and for 2016 respectively are shown in Figure 4.7. A strong

relationship between NDVI and K_c values was showed with coefficient of determination

(r^2) values of 0.96 for 2015 and 0.93 for 2016 (Figure 4.7), which indicate that NDVI is a robust indicator of crop coefficients values. Higher coefficient of determination values in corn were reported by Rocha, Perdigão, Melo, and Henriques (2012) and Arturo Reyes-Gonzalez et al. (2015), they reported r^2 values of 0.99 and 0.97, respectively, however lower values of r^2 were found by Singh and Irmak (2009) (0.83) and Kamble et al. (2013) (0.81) in Nebraska, USA.

The NDVI computed from Landsat images and K_c's obtained from ASCE manual 70 (Appendix E) were used to develop the linear regression equations. The relationship between NDVI and K_c for 2015 and for 2016 growing seasons were found as the following linear equations:

$$K_c = 1.1887 \, \text{NDVI} - 0.033 \qquad (2015) \tag{6}$$

$$K_c = 1.2508 \, \text{NDVI} - 0.093 \qquad (2016) \tag{7}$$

Several researchers have shown linear relationships for NDVI not only with K_c values but also with canopy ground cover e.g., (DeJonge et al., 2016; Er-Raki et al., 2013; Glenn et al., 2011; Zhang et al., 2015), corn dry weight (Hong, Schepers, Francis, & Schlemmer, 2007), corn grain yield (Thomason et al., 2007), and leaf area index (LAI) (Colombo et al., 2003; Duchemin et al., 2006; Nguy-Robertson et al., 2012; Paz-Pellat et al., 2007). Strong relationships ($r^2 = \pm 0.95$) were observed with canopy ground cover and LAI, while good relationship ($r^2 = \pm 0.80$) were observed with corn dry weight, and corn grain yield.
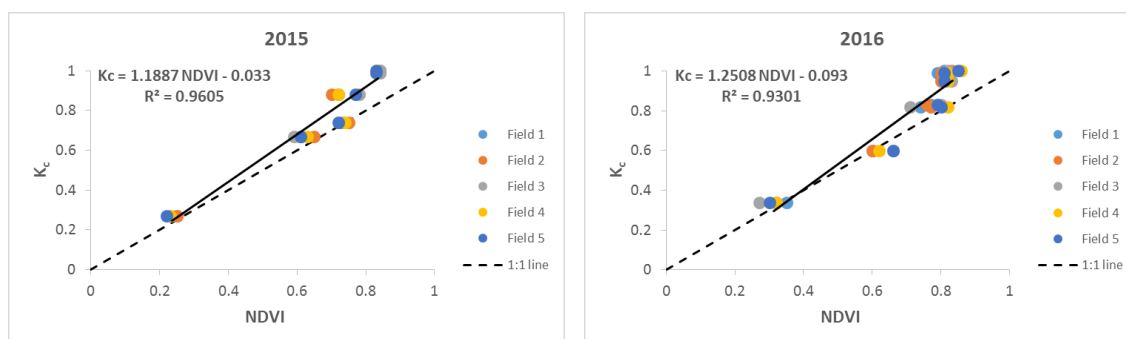
Figure 4.7 Linear correlation between NDVI and K_c of five maize fields during 2015 and 2016 growing seasons in eastern South Dakota. The black dashed line indicates 1:1 line.

4.4.4 K_c maps developed with ERDAS Imagine software using $K_{c\text{-NDVI}}$ method and K_c values throughout the growing seasons.

Based on the regressions developed in equations 6 and 7 and maps of NDVI from Landsat imagery, spatial maps of K_c was developed. Figure 4.8 shows an example of the spatial and temporal evolution of K_c of maize fields during the 2015 growing season. The lower K_c values are presented in early season (June 8) (light green color) and then gradually increased until mid-season, where the K_c values remains constant (July 18 - August 3) (dark blue color) and finally decreased at the end of the season (September 20) (light green color), indicating the crop maturity.

Similar spatial and temporal K_c maps derived from a vegetation index has been reported by different agricultural crops around the world. For example, Neale et al. (2005) developed K_c maps for potato in Idaho, USA, Garatuza-Payan and Watts (2005) developed K_c for wheat in Northwest México, Singh and Irmak (2009) developed K_c maps for corn, soybean, sorghum, and alfalfa in Nebraska, USA, Gontia and Tiwari (2010) developed K_c for wheat in West Bengal, India, Rocha et al. (2012) developed K_c maps for corn in Caia, Portugal, Vanino et al. (2015) developed K_c maps for vineyard in

Apulia, Italy, El-Shirbeny, Ali, Badr, and Bauomy (2014) developed K_c maps for wheat

in El-Kassaseen Egypt, Zhang et al. (2015) developed K_c maps for sugarcane in Maui,

Hawaii, and Reyes-González et al. (2016) developed K_c maps for silage corn in northern

México.

      Average K_c values derived from ten pixels for each satellite overpass date during

the 2015 and 2016 growing seasons are shown in Table 4.2. In both seasons the K_c values

increased from initial stage (0.27) to mid-season stage (0.95) reached their full canopy

cover and transpired water at potential rates and then decreased at the end of the growing

season (0.7). During the development stage (July 10 for 2015 and June 26 for 2016) and

late season (September 20 for 2015 and September 14 for 2016) crop presented more

variability in K_c, this probably due to variation in management practice, different soil

moisture content and different maize hybrids maturity or simply K_c values varied due to

soil background and vegetation senescence as reported by Bausch (1993), González-

Dugo and Mateos (2008), and Martha C. Anderson et al. (2012).
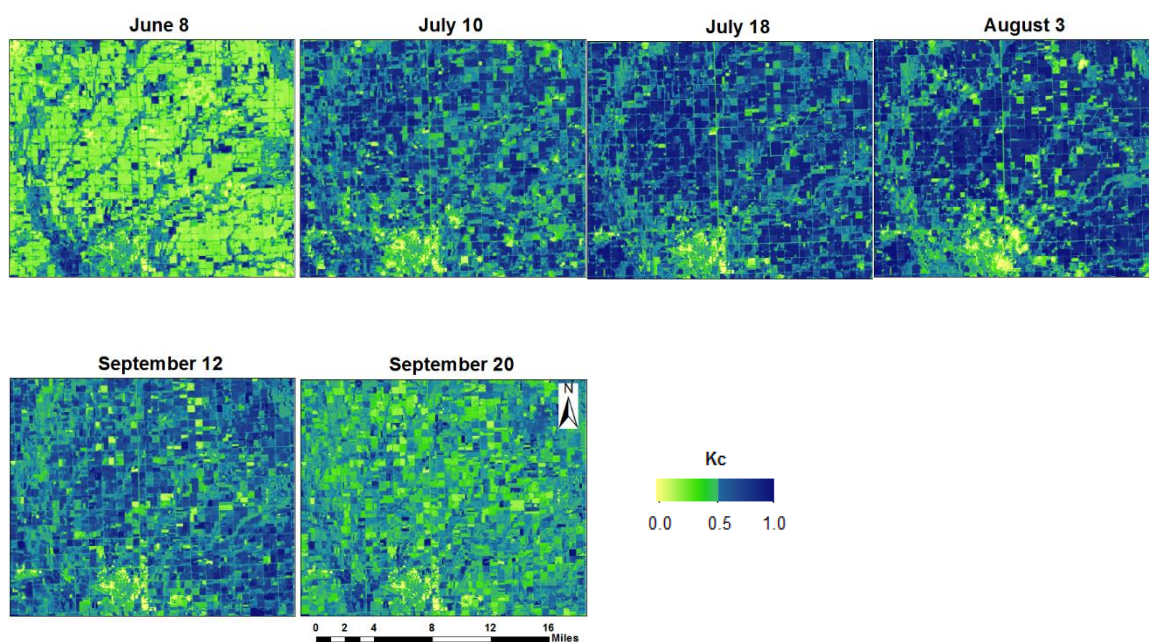
Figure 4.8 Spatial and temporal K_c maps generated using the ERDAS Imagine software (model maker) and ArcGIS version 10.3.1 for the 2015 growing season.

Table 4.2 Average K_c values derived from ten pixels for five maize fields in each overpass date throughout the 2015 and 2016 growing seasons.

	2015					
	K_c					
Corn field	Jun 8	Jul 10	Jul 18	Aug 3	Sep 12	Sep 20
Field 1	0.27	0.88	0.98	0.96	0.84	0.69
Field 2	0.27	0.82	0.97	0.96	0.85	0.74
Field 3	0.24	0.90	0.97	0.97	0.83	0.67
Field 4	0.24	0.83	0.96	0.95	0.84	0.70
Field 5	0.23	0.89	0.96	0.96	0.82	0.69

	2016						
	K_c						
Corn field	Jun 2	Jun 26	Jul 12	Jul 20	Aug 5	Aug 21	Sep
Field 1	0.32	0.87	0.95	0.94	0.92	0.86	0.61
Field 2	0.28	0.90	0.96	0.94	0.94	0.90	0.62
Field 3	0.26	0.84	0.94	0.95	0.96	0.90	0.71
Field 4	0.31	0.94	0.98	0.95	0.94	0.89	0.69
Field 5	0.27	0.90	0.97	0.94	0.92	0.89	0.73

4.4.5 ET$_a$ maps and Daily Spatial distribution of ET$_a$ Comparison

The METRIC model was used to estimate daily ET$_a$ maps using all input parameters (EB method) and ERDAS Imagine software (model maker) was used to estimate daily ET$_a$ maps using only two input parameters (K$_{c\text{-NDVI}}$ method) for ET$_a$ comparisons of both growing seasons. Figure 4.9 shows an example of ET$_a$ maps developed by EB method and developed by K$_{c\text{-NDVI}}$ method on July 20, 2016. The ET$_a$ K$_{c\text{-NDVI}}$ method map shows more dark blue color than in ET$_a$ EB method, this is due to mainly to pixel resolution between these methods. The pixel resolution in the ET$_a$ K$_{c\text{-NDVI}}$ method is 30 by 30 m, while in ET$_a$ EB method the thermal pixel resolution for Landsat 7 is 60 by 60 m and for Landsat 8 is 100 by 100 m. Thus, this visual difference is because the ET$_a$ EB method was affected by the thermal band at 100 m for Landsat 8.
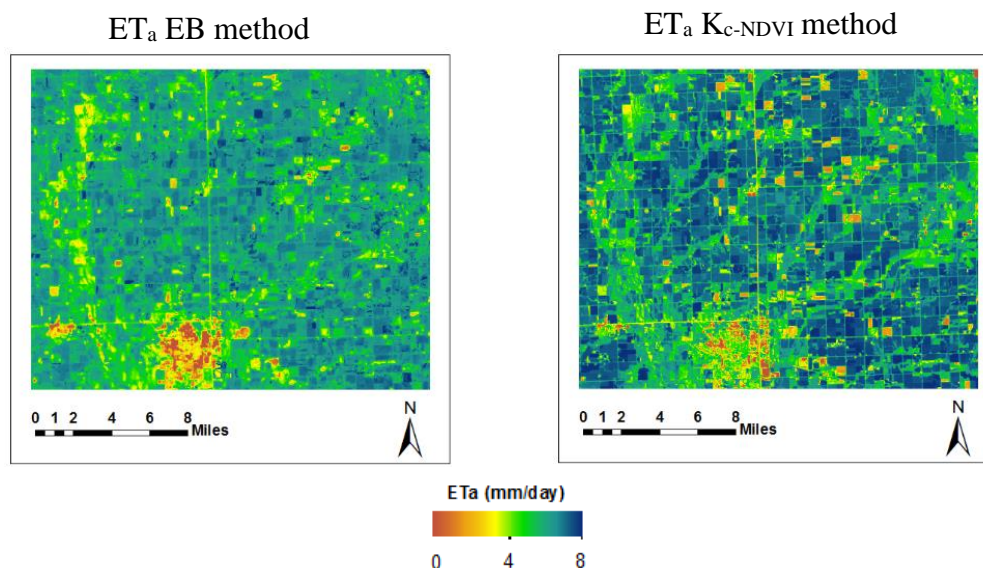
Figure 4.9 ET$_a$ maps generated using EB method and using K$_{c\text{-NDVI}}$ method on July 20, 2016.

Similar comparison of ET_a maps over agricultural areas generated by the METRIC model using energy balance and using vegetation index data were reported by R. Allen, A. Irmak, R. Trezza, J. M. H. Hendrickx, et al. (2011) and Martha C. Anderson et al. (2012) in Twin Falls, Idaho. Mokhtari et al. (2013), found that the METRIC-based ET is highly sensitive to surface temperature, but less sensitive to NDVI.

For the 2015 season, Figure 4.10 shows that the ET_a values were lower at the beginning and at the end of the season for EB method was around 4.2 mm day^{-1} and for K_{c-NDVI} method was around 3.0 mm day^{-1}, indicating that less water is transpired by the crop. However, the highest ET_a values were showed in the mid-season (July 18) 7.93 and 7.68 mm day^{-1} for EB method and K_{c-NDVI} method, respectively.

For the 2016 season, Figure 4.10 shows that the low ET_a values were observed at the beginning of the growing season 2.78 and 1.72 mm day^{-1} for EB method and for K_{c-NDVI} method, respectively. Moderate ET_a values were presented at the end of the season for EB method was 4.23 mm day^{-1} and for K_{c-NDVI} method was 3.04 mm day^{-1}. High ET_a values were observed in the mid-season (July 12) with 8.87 mm day^{-1} for EB method and 8.66 mm day^{-1} for K_{c-NDVI} method.

In general, the ET_a values estimated with EB method were higher than the ET_a values estimated with K_{c-NDVI} method by 18 and 11% for 2015 and 2016 growing seasons, respectively. Because the K_{c-NDVI} method overwhelmingly considers transpiration from green vegetation, and only to a small extent evaporation from bare soil, some underestimation during the shoulder periods of the growing season is common. These results coincides with those in previous studies reported by Martha C. Anderson et

al. (2012), they reported that ET_a calculated from vegetation index data only underestimate seasonal ET_a values in irrigated area in Idaho.
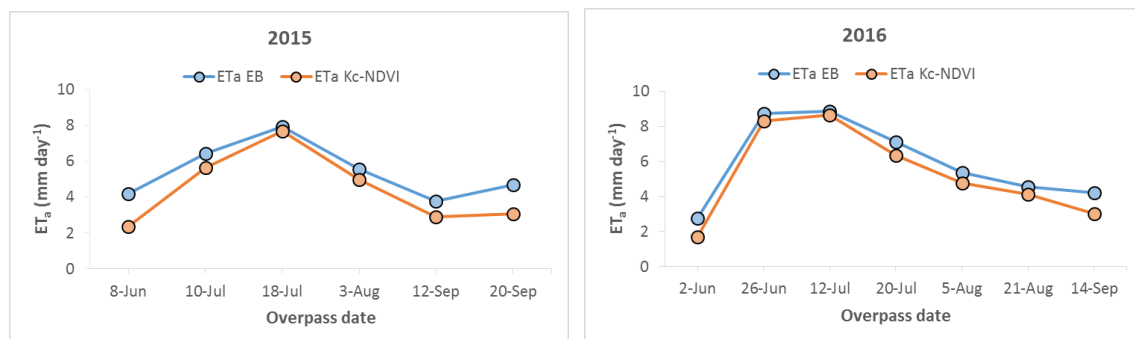
Figure 4.10 ET_a EB and ET_a K_{c-NDVI} values comparisons throughout the 2015 and 2016 growing seasons.

4.4.6   Average ratio of ET_a K_{c-NDVI} method to ET_a EB method

The average ratio distribution of ET_a K_{c-NDVI} to ET_a EB method for 2015 and 2016 corn growing seasons are showed in Figure 4.11. This figure shows that all average ratios are below 1, which is denoted by the thick blue line. This means that the K_{c-NDVI} method underestimated the ET_a EB values during the two growing seasons. In early and late season the K_{c-NDVI} method showed the far values from 1, while in the mid-season the values were close to 1. Indicating that K_{c-NDVI} is more accurate for ET_a estimations during the mid-season than early and late seasons, this probably due to in the early and late seasons the crop had low vegetation cover, high soil evaporation, and leaf senescence (R. Allen, A. Irmak, R. Trezza, J. M. H. Hendrickx, et al., 2011; Martha C. Anderson et al., 2012; González-Dugo & Mateos, 2008; Tasumi et al., 2005). Therefore, K_{c-NDVI} method give less accurate estimation of ET_a during early and late season periods, but for irrigation scheduling purposes, where the crop water demand is highest during the middle of the growing season, the K_{c-NDVI} method may be acceptable. However, ET_a values from

K$_{c\text{-NDVI}}$ method need to be adjusted during early and during late season to get close or accurate estimates to ET$_a$ EB values. The adjustment factor (ET$_a$ K$_{c\text{-NDVI}}$ / 0.66 = ET$_a$ EB) for 2015 growing season was 0.66 and adjustment factor (ET$_a$ K$_{c\text{-NDVI}}$ / 0.71 = ET$_a$ EB) for 2016 growing season was 0.71.

For entire 2015 growing season the percent of error or underestimation was 21 and for the mid-season only (excluding early and late seasons) was 12%, while for entire 2016 growing season the percent of error was 13 and for mid-season was 7%. The total average percent of error for two growing seasons was 17%. This general percent of underestimation with the K$_{c\text{-NDVI}}$ method is satisfactory compared with error for an experienced expert reported by R. G. Allen et al. (2011b), who reported error of 10-30% with remote sensing using vegetation indices. However, the average error for both growing seasons during the mid-season stage was less than 10%.
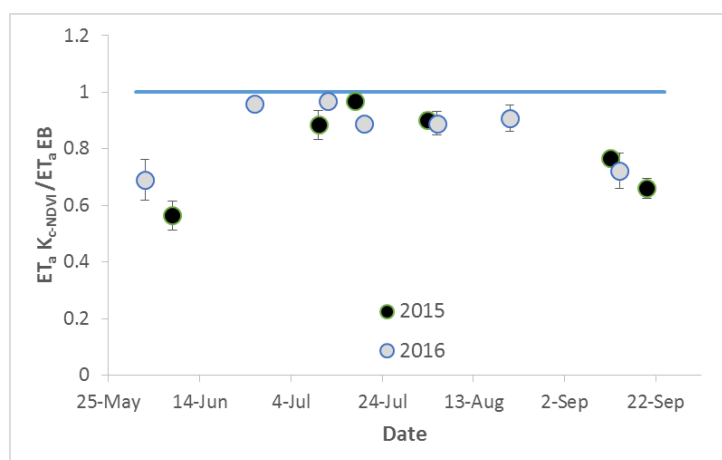
Figure 4.11 Average ratio of ET$_a$ K$_{c\text{-NDVI}}$ to ET$_a$ EB for 2015 and 2016 growing seasons. The thick blue line denotes 1 or 100% accuracy with ET$_a$ EB method. Bars in time series indicates standard deviation of ET$_a$ values.

4.4.7 Relationship between ET_a EB method and ET_a $K_{c\text{-NDVI}}$ method

A strong relationship was found between ET_a EB method and ET_a $K_{c\text{-NDVI}}$ method during the period of study (2015 and 2016 seasons) with r^2 of 0.97 (Figure 4.12). The corresponding mean bias error (MBE) (0.81 mm day^{-1}) and root mean square error (RMSE) (0.37 mm day^{-1}) were acceptable, assuming an average daily ET_a of 5.3 mm day^{-1}.

In this study, the $K_{c\text{-NDVI}}$ method performed well for ET_a estimations during the two growing seasons, indicating that $K_{c\text{-NDVI}}$ method can be a robust and reliable method to estimate crop water requirements at regional and field scale in regions where digital elevation, land cover map and thermal infrared data are not available for ET estimations.
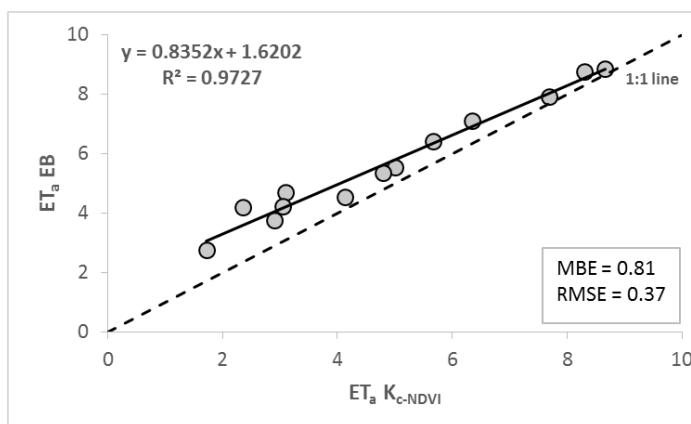
Figure 4.12 Relationship between ET_a EB method and ET_a $K_{c\text{-NDVI}}$ for maize fields during two growing seasons in eastern South Dakota. The black dashed line indicates the 1:1 line.

4.5 Conclusions

The linear relationships between NDVI derived from NDVI maps and K_c obtained based on literature values (ASCE manual 70) were $K_c = 1.1887 \, \text{NDVI} - 0.033$ for 2015

and $K_c = 1.2508$ NDVI $- 0.093$for 2016. These linear equations were used to generate

K_c maps. The K_c values derived from the K_c maps were multiplied by ET_r to estimate ET_a

values during two growing seasons using the $K_{c\text{-NDVI}}$ method. The METRIC model was

used to estimate ET_a using the full suite of input parameters (Landsat image, weather

data, digital elevation map, and land cover map) (EB method).

Results showed that the ET_a values estimated with $K_{c\text{-NDVI}}$ method were lower than

the ET_a values estimated with EB method by 18% for 2015 and 11% for 2016 growing

season. The ET_a $K_{c\text{-NDVI}}$ values were less than the ET_a EB values during the two seasons

especially early and late in the growing seasons when the vegetation cover is incomplete

and soil evaporation is not fully captured by the $K_{c\text{-NDVI}}$ method. As a result, the accuracy

of ET_a estimation with the $K_{c\text{-NDVI}}$ method decreased 17% compared with EB method

during the period of study (2015 and 2016 growing seasons). Finally, $K_{c\text{-NDVI}}$ method

give less accurate estimation of ET_a during early and late seasons, but for irrigation

scheduling purposes, where the crop water demand is highest during the middle of the

growing season, the $K_{c\text{-NDVI}}$ method may be acceptable. Nevertheless, ET_a values from

$K_{c\text{-NDVI}}$ method need to be adjusted during early and late seasons to get close or accurate

estimates to ET_a EB values.

The results of this study showed a strong relationship between the $K_{c\text{-NDVI}}$ method

and the EB method throughout two growing seasons with r^2 of 0.97 and RMSE of

0.37mm day^{-1}. In conclusion, the $K_{c\text{-NDVI}}$ method performed well for ET_a estimations

during two seasons, indicating that this method can be a robust and reliable method to

estimate ET_a with minimum input parameters at regional and field scales for short time

periods.

4.6   References

Allen, R., Irmak, A., Trezza, R., Hendrickx, J. M. H., Bastiaanssen, W., & Kjaersgaard, J. (2011a). Satellite-based ET estimation in agriculture using SEBAL and METRIC. *Hydrological Processes, 25*(26), 4011-4027. doi:10.1002/hyp.8408

Allen, R. G., Pereira, L. S., Howell, T. A., & Jensen, M. E. (2011b). Evapotranspiration information reporting: I. Factors governing measurement accuracy. *Agricultural Water Management, 98*(6), 899-920.

Allen, R. G., Pereira, L. S., Raes, D., & Smith, M. (1998). Crop evapotranspiration-Guidelines for computing crop water requirements-FAO Irrigation and drainage paper 56. *FAO, Rome, 300*(9), D05109.

Allen, R. G., Tasumi, M., Morse, A., & Trezza, R. (2005). A Landsat-based energy balance and evapotranspiration model in Western US water rights regulation and planning. *Irrigation and Drainage Systems, 19*(3), 251-268.

Allen, R. G., Tasumi, M., Morse, A., Trezza, R., Wright, J. L., Bastiaanssen, W., . . . Robison, C. W. (2007b). Satellite-based energy balance for mapping evapotranspiration with internalized calibration (METRIC)—Applications. *Journal of Irrigation and Drainage Engineering, 133*(4), 395-406.

Allen, R. G., Tasumi, M., & Trezza, R. (2007a). Satellite-based energy balance for mapping evapotranspiration with internalized calibration (METRIC)—Model. *Journal of Irrigation and Drainage Engineering, 133*(4), 380-394.

Anderson, M. C., Allen, R. G., Morse, A., & Kustas, W. P. (2012). Use of Landsat thermal imagery in monitoring evapotranspiration and managing water resources. *Remote*

Sensing of Environment, 122, 50-65. doi:http://dx.doi.org/10.1016/j.rse.2011.08.025

ASCE-EWRI. (2005). *The ASCE standardized reference evapotranspiration equation; ASCE-EWRI Standardization of Reference Evapotranspiration Task Committee Report; ASCE: Reston, VA, USA*.

Bannari, A., Morin, D., Bonn, F., & Huete, A. (1995). A review of vegetation indices. *Remote sensing reviews, 13*(1-2), 95-120.

Barbagallo, S., Consoli, S., & Russo, A. (2009). A one-layer satellite surface energy balance for estimating evapotranspiration rates and crop water stress indexes. *Sensors, 9*(1), 1-21.

Bausch, W. C. (1993). Soil background effects on reflectance-based crop coefficients for corn. *Remote Sensing of Environment, 46*(2), 213-222.

Bausch, W. C. (1995). Remote sensing of crop coefficients for improving the irrigation scheduling of corn. *Agricultural Water Management, 27*(1), 55-68.

Campos, I., Neale, C. M., Calera, A., Balbontín, C., & González-Piqueras, J. (2010). Assessing satellite-based basal crop coefficients for irrigated grapes (Vitis vinifera L.). *Agricultural Water Management, 98*(1), 45-54.

Carrasco-Benavides, M., Ortega-Farías, S., Lagos, L. O., Kleissl, J., Morales-Salinas, L., & Kilic, A. (2014). Parameterization of the Satellite-Based Model (METRIC) for the estimation of instantaneous surface energy balance components over a drip-irrigated vineyard. *Remote Sensing, 6*(11), 11342-11371.

Chavez, J. L., Gowda, P. H., Howell, T. A., Marek, T. H., & New, L. L. (2007). *Evapotranspiration mapping using METRICTM for a region with highly advective*

conditions. Paper presented at the 2007 ASABE Annual International Meeting, Technical Papers.

Chen, P.-Y., Fedosejevs, G., Tiscareno-Lopez, M., & Arnold, J. G. (2006). Assessment of MODIS-EVI, MODIS-NDVI and VEGETATION-NDVI composite data using agricultural measurements: an example at corn fields in western Mexico. *Environmental monitoring and assessment, 119*(1-3), 69-82.

Choi, M., Kustas, W. P., Anderson, M. C., Allen, R. G., Li, F., & Kjaersgaard, J. H. (2009). An intercomparison of three remote sensing-based surface energy balance algorithms over a corn and soybean production region (Iowa, US) during SMACEX. *Agricultural and Forest Meteorology, 149*(12), 2082-2097.

Colombo, R., Bellingeri, D., Fasolini, D., & Marino, C. M. (2003). Retrieval of leaf area index in different vegetation types using high resolution satellite data. *Remote Sensing of Environment, 86*(1), 120-131.

de Souza, C. H. W., Mercante, E., Johann, J. A., Lamparelli, R. A. C., & Uribe-Opazo, M. A. (2015). Mapping and discrimination of soya bean and corn crops using spectro-temporal profiles of vegetation indices. *International journal of remote sensing, 36*(7), 1809-1824.

DeJonge, K. C., Mefford, B. S., & Chávez, J. L. (2016). Assessing corn water stress using spectral reflectance. *International journal of remote sensing, 37*(10), 2294-2312.

Droogers, P., Immerzeel, W., & Lorite, I. (2010). Estimating actual irrigation application by remotely sensed evapotranspiration observations. *Agricultural Water Management, 97*(9), 1351-1359.

Duchemin, B., Hadria, R., Erraki, S., Boulet, G., Maisongrande, P., Chehbouni, A., . . . Kharrou, M. (2006). Monitoring wheat phenology and irrigation in Central Morocco: On the use of relationships between evapotranspiration, crops coefficients, leaf area index and remotely-sensed vegetation indices. *Agricultural Water Management, 79*(1), 1-27.

El-Shirbeny, M. A., Ali, A., Badr, M. A., & Bauomy, E. M. (2014). Assessment of wheat crop coefficient using remote sensing techniques. *World Research Journal of Agricultural Sciences, 1*(2), 12-17.

Er-Raki, S., Rodriguez, J., Garatuza-Payan, J., Watts, C., & Chehbouni, A. (2013). Determination of crop evapotranspiration of table grapes in a semi-arid region of Northwest Mexico using multi-spectral vegetation index. *Agricultural Water Management, 122*, 12-19.

Folhes, M. T., Rennó, C. D., & Soares, J. V. (2009). Remote sensing for irrigation water management in the semi-arid Northeast of Brazil. *Agricultural Water Management, 96*(10), 1398-1408.

French, A. N., Hunsaker, D. J., & Thorp, K. R. (2015). Remote sensing of evapotranspiration over cotton using the TSEB and METRIC energy balance models. *Remote Sensing of Environment, 158*, 281-294.

Gao, F., Anderson, M. C., Zhang, X., Yang, Z., Alfieri, J. G., Kustas, W. P., . . . Prueger, J. H. (2017). Toward mapping crop progress at field scales through fusion of Landsat and MODIS imagery. *Remote Sensing of Environment, 188*, 9-25.

Garatuza-Payan, J., Tamayo, A., Watts, C., & Rodríguez, J. C. (2003). *Estimating large area wheat evapotranspiration from remote sensing data.* Paper presented at the

Geoscience and Remote Sensing Symposium, 2003. IGARSS'03. Proceedings. 2003 IEEE International.

Garatuza-Payan, J., & Watts, C. J. (2005). The use of remote sensing for estimating ET of irrigated wheat and cotton in Northwest Mexico. *Irrigation and Drainage Systems, 19*(3), 301. doi:10.1007/s10795-005-5192-2

George, B. A., Reddy, B., Raghuwanshi, N., & Wallender, W. (2002). Decision support system for estimating reference evapotranspiration. *Journal of Irrigation and Drainage Engineering, 128*(1), 1-10.

Glenn, E. P., Neale, C. M., Hunsaker, D. J., & Nagler, P. L. (2011). Vegetation index-based crop coefficients to estimate evapotranspiration by remote sensing in agricultural and natural ecosystems. *Hydrological Processes, 25*(26), 4050-4062.

Gontia, N. K., & Tiwari, K. N. (2010). Estimation of crop coefficient and evapotranspiration of wheat (Triticum aestivum) in an irrigation command using remote sensing and GIS. *Water resources management, 24*(7), 1399-1414.

González-Dugo, M., & Mateos, L. (2008). Spectral vegetation indices for benchmarking water productivity of irrigated cotton and sugarbeet crops. *Agricultural Water Management, 95*(1), 48-58.

Gordillo Salinas, V. M., Flores Magdaleno, H., Tijerina Chávez, L., & Arteaga Ramírez, R. (2014). Estimación de la evapotranspiración utilizando un balance de energía e imágenes satelitales. *Revista mexicana de ciencias agrícolas, 5*(1), 143-155.

Gowda, P. H., Chavez, J. L., Colaizzi, P. D., Evett, S. R., Howell, T. A., & Tolk, J. A. (2008). ET mapping for agricultural water management: present status and challenges. *Irrigation Science, 26*(3), 223-237. doi:10.1007/s00271-007-0088-6

Hankerson, B., Kjaersgaard, J., & Hay, C. (2012). Estimation of evapotranspiration from fields with and without cover crops using remote sensing and in situ methods. *Remote Sensing, 4*(12), 3796-3812.

Hanson, R. L. (1991). Evapotranspiration and droughts. *US Geological Survey Water-Supply Paper, 2375*, 99-104.

Hong, S. D., Schepers, J., Francis, D. D., & Schlemmer, M. R. (2007). Comparison of Ground-Based Remote Sensors for Evaluation of Corn Biomass Affected by Nitrogen Stress. *Communications in soil science and plant analysis, 38*(15-16), 2209-2226.

Hunsaker, D. J., Pinter Jr, P. J., Barnes, E. M., & Kimball, B. A. (2003). Estimating cotton evapotranspiration crop coefficients with a multispectral vegetation index. *Irrigation Science, 22*(2), 95-104.

Hunsaker, D. J., Pinter, P. J., & Kimball, B. A. (2005). Wheat basal crop coefficients determined by normalized difference vegetation index. *Irrigation Science, 24*(1), 1-14.

Irmak, A., Ratcliffe, I., Ranade, P., Hubbard, K. G., Singh, R. K., Kamble, B., & Kjaersgaard, J. (2011). Estimation of land surface evapotranspiration with a satellite remote sensing procedure. *Great plains research*, 73-88.

Jackson, T. J., Chen, D., Cosh, M., Li, F., Anderson, M., Walthall, C., . . . Hunt, E. R. (2004). Vegetation water content mapping using Landsat data derived normalized difference water index for corn and soybeans. *Remote Sensing of Environment, 92*(4), 475-482.

Jayanthi, H., Neale, C. M., & Wright, J. L. (2007). Development and validation of canopy reflectance-based crop coefficient for potato. *Agricultural Water Management, 88*(1), 235-246.

Jensen, M. E., & Allen, R. G. (2016). *Evaporation, Evapotranspiration, and Irrigation Water Requirements*.

Jensen, M. E., Burman, R. D., & Allen, R. G. (1990). *Evapotranspiration and irrigation water requirements*.

Kamble, B., Kilic, A., & Hubbard, K. (2013). Estimating crop coefficients using remote sensing-based vegetation index. *Remote Sensing, 5*(4), 1588-1602.

Keim, B. D. (2010). The lasting scientific impact of the Thornthwaite water–balance model. *Geographical Review, 100*(3), 295-300.

Kjaersgaard, J., & Allen, R. (2010). Remote sensing technology to produce consumptive water use maps for the Nebraska Panhandle. *Final completion report submitted to the University of Nebraska, 88*.

Kjaersgaard, J., Allen, R., & Irmak, A. (2011). Improved methods for estimating monthly and growing season ET using METRIC applied to moderate resolution satellite imagery. *Hydrological Processes, 25*(26), 4028-4036.

Mkhwanazi, M., & Chávez, J. L. (2012). Using METRIC to estimate surface energy fluxes over an alfalfa field in Eastern Colorado. *Hydrology Days, Colorado State University USA (Accessed on August 26th 2014 from: http:// hydrologydays. colostate. edu/ Papers_ 2012/ Mcebisi_ paper. pdf)*.

Mokhtari, M., Ahmad, B., Hoveidi, H., & Busu, I. (2013). Sensitivity analysis of METRIC–based evapotranspiration algorithm. *International Journal of Environmental Research, 7*(2), 407-422.

Morton, C. G., Huntington, J. L., Pohll, G. M., Allen, R. G., McGwire, K. C., & Bassett, S. D. (2013). Assessing calibration uncertainty and automation for estimating evapotranspiration from agricultural areas using METRIC. *JAWRA Journal of the American Water Resources Association, 49*(3), 549-562.

Neale, C. M., Bausch, W. C., & Heerman, D. (1989). Development of reflectance-based crop coefficients for corn. *Trans. ASAE, 32*(6), 1891-1899.

Neale, C. M., Jayanthi, H., & Wright, J. L. (2005). Irrigation water management using high resolution airborne remote sensing. *Irrigation and Drainage Systems, 19*(3), 321-336.

Nguy-Robertson, A., Gitelson, A., Peng, Y., Viña, A., Arkebauer, T., & Rundquist, D. (2012). Green leaf area index estimation in maize and soybean: combining vegetation indices to achieve maximal sensitivity. *Agronomy Journal, 104*(5), 1336-1347.

Numata, I., Khand, K., Kjaersgaard, J., Cochrane, M. A., & Silva, S. S. (2017). Evaluation of Landsat-Based METRIC Modeling to Provide High-Spatial Resolution Evapotranspiration Estimates for Amazonian Forests. *Remote Sensing, 9*(1), 46.

Paço, T. A., Pôças, I., Cunha, M., Silvestre, J. C., Santos, F. L., Paredes, P., & Pereira, L. S. (2014). Evapotranspiration and crop coefficients for a super intensive olive orchard. An application of SIMDualKc and METRIC models using ground and satellite observations. *Journal of Hydrology, 519*, 2067-2080.

Paz-Pellat, F., Palacios-Velez, E., Bolanos-Gonzalez, M., Palacios-Sanchez, L. A., Martinez-Menes, M., Mejia-Saenz, E., & Huete, A. (2007). Design of a vegetation spectral index: NDVIcp. *Agrociencia, 41*(5), 539-554.

Pôças, I., Paço, T. A., Paredes, P., Cunha, M., & Pereira, L. S. (2015). Estimation of actual crop coefficients using remotely sensed vegetation indices and soil water balance modelled data. *Remote Sensing, 7*(3), 2373-2400.

Rafn, E. B., Contor, B., & Ames, D. P. (2008). Evaluation of a method for estimating irrigated crop-evapotranspiration coefficients from remotely sensed data in Idaho. *Journal of Irrigation and Drainage Engineering, 134*(6), 722-729.

Reyes-Gonzalez, A., Hay, C., Kjaersgaard, J., & Neale, C. (2015). *Use of Remote Sensing to Generate Crop Coefficient and Estimate Actual Crop Evapotranspiration.* Paper presented at the 2015 ASABE Annual International Meeting.

Reyes-González, A., Trooien, T., Kjaersgaard, J., Hay, C., & Reta-Sánchez, D. G. (2016). *Development of Crop Coefficients Using Remote Sensing-Based Vegetation Index and Growing Degree Days.* Paper presented at the 2016 ASABE Annual International Meeting.

Reyes-Gonzalez, A., U., F., J.G., M., & Reta-Sánchez, D. G. (2012). Estimacion de la evapotranspiracion actual utilizando sensores remotos y mediciones in situ. 18.

Rocha, J., Perdigão, A., Melo, R., & Henriques, C. (2012). Remote sensing based crop coefficients for water management in agriculture *Sustainable Development-Authoritative and Leading Edge Content for Environmental Management*: InTech.

Rouse Jr, J. W., Haas, R., Schell, J., & Deering, D. (1974). Monitoring vegetation systems in the Great Plains with ERTS.

Santos, C., Lorite, I., Tasumi, M., Allen, R., & Fereres, E. (2008). Integrating satellite-based evapotranspiration with simulation models for irrigation management at the scheme level. *Irrigation Science, 26*(3), 277-288.

Singh, R. K., & Irmak, A. (2009). Estimation of crop coefficients using satellite remote sensing. *Journal of Irrigation and Drainage Engineering, 135*(5), 597-608.

Tasumi, M., Allen, R. G., Trezza, R., & Wright, J. L. (2005). Satellite-based energy balance to assess within-population variance of crop coefficient curves. *Journal of Irrigation and Drainage Engineering, 131*(1), 94-109.

Thomason, W. E., Phillips, S. B., & Raymond, F. D. (2007). Defining useful limits for spectral reflectance measures in corn. *Journal of plant nutrition, 30*(8), 1263-1277.

Trout, T. J., Johnson, L. F., & Gartung, J. (2008). Remote sensing of canopy cover in horticultural crops. *HortScience, 43*(2), 333-337.

Vanino, S., Pulighe, G., Nino, P., De Michele, C., Bolognesi, S. F., & D'Urso, G. (2015). Estimation of evapotranspiration and crop coefficients of tendone vineyards using multi-sensor remote sensing data in a mediterranean environment. *Remote Sensing, 7*(11), 14708-14730.

Wright, J. L. (1982). New evapotranspiration crop coefficients. *Proceedings of the American Society of Civil Engineers, Journal of the Irrigation and Drainage Division, 108*(IR2), 57-74.

Yebra, M., Van Dijk, A., Leuning, R., Huete, A., & Guerschman, J. P. (2013). Evaluation of optical remote sensing to estimate actual evapotranspiration and canopy conductance. *Remote Sensing of Environment, 129*, 250-261.

Zhang, H., Anderson, R. G., & Wang, D. (2015). Satellite-based crop coefficient and regional water use estimates for Hawaiian sugarcane. *Field Crops Research, 180*, 143-154.

CHAPTER 5: Estimation of Crop Evapotranspiration using Satellite Remote Sensing-based Vegetation Index

5.1   Abstract

As population increases, the scarcity of fresh water increases. Thus better estimations of irrigation water requirements are essential to conserve fresh water. The objective was estimate crop evapotranspiration (ET_c) using satellite remote sensing-based vegetation index. The study was carried out in northern México during four growing seasons. Six, eleven, three, and seven clear Landsat images were acquired for 2013, 2014, 2015, and 2016, respectively for the analysis. The NDVI was calculated using near-infrared and red wavebands. The relationship between NDVI and tabulated K_c's was used to generate K_c maps using Model Maker tool of ERDAS Imagine Software. Spatially ET_c maps were generated as an output of K_c maps multiplied by reference evapotranspiration (ET_r), which was taken from a local automatic weather station. The results showed that ET_c was low at initial and early development stages, while high ET_c was found from mid-season to harvest stage. Daily ET_c maps helped to explain the variability of crop water use during the growing season. Based on the results we can conclude that ET_c maps developed from remotely sensed multispectral vegetation indices are a useful tool for quantifying crop water consumption at regional and field scales. Using ET_c maps, farmers can supply appropriate amount of irrigation water corresponding to each growth stage, leading to water conservation.

5.2   Introduction

As population increases, the scarcity of fresh water increases. Agriculture is the major consumer of fresh water (Gontia & Tiwari, 2010; Heermann & Solomon, 2007), but it is not necessary used efficiently due to farmers supplying more water than is consumed by the crop. Thus better estimation of irrigation water requirements is essential to conserve fresh water and avoid threatened food security. To achieve water conservation is necessary that the farmers adopt new technologies for estimating crop water requirements more efficiently.

Crop evapotranspiration (ET_c) represents crop water requirements and is affected by microclimate and actual crop conditions (Adamala, Rajwade, & Reddy, 2016; Parmar & Gontia, 2016). A useful method to estimate ET_c or crop water requirements in cropland areas is to multiplying reference evapotranspiration (ET_r) by a crop coefficient (K_c) values (Eq. 1). ET_r is estimated based on meteorological information (e.g., solar radiation, wind speed, air temperature, and air vapor pressure deficit) from a local weather station, using the Penman-Monteith equation. The K_c is typically taken from literature values and is affected by soil water content, crop variety, and crop density (R. G. Allen, Clemmens, Burt, Solomon, & O'Halloran, 2005; R. G. Allen et al., 1998; Marvin E Jensen & Allen, 2016). ET_c has been estimated using conventional methods e.g., weighing lysimeters, evaporation pan, soil water balance, atmometer, Bowen Ratio Energy Balance System (BREBS), and Eddy covariance (EC). However, these methods are recognized as the point-based measurements. To overcome this problem, satellite-based remote sensing can estimate crop water requirements and its spatial and temporal distribution on a field-by-field basis at a regional scale (R. Allen, A. Irmak, R. Trezza, J.

M. H. Hendrickx, et al., 2011; R. G. Allen, Tasumi, & Trezza, 2007; Bastiaanssen et al., 2005; J Kjaersgaard et al., 2011).

$$ET_c = ET_r \times K_c \tag{1}$$

Remote sensing is a technology that can estimate ET_c at regional and local scale in less time and with less cost (R. G. Allen, Tasumi, & Trezza, 2007; J Kjaersgaard et al., 2011). Remotely sensed can also estimate crop coefficients based on spectral reflectance of vegetation indices (VIs) (Adamala et al., 2016; Neale et al., 2005). The normalized difference vegetation index (NDVI) is the most common VIs (Glenn et al., 2011). NDVI takes into account the reflectance of red and near infrared wavebands (Rouse Jr et al., 1974), where red waveband is strong absorbed by chlorophyll in leaves of the top layers, while near infrared wavebands is reflected by the mesophyll structure in leaves, penetrating into deeper leaf layers in a healthy vegetation (Figure 5.2) (Glenn, Nagler, & Huete, 2010; Glenn et al., 2011; Romero-Trigueros et al., 2016). High values of NDVI are related with healthy and dense vegetation, which presents high reflectance values in the NIR band and low reflectance values in the red band (Toureiro, Serralheiro, Shahidian, & Sousa, 2016). Crop coefficients generated from VIs determine ET_c better than a tabulated K_c because it represents the actual crop growth conditions and capture the spatial variability among different fields (Gontia & Tiwari, 2010; Kullberg et al., 2017; Lei & Yang, 2012).

Several studies have used multispectral vegetation indices derived from remote sensing to estimate K_c values on agricultural crops including corn crop (e.g., (Bausch, 1995; Campos et al., 2010; Duchemin et al., 2006; Garatuza-Payan et al., 2003; Gontia & Tiwari, 2010; González-Dugo & Mateos, 2008; Hunsaker et al., 2003; Jayanthi et al.,

2007; Kamble et al., 2013; Neale et al., 1989; Arturo Reyes-Gonzalez et al., 2015; Tasumi et al., 2005; Trout et al., 2008). Crop coefficients derived from remotely sensed vegetation index also have used to generate local and regional ET_c maps (Farg, Arafat, El-Wahed, & El-Gindy, 2012; Gontia & Tiwari, 2010; Vanino et al., 2015; Zhang et al., 2015), however in northern México ET_c maps using satellite remote sensing-based vegetation index remains unexplored.

The objectives of this study were to 1) calculate NDVI values for each corn field for each growing season, 2) develop a simple linear regression model between NDVI derived from satellite-based remote sensing and tabulated K_c obtained of alfalfa-based crop coefficient from ASCE Manual 70, 3) generate K_c maps using the linear regression equation obtained between NDVI and K_c values, and 4) create ET_c maps with high spatial resolution at regional and field scales.

5.3   Material and methods

5.3.1   Study Area

The study was carried out in northern México (Comarca Lagunera) during four growing seasons. The Comarca Lagunera had an average latitude of 25° 40' N and longitude of 103° 18' W, and elevation of 1115 m above mean sea level (Figure 5.1). In the Comarca Lagunera forage crops (alfalfa, corn, sorghum, and oat (planted in winter season)) occupied more than 75% of the total irrigated area (SAGARPA, 2016). Silage corn is the most important crop after alfalfa in this region. Five silage corn fields in each growing season were selected for NDVI calculations. The corn fields were irrigated using surface irrigation system. The plant population density was 78, 000 plants ha^{-1}. Silage

corn is typically planted from late March to early April and chopped for silage from late

July to early August depends on the crop variety. The corn fields selected ranged between

10 and 20 hectares in size. The soil texture for this region is clay loam soil. The mean

annual maximum temperature is 28 °C, minimum 13 °C, and mean 21 °C. (Pedro & del

Consuelo, 2002). The mean annual precipitation is 200 mm, while the annual potential

evapotranspiration is 2,000 mm (Levine, 1998).
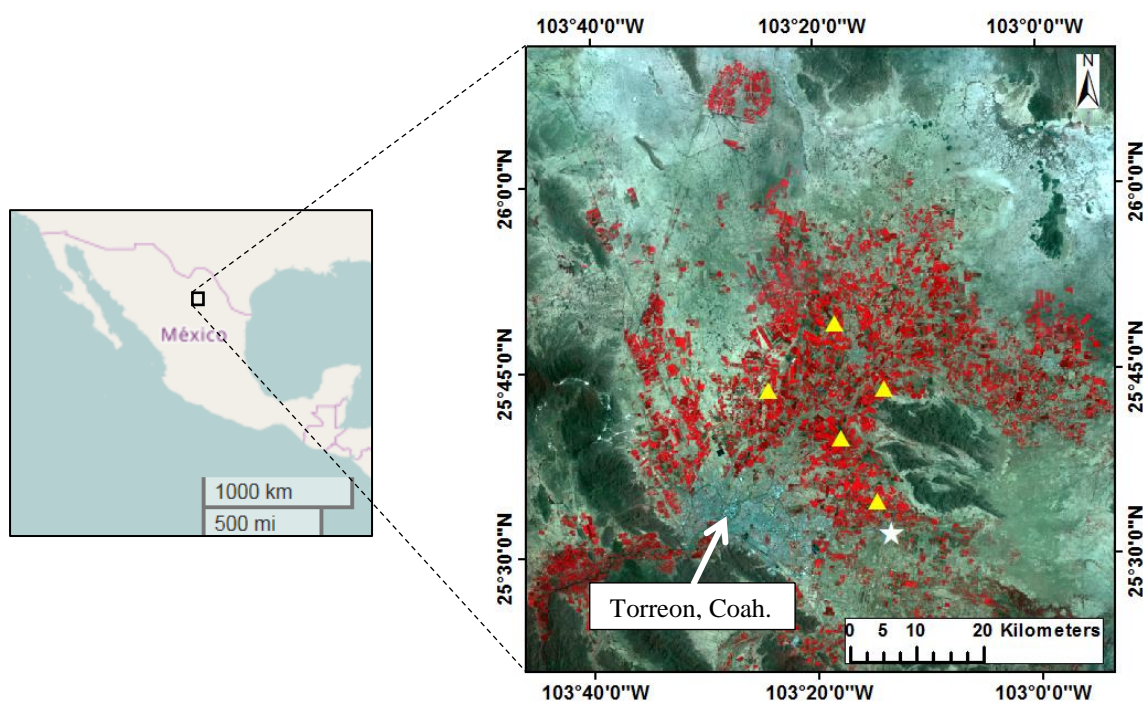
Figure 5.1 Location of the study area at northern México (left map). The subset of the area of interest, Landsat with false color composite (bands 4, 3, 2), the yellow rectangles represent five locations where we selected the corn fields, and the white star indicates weather station (right image).

5.3.2 Landsat Images

Clear sky images from Landsat 7 Enhanced Thematic Mapper Plus (ETM+) and

Landsat 8 Operational Land Imager (OLI) and Thermal Infrared Sensor (TIRS) (Path 30,

Row 42) were used to estimate NDVI, K_c and ET_c values. The images were downloaded

from the United States Geological Survey (USGS) EROS Datacenter. Six, eleven, three,

and seven clear Landsat images were acquired for 2013, 2014, 2015, and 2016,

respectively (Table 5.1). The satellite images were processed using the Model Maker tool

of ERDAS Imagine Software.

Table 5.1 The year, acquisition dates, day after planting (DAP), Landsat satellite, and
path/row for 2013, 2014, 2015, and 2016 growing seasons.

Year	Acquisition dates	DAP	Satellite	Path/Row
2013	April 14	10	Landsat 8	30/42
	April 22	18	Landsat 7	30/42
	April 30	26	Landsat 8	30/42
	May 16	42	Landsat 8	30/42
	June 9	66	Landsat 7	30/42
	June 17	74	Landsat 8	30/42
2014	April 17	8	Landsat 8	30/42
	May 3	24	Landsat 8	30/42
	May 11	32	Landsat 7	30/42
	May 19	40	Landsat 8	30/42
	May 27	48	Landsat 7	30/42
	June 4	56	Landsat 8	30/42
	June 12	64	Landsat 7	30/42
	June 28	80	Landsat 7	30/42
	July 6	88	Landsat 8	30/42
	July 14	96	Landsat 7	30/42
	July 22	104	Landsat 8	30/42
2015	April 28	22	Landsat 7	30/42
	May 30	54	Landsat 7	30/42
	July 17	102	Landsat 7	30/42
2016	April 14	8	Landsat 7	30/42
	May 16	40	Landsat 7	30/42
	June 9	64	Landsat 8	30/42
	June 25	80	Landsat 8	30/42
	July 3	88	Landsat 7	30/42
	July 11	96	Landsat 8	30/42
	July 19	104	Landsat 7	30/42

5.3.3 Pixel selection

Ten pixels for each corn field and each season were selected and extracted from NDVI maps. The pixels were located in the center of each corn field for each overpass date during the four growing seasons. The same pixels were observed throughout the corn growing season. We assumed that the pixels are representative of the entire corn field. All corn fields had flat terrain. The number of pixels per year are presented in Table 5.2.

Table 5.2 The year and number of pixels selected throughout the growing season.

Year	No. pixels
2013	300
2014	550
2015	150
2016	350

5.3.4 NDVI Calculations

The NDVI is the difference between near-infrared (NIR) and red waveband reflectances divided by their sum (Rouse Jr et al., 1974). NIR and red wavebands present different reflectance on healthy vegetation as shown in Figure 5.2. NDVI values range between -1 and +1, where water presents negative values and dense canopy presents high positive values (Bannari et al., 1995; Bausch, 1993; Toureiro et al., 2016). The NDVI was calculated for each overpass date and for each growing season using Model Maker tool of ERDAS Imagine Software as shown in the next equations:

For Landsat 7 was calculated as:

$$NDVI = \frac{(NIR_{band\ 4} - Red_{band\ 3})}{(NIR_{band\ 4} + Red_{band\ 3})} \tag{2}$$

For Landsat 8 was calculated as:

$$NDVI = \frac{(NIR_{band\,5} - Red_{band\,4})}{(NIR_{band\,5} + Red_{band\,4})}$$ (3)

where NIR_{band} and Red_{band} are the near-infrared and red wavebands,

respectively.
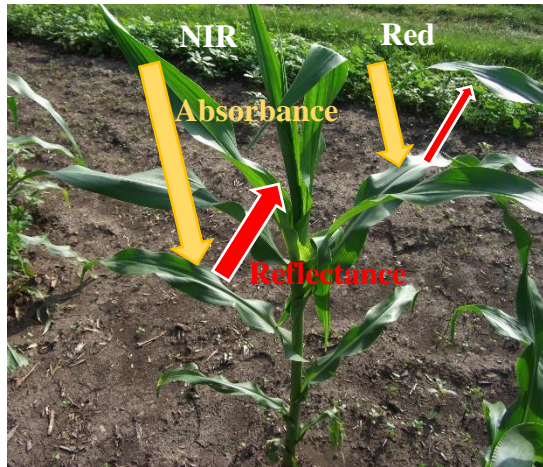
Figure 5.2 Absorbance and reflectance of NIR and Red wavebands on healthy vegetation.

5.3.5 Crop coefficient (K_c) values from Manual 70

The K_c values were taken from ASCE Manual 70 (Appendix E) and were adjusted

according to different corn growth stages throughout the growing season. For K_c

estimations the ASCE Manual 70 divides the growing season into two periods, viz.

percent of time from planting to effective cover and days after effective cover to harvest.

The effective cover and harvest of corn in our study occurred around 55 and 105 DAP,

respectively based on the crop phenology.

5.3.6 Relationship between NDVI and K_c and K_c maps development

The relationships between NDVI derived from Landsat images and tabulated K_c's

values obtained from ASCE Manual 70 (Appendix E) (Marvin E Jensen & Allen, 2016)

corresponding to each satellite overpass date for 2013, 2014, 2015, and 2016 corn

growing seasons were established. These relationships were used to generate an average

linear regression equation for entire period of study.

5.3.7 Reference Evapotranspiration (ET$_r$) calculations

The meteorological information was taken from an automated weather station.

The weather station was located at the National Institute of Forestry, Agriculture, and

Livestock Research (INIFAP) Matamoros Coahuila, México (Figure 5.1). The ET$_r$ values

were taken from the weather station, where ET$_r$ was calculated using the Penman-

Monteith equation (R. G. Allen et al., 1998; ASCE-EWRI, 2005) as follows:

$$ET_{ref} = \frac{0.408\,\Delta(R_n - G) + \gamma\frac{C_n}{T+273}u_2(e_s - e_a)}{\Delta + \gamma(1 + C_d u_2)} \tag{4}$$

where ET_{ref} is the alfalfa reference (mm day^{-1}), Δ is the slope pressure versus air

temperature curve (kPa °C^{-1}), R_n is the net radiation at the crop surface (MJ m^{-2} day^{-1}), G

is the soil heat flux at the soil surface (MJ m^{-2} day^{-1}), T is the mean air temperature at 1.5

to 2.5 m height (°C), u_2 is the mean daily wind speed at 2 m height (m s^{-1}), e_s is the

saturation vapor pressure of the air (kPa), e_a is the actual vapor pressure of the air (kPa),

γ is the psychrometric constant (0.0671 kPa °C^{-1}), $e_s - e_a$ is the vapor pressure deficit

(kPa), C_n is the numerator constant (1600 K mm s^3 Mg^{-1} day^{-1}), C_d is the denominator

constant (0.38 s m^{-1}) for alfalfa reference, and 0.408 is the coefficient constant (m^2 mm

MJ^{-1}).

5.3.8 Crop Evapotranspiration (ET$_c$) maps

The K$_c$ values taken from the K$_c$ maps were multiplied by ET$_r$ (Eq. 1) to create

ET$_c$ maps with high spectral resolution (30 m) for 2014 growing season, using Model

Maker tool of ERDAS Imagine Software and ArcGIS version 10.3.1. The ET_c maps were designed to monitoring the spatial distribution and temporal evolution of the crop water requirements during the growing season.

5.3.9   Flowchart of estimation of ET_c

A summary of estimation of ET_c using satellite remote sensing-based vegetation index is showed in Figure 5.3. The Landsat images and weather data are the two major inputs parameters in the vegetation index method.
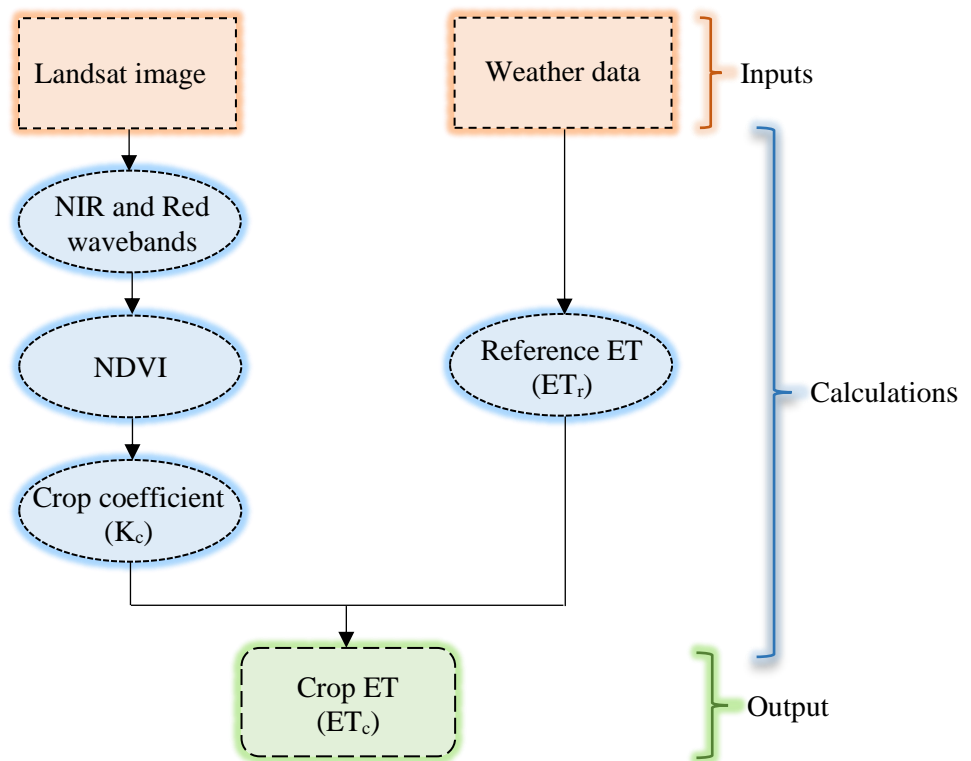
Figure 5.3 Flowchart of crop evapotranspiration estimation.

5.4 Result and Discussion

5.4.1 NDVI curves

The NDVI average values (10 pixels) selected and extracted from NDVI maps for five corn fields and for different corn growing seasons are shown in Figure 5.4. The figures show similar NDVI curves for 2014 and 2016, while for 2013 and 2015 the curves are not well pronounced due to lack of clear sky images during the growing seasons. In general NDVI values at initial stage were low around 0.15 in early April (DAP 8), and then increase as the crop develops reaching its maximum value (0.8) at mid-season stage followed by plateau from late May to middle July (DAP 55-95) and slight decreasing (0.7) at the end of the season by the end of July (DAP 105). Several researchers reported similar seasonal NDVI curves for corn (P.-Y. Chen et al., 2006; de Souza et al., 2015; F. Gao et al., 2017; Jackson et al., 2004; Kamble et al., 2013; Neale et al., 1989; Singh & Irmak, 2009; Tasumi et al., 2005; Thomason et al., 2007; Toureiro et al., 2016). All NDVI curves developed by these researchers showed low corn NDVI values at early stage and then increased at mid-season stage and decline at late stage. However, Thomason et al. (2007) reported NDVI curves of forage corn, where NDVI values gradually increase and then remains longer plateau until the end of the season.

In this study, the NDVI values derived from Landsat 8 (L8) were greater than NDVI derived from Landsat 7 (L7), not only in mid-season stage (Figure 5.4 (2014 and 2016)) but also in early stage (Figure 5.4 (2013)). The difference between L8 and L7 ranged from 0.03 to 0.09 (data no shown), those difference values are in agreement with values reported by Flood (2014) (0.04) and Ke, Im, Lee, Gong, and Ryu (2015) (0.06), but greater than reported by D. Roy et al. (2016) (0.02). The difference between L8 and

L7 was due to L8 has narrowed near-infrared waveband (L7 = 0.77-0.90μm, L8 = 0.85-0.88μm), higher signal to noise ratio (SNR), and higher 12-bit radiometric resolution (Flood, 2014; Holden & Woodcock, 2016; Ke et al., 2015; D. P. Roy et al., 2014). These features provide less influenced by atmospheric conditions, more sensitive to surface reflectance and more precise measurements (Flood, 2014; Holden & Woodcock, 2016; Ke et al., 2015). Although the comparison of NDVI between L8 and L7 was not objective of this study, it is important to mention that inconsistent or unreliable values of NDVI can produce poor estimates of crop evapotranspiration (Ke et al., 2015).
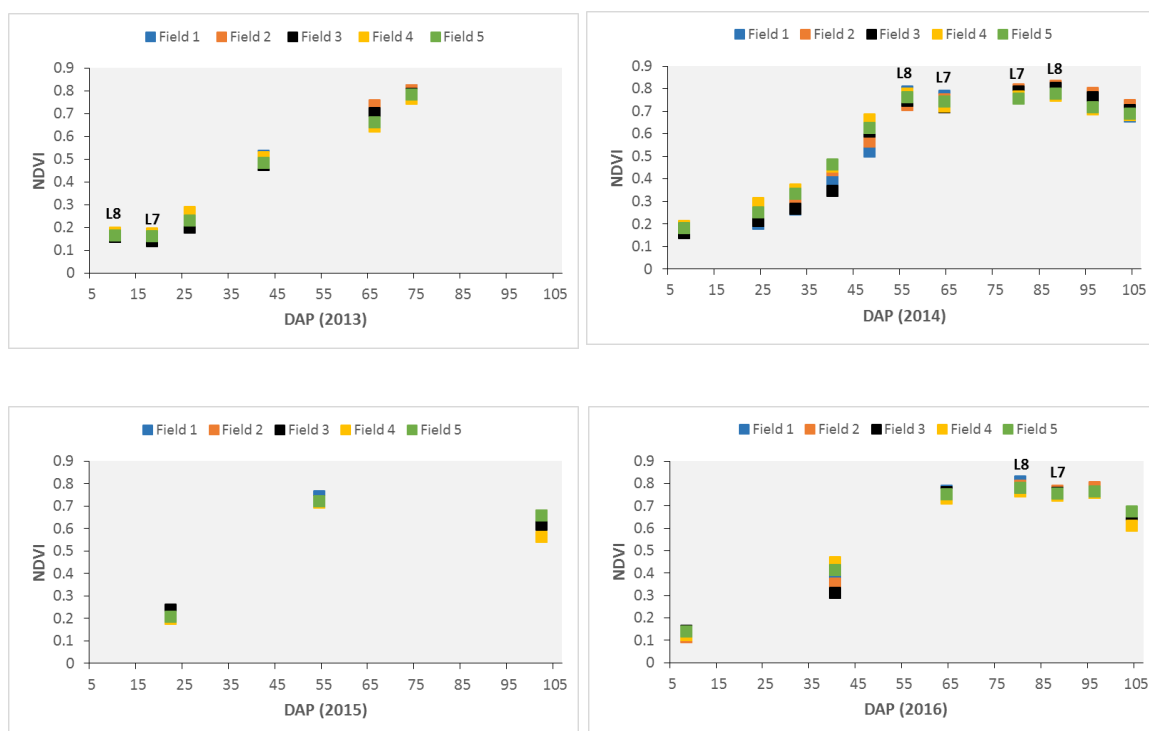
Figure 5.4 Seasonal evolution of NDVI at five corn fields for 2013, 2014, 2015, and 2016 growing seasons in northern México.

5.4.2 Relationship between NDVI and K_c

The NDVI values were taken from NDVI maps generated as an output using Landsat 7 and Landsat 8, while K_c's values were taken from ASCE Manual 70 (Appendix

E) table for 2013, 2014, 2015, and 2016 corn growing seasons. Figure 5.5 shows the

relationship between NDVI of five corn fields and tabulated K_c values for four growing

seasons. Strong relationships were observed for 2013 and 2015 growing seasons, with r^2

equal to 0.99, whereas for 2014 and 2016 the r^2 was equal to 0.96. The slightly low

values of r^2 found in 2014 and 2016 seasons, probably were due to major numbers of

NDVI values, where some of them were lower than K_c values, especially in development

growth stage. Similar values of coefficients of determination (0.99) between NDVI and

K_c for corn crop were found by Rocha et al. (2012) and Reyes-González et al. (2016) but

low coefficients were reported by Singh and Irmak (2009), Kamble et al. (2013), and

Toureiro et al. (2016), who reported values of r^2 equal to 0.83, 0.81, and 0.82,

respectively.

The NDVI computed from Landsat images and K_c's obtained from ASCE manual

70 (Appendix E) were used to develop the linear regression equations. Linear

relationships between NDVI and K_c for 2013, 2014, 2015, and 2016 were establish as the

following equations:

$$K_c = 1.3301\ NDVI + 0.0021 \qquad (2013) \tag{5}$$

$$K_c = 1.2234\ NDVI + 0.0242 \qquad (2014) \tag{6}$$

$$K_c = 1.4556\ NDVI + 0.0618 \qquad (2015) \tag{7}$$

$$K_c = 1.0968\ NDVI + 0.1054 \qquad (2016) \tag{8}$$

Similar linear equations for corn were reported by other researchers e.g., (Neale et

al., 1989; Rafn et al., 2008; Reyes-González et al., 2016; Rocha et al., 2012), all these

authors used alfalfa-reference crop coefficient for generating linear equations.
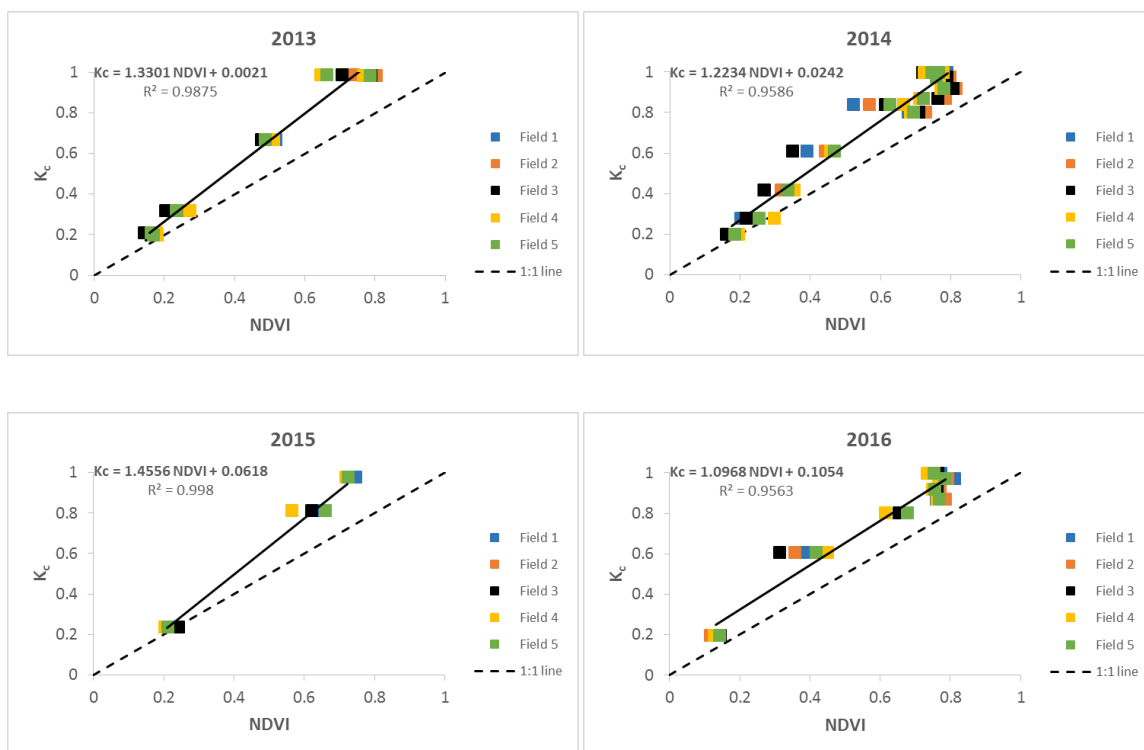
Figure 5.5 Linear relationship between NDVI derived from NDVI maps and K_c from ASCE manual 70 for four growing seasons. The dashed line indicates the 1:1 line.

The four year linear regression equations were compared using the *t* test method to test statistical difference between two independent regressions (Steel & Torrie, 1980). Table 5.3 shows the results of all comparisons, where all *t* values were less than tabulated *t* values, which means that there were no statistical differences between linear regression equations. Based on these results all data from the four years were pooled to create a general linear equation as shown in Figure 5.6. This linear equation was used to create K_c maps for 2014 season.

Table 5.3 Comparisons between linear regression equations using the t test method.

Compared years	t value	t from table
2013 to 2014	1.14	2.16
2013 to 2015	0.96	2.57
2013 to 2016	2.13	2.26
2014 to 2015	1.53	2.22
2014 to 2016	1.08	2.14
2015 to 2016	2.31	2.44
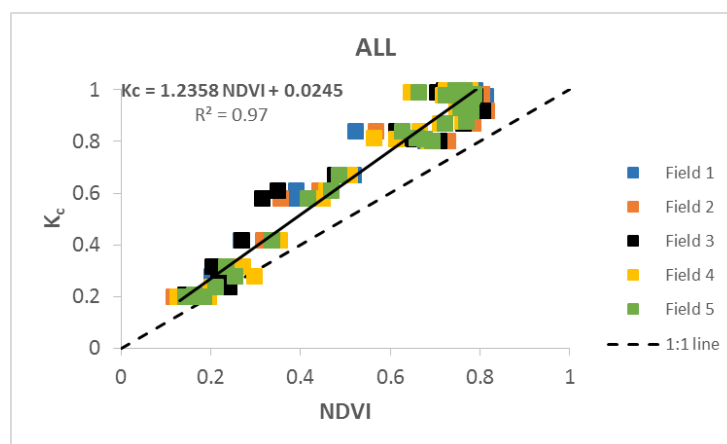
Figure 5.6 Linear relationship between NDVI and K_c for all data. The dashed line indicates the 1:1 line.

5.4.3 K_c maps and K_c values

Previous empirical linear equation between NDVI and K_c were used to generate K_c maps using Landsat images processed in ERDAS Imagine (Model Maker) for 2014 growing season. Figure 5.7 shows spatial and temporal variability of K_c values throughout the 2014 growing season. The K_c maps showed low K_c values early in the growing season (DAP 8) (light blue-green color) and gradually increase at mid-season stage (DAP 56), where remains plateau until harvest (DAP 105) (brown color). Similar K_c maps of corn were developed by Singh and Irmak (2009), Ayse Irmak et al. (2011),

Rocha et al. (2012), and Reyes-González et al. (2016), who reported maps of daily spatial distribution of K_c for six, four, seven, and four overpass dates, respectively. However, satellite overpasses date used in this study for 2014 growing season were almost an 8-day observation intervals. These K_c maps show how the K_c values increase (from 0.2 to 1.0), as the silage crops develop increases.

Figure 5.7 Spatial and temporal evolution of K_c generated with ERDAS Imagine Software (Model Maker) and ArcGIS version 10.3.1 during the 2014 growing season in northern México.

The K$_c$ values obtained from K$_c$ maps based on ten selected pixels average within

a corn field in five corn fields for each overpass date are shown in Table 5.4. In general,

the minimum K$_c$ value (0.24) was presented in early season, while the maximum K$_c$ value

(1.00) was presented in the mid-season stage. The standard deviation values of K$_c$ were

equal or lower than 0.07 throughout the growing season (Table 5.4), this means that

planting dates, management practice, and maturity dates among corn fields did not affect

too much the K$_c$ values during the season.

Table 5.4 DAP, Landsat satellite, crop coefficient (K$_c$), and standard deviation (Std. Dev.) throughout the 2014 growing season.

DAP	Satellite	Kc	Std. Dev.
8	Landsat 8	0.24	0.01
24	Landsat 8	0.32	0.05
32	Landsat 7	0.40	0.05
40	Landsat 8	0.56	0.07
48	Landsat 7	0.76	0.07
56	Landsat 8	0.97	0.03
64	Landsat 7	0.94	0.03
80	Landsat 7	0.98	0.02
88	Landsat 8	1.00	0.02
96	Landsat 7	0.97	0.04
104	Landsat 8	0.88	0.02

The relationship between K$_c$ calculated derived from K$_c$ maps and K$_c$ from tables

is showed in Figure 5.8. A strong relationship was found with r^2 = 0.96. This means that

K$_c$ values derived from vegetation index (K$_c$ calculated) can be a robust parameter to

calculate actual crop evapotranspiration. The main difference between K$_c$ calculated and

K$_c$ tabulated is that the K$_c$ tabulated comes from well-water reference crop (e.g. alfalfa),

whereas K$_c$ calculated comes from the actual crop growth conditions, where some K$_c$

values derived from reflectance of vegetation index are reduced by soil water content. In

this study the little difference between K_c calculated and K_c tabulated was found in the development growth stage (DAP 40-48).
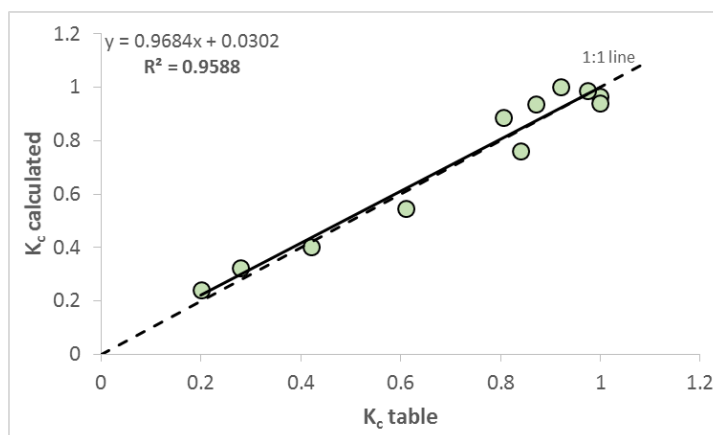
Figure 5.8 Relationship between K_c calculated and K_c tabulated for corn during 2014 growing season. The dashed line indicates the 1:1 line.

5.4.4   ET$_c$ maps and ET$_c$ values

Spatially ET$_c$ maps of 30 m resolution were generated as an output of K_c maps multiplied by ET$_r$ values for corresponding day using ERDAS Imagine Software (Model Maker) for 2014 growing season (Figure 5.9). The maps showed low ET$_c$ values (2.0 mm day^{-1}) (light green color) at initial stage and high ET$_c$ values (8.0 mm day^{-1}) (red color) at mid-season stage. The ET$_c$ maps created in this study are in agreement with other researchers e.g., (Adamala et al., 2016; Gontia & Tiwari, 2010; Rossato, Alvala, Ferreira, & Tomasella, 2005). They generated crop evapotranspiration maps using K_c derived from remote sensing based vegetation indices. Other researchers reported that the K_c derived from canopy reflectance based vegetation index had the potential to estimate crop evapotranspiration at regional and field scale e.g., (Campos et al., 2010; Gonzalez-Dugo et al., 2009; Lei & Yang, 2012; Murray, Nagler, Morino, & Glenn, 2009; Rafn et al., 2008; Toureiro et al., 2016).
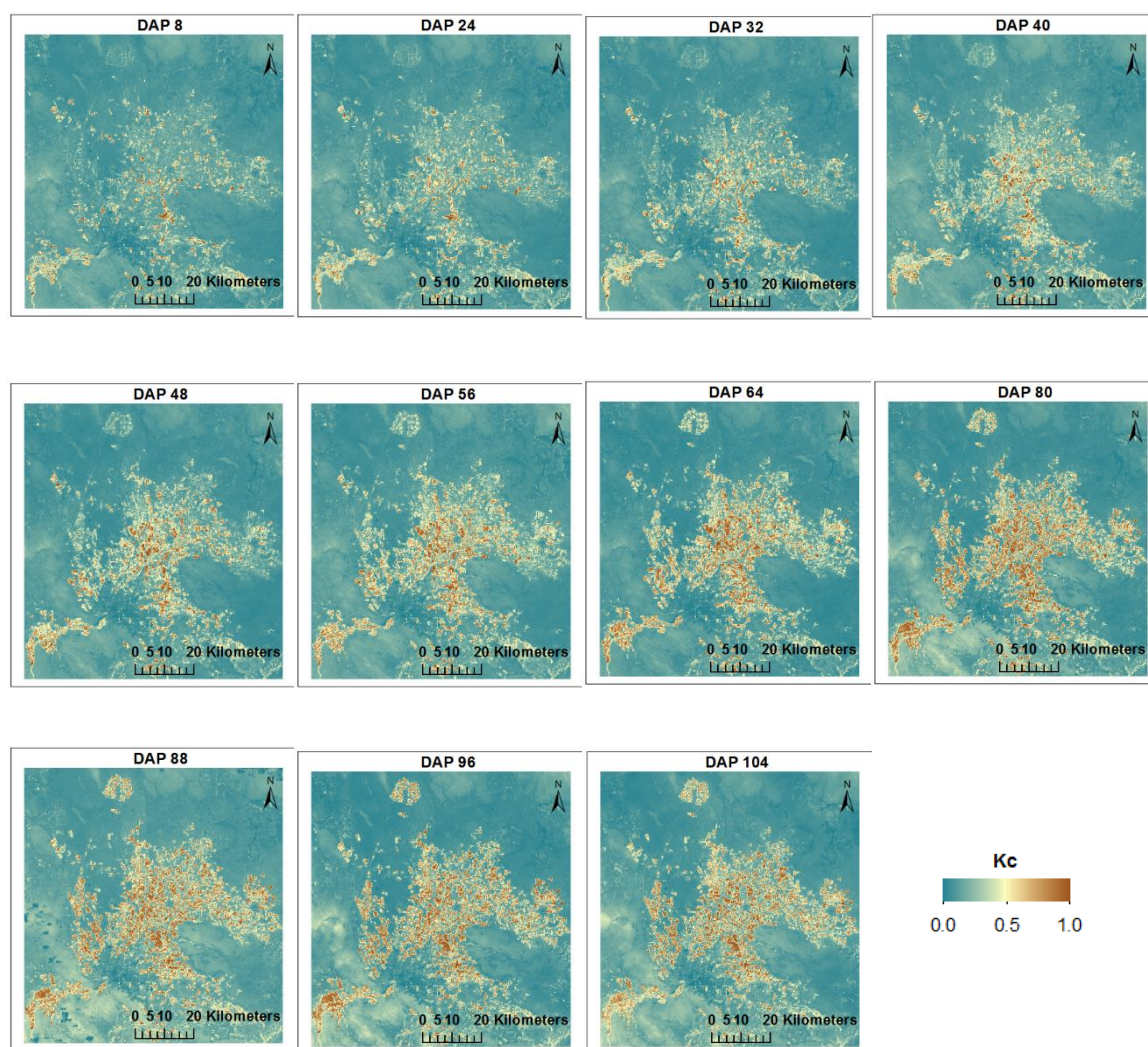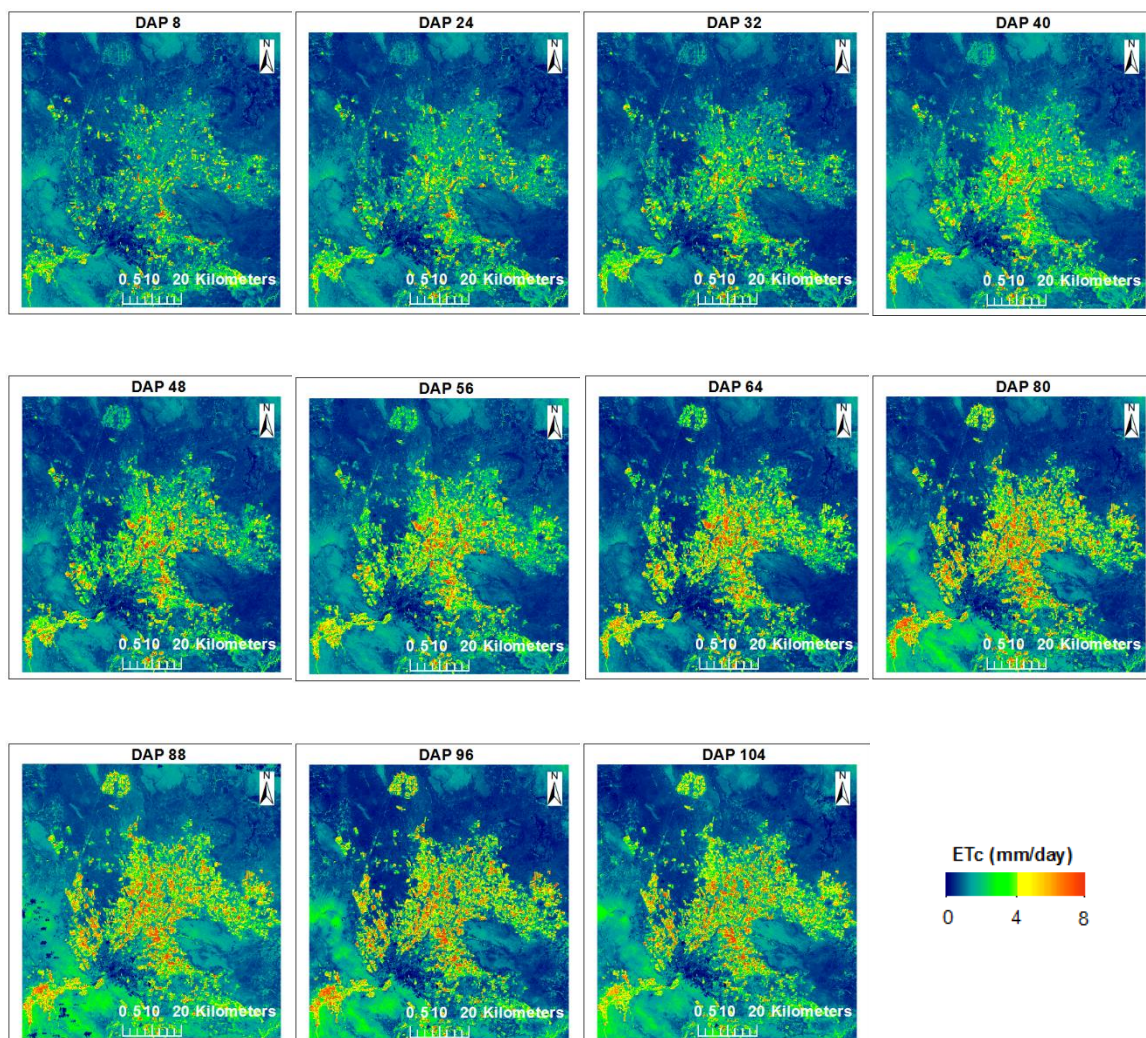
Figure 5.9 Spatial and temporal ET_c maps generated with ERDAS Imagine Software (Model Maker) and ArcGIS version 10.3.1 for 2014 growing season in northern México.

Daily ET_c values for 2014 growing season are shown in Table 5.5. The ET_c values were obtained from ten selected pixels average within a corn field in five corn field for each overpass date. It can be observed from Table 5.5 that the ET_c values varied during the growing season from 1.40 to 7.41 mm day^{-1}. The results showed that ET_c was low at initial and early development stage, while high ET_c were found from mid-season to harvest stage. These two seasons were characterized because in the initial stage crop needs smaller water requirements, whereas in the mid-season crop needs higher water

requirements, as we can see in the next section. Low standard deviation values (<0.5 mm day^{-1}) were registered among corn fields during the growing season (Table 5.5), however the higher standard deviation were found in development stage. In this particular stage the crop evapotranspiration is affected by soil type, soil water content, and crop architecture.

Table 5.5 DAP, Landsat satellite, crop evapotranspiration (ET$_c$), and standard deviation (Std. Dev.) for 2014 growing season.

DAP	Satellite	ET$_c$	Std. Dev.
8	Landsat 8	1.40	0.09
24	Landsat 8	1.87	0.26
32	Landsat 7	2.62	0.33
40	Landsat 8	3.87	0.48
48	Landsat 7	4.95	0.43
56	Landsat 8	6.46	0.18
64	Landsat 7	5.37	0.15
80	Landsat 7	4.78	0.10
88	Landsat 8	7.41	0.17
96	Landsat 7	4.78	0.20
104	Landsat 8	5.32	0.15

5.4.5   ET$_c$ maps at a field scale

Daily ET$_c$ maps helps explain the variability of crop water requirement during the growing season of croplands as shown in Figure 5.10. These images at a field scale level show the corresponding ET values according to each growth stage, this indicates that each stage requires different amount of water throughout the growing season. For example minimum water requirements (2.0 mm day^{-1}) are need at the initial stage, whereas maximum water requirements are needed at mid-season stage (8.0 mm day^{-1}). Understating the different crop growth stages and applying the accurate amount of

volumetric water, farmers can improve their irrigation scheduling, improve water management, and enhance irrigation water sustainability.

Similar ET_c maps at a field scale for agricultural crops including corn were reported by Farg et al. (2012), Zipper and Loheide II (2014), and Senay et al. (2016), they reported minimum and maximum ET_c values at different crop growth stages, where the higher evapotranspiration rates were found at the mid-season growth stage and lowest evapotranspiration rates were found at early growth stage.
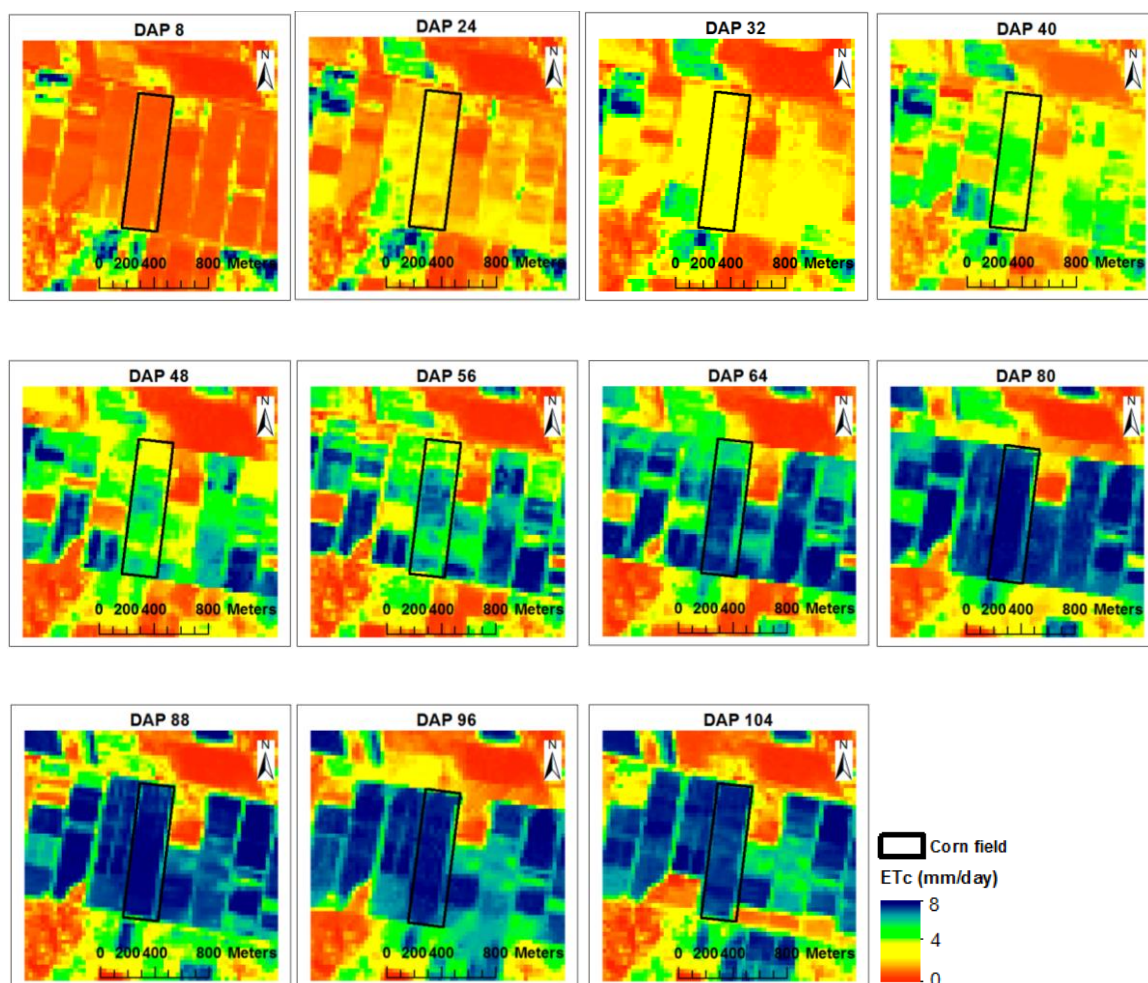

Figure 5.10 ET_c maps at a field scale (e.g., silage corn) generated with ERDAS Imagine Software (Model Maker) and ArcGIS version 10.3.1 using Landsat 7 and Landsat 8 satellite images for the 2014 growing season. The red, light green, and dark blue color within the corn field (black rectangle) indicates low, medium and high ET_c values.

5.4.6   Comparison between ET_r and ET_c

The ET_r values were taken directly from a local weather station, while ET_c values were derived from ET_c maps. Figure 5.11 shows the comparison between ET_r and ET_c for 2014 growing season. This figure illustrated that the daily ET_r were higher than the daily ET_c outputs at the beginning of the growing season, but similar outputs were recorded at mid-season stage. For 2014 growing season, in early stage (DAP 1-20) the ET_r values were around 6.0 mm day^{-1}, while the ET_c values were around 2.0 mm day^{-1}. In development stage (DAP 20-55) the ET_r values continue around 6 mm day^{-1}, while ET_c values increase from 2 to 6 mm day^{-1}. In the mid-season stage (DAP 55-95) both ET_r and ET_c values were very similar around 7.0 mm day^{-1}. At the end of the growing season (DAP 95-105) the ET_r values were slightly greater than ET_c values by 0.5 mm day^{-1}. From early to mid-development stage the ET_c values were lower than ET_r values, this means that in those particular stages we can save irrigation water (grey wide column in the graph), because in those stages the crops need small water requirements, due to the crop canopy is no yet fully developed. In general, the ET_c values from ET_c maps could be used by farmers in their irrigation scheduling programs because it shows when and how much water is required by the crop during different growth stages.

Reyes-González et al. (2016), reported that the farmers should be use ET_c instead of ET_r for irrigation scheduling in arid and semi-arid regions where irrigation water is scarce. Kebede, Fisher, Sui, and Reddy (2014) reported that the farmers in the Mississippi Delta use four primarily methods to determine to irrigate: the first was visual observation of crop condition method (47%), the second was the soil feel method (24%), the third was daily crop evapotranspiration method (10%), and the fourth was personal

calendar schedule method (8%). Also they reported that these methods were similar to the national average, however personal calendar scheduling was slightly higher (10%) than crop evapotranspiration method (3%). Thus, there is a necessity to the farmers adopt new technologies or new methods (crop evapotranspiration) to determine when to supply irrigation water.
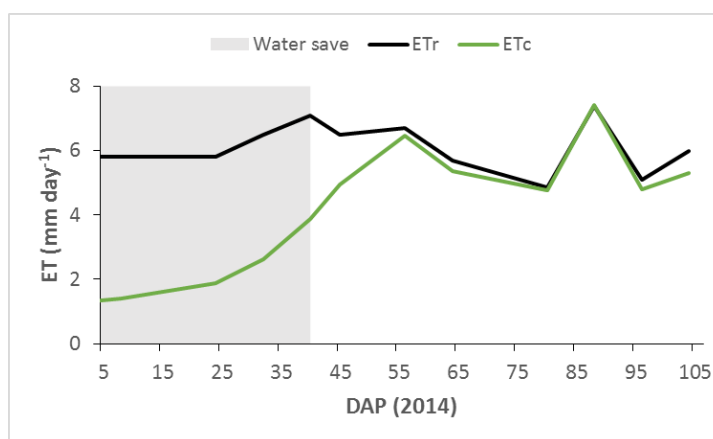
Figure 5.11 Comparison between ET_r and ET_c for 2014 growing season in northern México. The grey wide column indicates the time interval where producers can save irrigation water.

5.5   Conclusions

The general objective of this study was estimate crop evapotranspiration using satellite remote sensing-based vegetation index in northern México.

The relationships between NDVI derived from Landsat images and tabulated K_c's obtained from ASCE Manual 70 (Appendix E) were established for four growing seasons. These empirical linear equations were used to generate an average linear regression equation.

Spatially ET_c maps were created as an output of K_c maps multiplied by ET_r values. The ET_c values ranged from 1.40 to 7.41 mm day^{-1} during the period of study.

The results showed that ET_c values were low at the beginning of the growing season, while high ET_c values were found from mid-season to harvest season. Daily ET_c maps helped to explain the variability of crop water use throughout the growing season.

Farmers in the northern México region currently use ET_r in their irrigation scheduling methods. The results indicate that farmers could reduce their seasonal water application amounts by 18% just by using ET_c appropriately in their irrigation scheduling methods.

The information generated in this study is essential for irrigation scheduling because it shows when and how much water is required by the crop during different crop growth stages.

Based on the results we can conclude that ET_c maps developed from remotely sensed multispectral vegetation indices are a useful tool for quantifying accurate crop water consumption from space at regional and field scales.

5.6   References

Adamala, S., Rajwade, Y. A., & Reddy, Y. K. (2016). Estimation of wheat crop evapotranspiration using NDVI vegetation index. *Journal of Applied and Natural Science, 8*(1), 159-166.

Allen, R., Irmak, A., Trezza, R., Hendrickx, J. M., Bastiaanssen, W., & Kjaersgaard, J. (2011). Satellite-based ET estimation in agriculture using SEBAL and METRIC. *Hydrological Processes, 25*(26), 4011-4027.

Allen, R. G., Clemmens, A. J., Burt, C. M., Solomon, K., & O'Halloran, T. (2005). Prediction accuracy for projectwide evapotranspiration using crop coefficients and

reference evapotranspiration. *Journal of Irrigation and Drainage Engineering, 131*(1), 24-36.

Allen, R. G., Pereira, L. S., Raes, D., & Smith, M. (1998). Crop evapotranspiration-Guidelines for computing crop water requirements-FAO Irrigation and drainage paper 56. *FAO, Rome, 300*(9), D05109.

Allen, R. G., Tasumi, M., & Trezza, R. (2007). Satellite-based energy balance for mapping evapotranspiration with internalized calibration (METRIC)—Model. *Journal of Irrigation and Drainage Engineering, 133*(4), 380-394.

ASCE-EWRI. (2005). *The ASCE standardized reference evapotranspiration equation; ASCE-EWRI Standardization of Reference Evapotranspiration Task Committee Report; ASCE: Reston, VA, USA.*

Bannari, A., Morin, D., Bonn, F., & Huete, A. (1995). A review of vegetation indices. *Remote sensing reviews, 13*(1-2), 95-120.

Bastiaanssen, W., Noordman, E., Pelgrum, H., Davids, G., Thoreson, B., & Allen, R. (2005). SEBAL model with remotely sensed data to improve water-resources management under actual field conditions. *Journal of Irrigation and Drainage Engineering, 131*(1), 85-93.

Bausch, W. C. (1993). Soil background effects on reflectance-based crop coefficients for corn. *Remote Sensing of Environment, 46*(2), 213-222.

Bausch, W. C. (1995). Remote sensing of crop coefficients for improving the irrigation scheduling of corn. *Agricultural Water Management, 27*(1), 55-68.

Campos, I., Neale, C. M., Calera, A., Balbontín, C., & González-Piqueras, J. (2010). Assessing satellite-based basal crop coefficients for irrigated grapes (Vitis vinifera L.). *Agricultural Water Management, 98*(1), 45-54.

Chen, P.-Y., Fedosejevs, G., Tiscareno-Lopez, M., & Arnold, J. G. (2006). Assessment of MODIS-EVI, MODIS-NDVI and VEGETATION-NDVI composite data using agricultural measurements: an example at corn fields in western Mexico. *Environmental monitoring and assessment, 119*(1-3), 69-82.

de Souza, C. H. W., Mercante, E., Johann, J. A., Lamparelli, R. A. C., & Uribe-Opazo, M. A. (2015). Mapping and discrimination of soya bean and corn crops using spectro-temporal profiles of vegetation indices. *International journal of remote sensing, 36*(7), 1809-1824.

Duchemin, B., Hadria, R., Erraki, S., Boulet, G., Maisongrande, P., Chehbouni, A., . . . Kharrou, M. (2006). Monitoring wheat phenology and irrigation in Central Morocco: On the use of relationships between evapotranspiration, crops coefficients, leaf area index and remotely-sensed vegetation indices. *Agricultural Water Management, 79*(1), 1-27.

Farg, E., Arafat, S., El-Wahed, M. A., & El-Gindy, A. (2012). Estimation of Evapotranspiration ETc and crop coefficient Kc of wheat, in south Nile Delta of Egypt using integrated FAO-56 approach and remote sensing data. *The Egyptian Journal of Remote Sensing and Space Science, 15*(1), 83-89.

Flood, N. (2014). Continuity of Reflectance Data between Landsat-7 ETM+ and Landsat-8 OLI, for both top-of-atmosphere and surface reflectance: A Study in the Australian landscape. *Remote Sensing, 6*(9), 7952-7970.

Gao, F., Anderson, M. C., Zhang, X., Yang, Z., Alfieri, J. G., Kustas, W. P., . . . Prueger, J. H. (2017). Toward mapping crop progress at field scales through fusion of Landsat and MODIS imagery. *Remote Sensing of Environment, 188*, 9-25.

Garatuza-Payan, J., Tamayo, A., Watts, C., & Rodríguez, J. C. (2003). *Estimating large area wheat evapotranspiration from remote sensing data.* Paper presented at the Geoscience and Remote Sensing Symposium, 2003. IGARSS'03. Proceedings. 2003 IEEE International.

Glenn, E. P., Nagler, P. L., & Huete, A. R. (2010). Vegetation index methods for estimating evapotranspiration by remote sensing. *Surveys in Geophysics, 31*(6), 531-555.

Glenn, E. P., Neale, C. M., Hunsaker, D. J., & Nagler, P. L. (2011). Vegetation index-based crop coefficients to estimate evapotranspiration by remote sensing in agricultural and natural ecosystems. *Hydrological Processes, 25*(26), 4050-4062.

Gontia, N. K., & Tiwari, K. N. (2010). Estimation of crop coefficient and evapotranspiration of wheat (Triticum aestivum) in an irrigation command using remote sensing and GIS. *Water resources management, 24*(7), 1399-1414.

González-Dugo, M., & Mateos, L. (2008). Spectral vegetation indices for benchmarking water productivity of irrigated cotton and sugarbeet crops. *Agricultural Water Management, 95*(1), 48-58.

Gonzalez-Dugo, M., Neale, C., Mateos, L., Kustas, W., Prueger, J., Anderson, M., & Li, F. (2009). A comparison of operational remote sensing-based models for estimating crop evapotranspiration. *Agricultural and Forest Meteorology, 149*(11), 1843-1853.

Heermann, D. F., & Solomon, K. (2007). Efficiency and uniformity. Design and operation of farm irrigation systems. Chapter 5. 108-119.

Holden, C. E., & Woodcock, C. E. (2016). An analysis of Landsat 7 and Landsat 8 underflight data and the implications for time series investigations. *Remote Sensing of Environment, 185*, 16-36.

Hunsaker, D. J., Pinter Jr, P. J., Barnes, E. M., & Kimball, B. A. (2003). Estimating cotton evapotranspiration crop coefficients with a multispectral vegetation index. *Irrigation Science, 22*(2), 95-104.

Irmak, A., Ratcliffe, I., Ranade, P., Hubbard, K. G., Singh, R. K., Kamble, B., & Kjaersgaard, J. (2011). Estimation of land surface evapotranspiration with a satellite remote sensing procedure. *Great plains research*, 73-88.

Jackson, T. J., Chen, D., Cosh, M., Li, F., Anderson, M., Walthall, C., . . . Hunt, E. R. (2004). Vegetation water content mapping using Landsat data derived normalized difference water index for corn and soybeans. *Remote Sensing of Environment, 92*(4), 475-482.

Jayanthi, H., Neale, C. M., & Wright, J. L. (2007). Development and validation of canopy reflectance-based crop coefficient for potato. *Agricultural Water Management, 88*(1), 235-246.

Jensen, M. E., & Allen, R. G. (2016). *Evaporation, Evapotranspiration, and Irrigation Water Requirements*.

Kamble, B., Kilic, A., & Hubbard, K. (2013). Estimating crop coefficients using remote sensing-based vegetation index. *Remote Sensing, 5*(4), 1588-1602.

Ke, Y., Im, J., Lee, J., Gong, H., & Ryu, Y. (2015). Characteristics of Landsat 8 OLI-derived NDVI by comparison with multiple satellite sensors and in-situ observations. *Remote Sensing of Environment, 164*, 298-313.

Kebede, H., Fisher, D. K., Sui, R., & Reddy, K. N. (2014). Irrigation methods and scheduling in the delta region of Mississippi: Current status and strategies to improve irrigation efficiency. *American Journal of Plant Sciences, 5*(20), 2917.

Kjaersgaard, J., Allen, R., & Irmak, A. (2011). Improved methods for estimating monthly and growing season ET using METRIC applied to moderate resolution satellite imagery. *Hydrological Processes, 25*(26), 4028-4036.

Kullberg, E. G., DeJonge, K. C., & Chávez, J. L. (2017). Evaluation of thermal remote sensing indices to estimate crop evapotranspiration coefficients. *Agricultural Water Management, 179*, 64-73.

Lei, H., & Yang, D. (2012). Combining the Crop Coefficient of Winter Wheat and Summer Maize with a Remotely Sensed Vegetation Index for Estimating Evapotranspiration in the North China Plain. *Journal of Hydrologic Engineering, 19*(1), 243-251.

Levine, G. (1998). *Performance of two transferred modules in the Lagunera Region: water relations* (Vol. 23): IWMI.

Murray, R. S., Nagler, P. L., Morino, K., & Glenn, E. P. (2009). An empirical algorithm for estimating agricultural and riparian evapotranspiration using MODIS Enhanced Vegetation Index and ground measurements of ET. II. Application to the Lower Colorado River, US. *Remote Sensing, 1*(4), 1125-1138.

Neale, C. M., Bausch, W. C., & Heerman, D. (1989). Development of reflectance-based crop coefficients for corn. *Trans. ASAE, 32*(6), 1891-1899.

Neale, C. M., Jayanthi, H., & Wright, J. L. (2005). Irrigation water management using high resolution airborne remote sensing. *Irrigation and Drainage Systems, 19*(3), 321-336.

Parmar, H., & Gontia, N. (2016). Remote sensing based vegetation indices and crop coefficient relationship for estimation of crop evapotranspiration in Ozat-II canal command. *Journal of Agrometeorology, 18*(1), 137.

Pedro, C. R., & del Consuelo, M. M. M. (2002). Tecnologia de produccion de nogal pecanero.

Rafn, E. B., Contor, B., & Ames, D. P. (2008). Evaluation of a method for estimating irrigated crop-evapotranspiration coefficients from remotely sensed data in Idaho. *Journal of Irrigation and Drainage Engineering, 134*(6), 722-729.

Reyes-Gonzalez, A., Hay, C., Kjaersgaard, J., & Neale, C. (2015). *Use of Remote Sensing to Generate Crop Coefficient and Estimate Actual Crop Evapotranspiration.* Paper presented at the 2015 ASABE Annual International Meeting.

Reyes-González, A., Trooien, T., Kjaersgaard, J., Hay, C., & Reta-Sánchez, D. G. (2016). *Development of Crop Coefficients Using Remote Sensing-Based Vegetation Index and Growing Degree Days.* Paper presented at the 2016 ASABE Annual International Meeting.

Rocha, J., Perdigão, A., Melo, R., & Henriques, C. (2012). Remote sensing based crop coefficients for water management in agriculture *Sustainable Development-Authoritative and Leading Edge Content for Environmental Management*: InTech.

Romero-Trigueros, C., Nortes, P. A., Alarcón, J. J., Hunink, J. E., Parra, M., Contreras, S., . . . Nicolás, E. (2016). Effects of saline reclaimed waters and deficit irrigation on

Citrus physiology assessed by UAV remote sensing. *Agricultural Water Management*.

Rossato, L., Alvala, R. C., Ferreira, N. J., & Tomasella, J. (2005). *Evapotranspiration estimation in the Brazil using NDVI data.* Paper presented at the Remote Sensing.

Rouse Jr, J. W., Haas, R., Schell, J., & Deering, D. (1974). Monitoring vegetation systems in the Great Plains with ERTS.

Roy, D., Kovalskyy, V., Zhang, H., Vermote, E., Yan, L., Kumar, S., & Egorov, A. (2016). Characterization of Landsat-7 to Landsat-8 reflective wavelength and normalized difference vegetation index continuity. *Remote Sensing of Environment, 185*, 57-70.

Roy, D. P., Wulder, M., Loveland, T., Woodcock, C., Allen, R., Anderson, M., . . . Kennedy, R. (2014). Landsat-8: Science and product vision for terrestrial global change research. *Remote Sensing of Environment, 145*, 154-172.

SAGARPA. (2016). Resumen sector agropecuario en la Region Lagunera. Publicacion especial el Siglo de Torreon, p. 24.

Senay, G. B., Friedrichs, M., Singh, R. K., & Velpuri, N. M. (2016). Evaluating Landsat 8 evapotranspiration for water use mapping in the Colorado River Basin. *Remote Sensing of Environment, 185*, 171-185.

Singh, R. K., & Irmak, A. (2009). Estimation of crop coefficients using satellite remote sensing. *Journal of Irrigation and Drainage Engineering, 135*(5), 597-608.

Steel, R. G., & Torrie, J. H. (1980). Principle and procedures of statistic: A biometrical approach: New York: McGraw-Hill.

Tasumi, M., Allen, R. G., Trezza, R., & Wright, J. L. (2005). Satellite-based energy balance to assess within-population variance of crop coefficient curves. *Journal of Irrigation and Drainage Engineering, 131*(1), 94-109.

Thomason, W. E., Phillips, S. B., & Raymond, F. D. (2007). Defining useful limits for spectral reflectance measures in corn. *Journal of plant nutrition, 30*(8), 1263-1277.

Toureiro, C., Serralheiro, R., Shahidian, S., & Sousa, A. (2016). Irrigation management with remote sensing: Evaluating irrigation requirement for maize under Mediterranean climate condition. *Agricultural Water Management*.

Trout, T. J., Johnson, L. F., & Gartung, J. (2008). Remote sensing of canopy cover in horticultural crops. *HortScience, 43*(2), 333-337.

Vanino, S., Pulighe, G., Nino, P., De Michele, C., Bolognesi, S. F., & D'Urso, G. (2015). Estimation of evapotranspiration and crop coefficients of tendone vineyards using multi-sensor remote sensing data in a mediterranean environment. *Remote Sensing, 7*(11), 14708-14730.

Zhang, H., Anderson, R. G., & Wang, D. (2015). Satellite-based crop coefficient and regional water use estimates for Hawaiian sugarcane. *Field Crops Research, 180*, 143-154.

Zipper, S. C., & Loheide II, S. P. (2014). Using evapotranspiration to assess drought sensitivity on a subfield scale with HRMET, a high resolution surface energy balance model. *Agricultural and Forest Meteorology, 197*, 91-102.

CHAPTER 6: General Conclusions

The first objective (chapter 2) of this research was to compare ET estimated from the satellite-based remote sensing METRIC model to *in situ* atmometer readings. Results of our study showed a good relationship between ET_a-METRIC and ET_a-atm with an r^2 of 0.87, "d" of 0.84, and RMSE of 0.65 mm day^{-1}. In general, the ET_a-atm values were lower than ET_a-METRIC values. Daily difference between ET_a-METRIC and ET_a-atm for Brookings site ranged from -0.95 to 1.32 mm day^{-1}, for Volga from -1.93 to 1.33 mm day^{-1}, and for Oak Lake ranged from -0.62 to 2.61 mm day^{-1}. Negative values indicated that the ET_a-METRIC estimates are lower than ET_a-atm, while positive values indicated that the ET_a-METRIC estimates exceeds ET_a-atm. The higher positive values were related with high wind speed values. Daily ET_a differences was attributed to high wind speed values (>4 m s^{-1}) at the time of satellite image overpass. Hence, as the wind speed increases, the ET_a difference increases. However, based on our results, ET_r values from atmometer need to be adjust during the windy days. The adjustment factors were 0.83, 0.87, and 0.68 for Brookings, Volga, and Oak Lake sites, respectively. In conclusion the results of this study can be used by policy makers, researchers, and producers for estimating actual evapotranspiration and improve irrigation water management at local and field scales, using both satellite-based remote sensing METRIC model method and atmometer method.

The second objective (chapter 3) was to assess the relationship between, leaf area index (LAI), surface temperature (T_s), and actual evapotranspiration (ET_a) estimated by remote sensing-based METRIC model and *in-situ* measurements at the same time of

satellite overpass over a corn field in eastern South Dakota. In order to assess the

METRIC model performance the coefficient of determination (r2), mean bias error

MBE), and root means square error (RMSE) were considered. The *in situ* measurements

of LAI obtained with AccuPAR during the time of satellite overpass was compared to the

LAI estimates by the METRIC model. The output of LAI values from the METRIC

model were slightly smaller (12%) than the LAI values derived from AccuPAR, this

slightly difference was attributed to the different LAI scales. METRIC model estimated

the average LAI for all plants with a 30 m by 30 m grid, while the AccuPAR measured

the LAI only in few plants within a pixel (30 x 30 m). However, good linear correlation

was found between *in situ* measured and estimated LAI, with a coefficient of

determination (r^2) of 0.76 and RMSE of 0.59 m^2 m^{-2}. For whole season the surface

temperature (T_s) estimated using the METRIC model was higher than the T_s measured *in*

situ using infrared thermometer by 0.85 °C. The slightly difference was attributed to the

measurements, which were carried out at different scales and different parts of the plant.

A good correlation ($r^2 = 0.87$), and acceptable value of RMSE (1.24 °C) were found

between estimated and measured T_s. Result of comparisons between estimated ET_a

during the 2016 corn growing season showed that ET_a values estimated with the

METRIC model were greater than ET_a values estimated by atmometer. Daily ET_a

estimations error for each image date between the METRIC model and the atmometer

ranged between 4 to 17%. The relationship revealed good agreement between ET_a

estimations, with high coefficient of determination ($r^2 = 0.89$) and low RMSE (0.71 mm

day^{-1}). Finally, the landscape position of observation locations were affected by soil water

content, which lead to low crop height, low LAI, and high T_s in both methods using remote sensing and *in situ* measurements.

The third objective (chapter 4) was to compare the accuracy of $K_{c\text{-NDVI}}$ method to calculate ET_a compared to EB method calculated by the METRIC model over two growing seasons. The linear relationships between NDVI derived from NDVI maps and K_c obtained based on literature values were $K_c = 1.1887 \text{ NDVI} - 0.033$ for 2015 and $K_c = 1.2508 \text{ NDVI} - 0.093$ for 2016. These linear equations were used to generate K_c maps. The K_c values derived from the K_c maps were multiplied by ET_r to estimate ET_a values during two growing seasons using the $K_{c\text{-NDVI}}$ method. The METRIC model was used to estimate ET_a using the full suite of input parameters (Landsat image, weather data, digital elevation map, and land cover map) (EB method). Results showed that the ET_a values estimated with $K_{c\text{-NDVI}}$ method were lower than the ET_a values estimated with EB method by 18% for 2015 and 11% for 2016 growing season. The ET_a $K_{c\text{-NDVI}}$ values were less than the ET_a EB values during the two seasons especially early and late in the growing seasons when the vegetation cover is incomplete and soil evaporation is not fully captured by the $K_{c\text{-NDVI}}$ method. As a result, the accuracy of ET_a estimation with the $K_{c\text{-NDVI}}$ method decreased 17% compared with EB method during the period of study. Finally, $K_{c\text{-NDVI}}$ method give less accurate estimation of ET_a during early and late seasons, but for irrigation scheduling purposes, where the crop water demand is highest during the middle of the growing season, the $K_{c\text{-NDVI}}$ method may be acceptable. The results of this study showed a strong relationship between the $K_{c\text{-NDVI}}$ method and the EB method throughout two growing seasons with r^2 of 0.97 and RMSE of 0.37mm day^{-1}. In conclusion, the $K_{c\text{-NDVI}}$ method performed well for ET_a estimations during two seasons,

indicating that this method can be a robust and reliable method to estimate ET_a with minimum input parameters at regional and field scales for short time periods.

The fourth objective (chapter 5) was to estimate crop evapotranspiration (ET_c) using satellite remote sensing-based vegetation index. Spatially ET_c maps were created as an output of K_c maps multiplied by ET_r values. The ET_c values ranged from 1.53 to 7.65 mm day^{-1} during period of study. The results showed that ET_c values were low at the beginning of the growing season, while high ET_c values were presented from mid-season to harvest season. Daily ET_c maps helped to explain the variability of crop water use throughout the growing seasons. Farmers in the northern México region currently use ET_r in their irrigation scheduling methods. The results indicate that farmers could reduce their seasonal water application amounts by 18% just by using ET_c appropriately in their irrigation scheduling methods. The information generated in this study is essential for irrigation scheduling because it shows when and how much water is required by the crop according to different growth stages. Based on the results we can conclude that ET_c maps developed from remotely sensed multispectral vegetation indices are a useful tool to quantifying accurate crop water consumptions from space at regional and field scales.

In conclusion, in all chapters satellite remote sensing was used to developed ET_a maps, which can be used by policy makers, researchers, and farmers for estimating crop water use to improve irrigation water management.

APPENDIX

Example of output of hourly quality control for solar radiation (Rs), air temperature (Ta) and dew point temperature (Td) in August 2016 growing season.
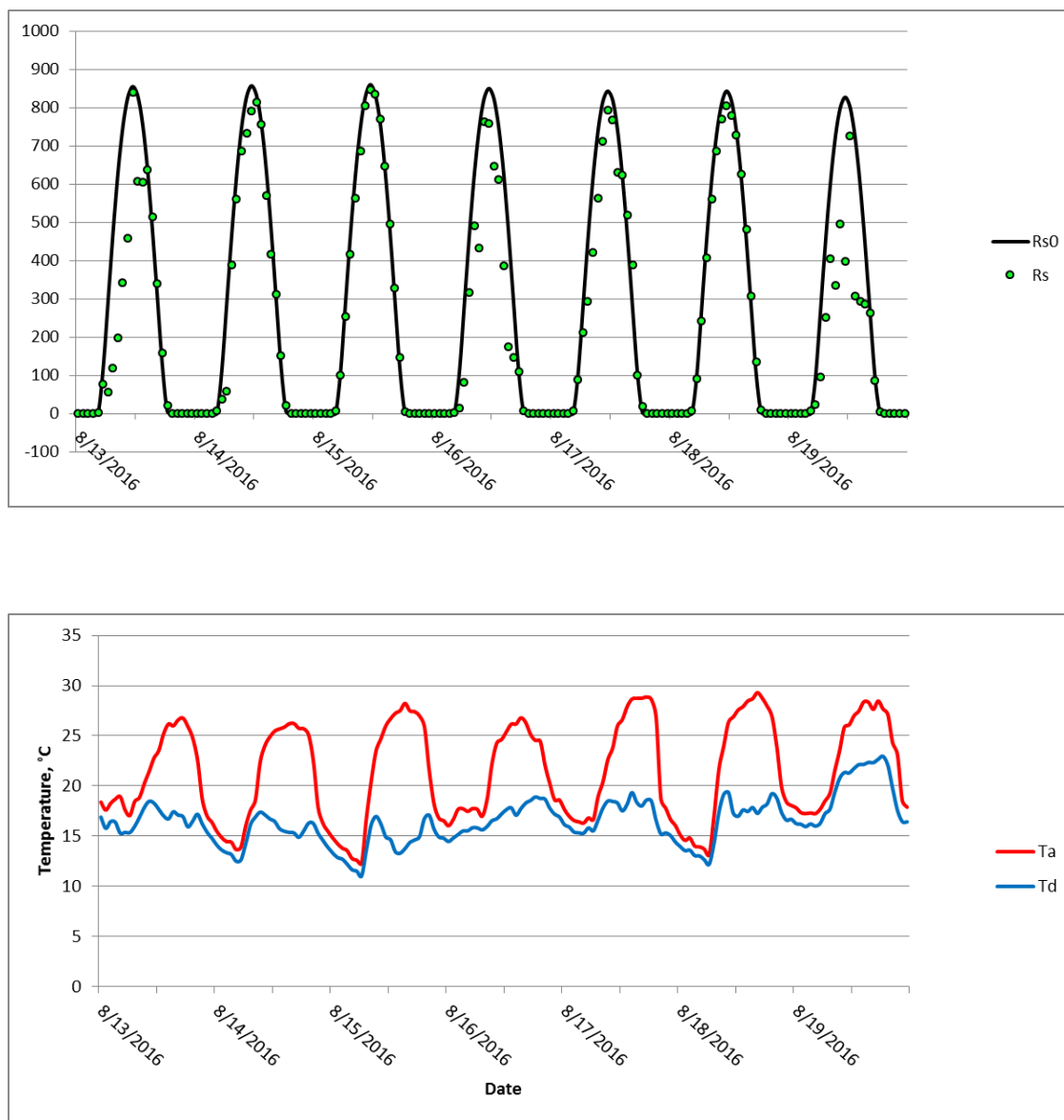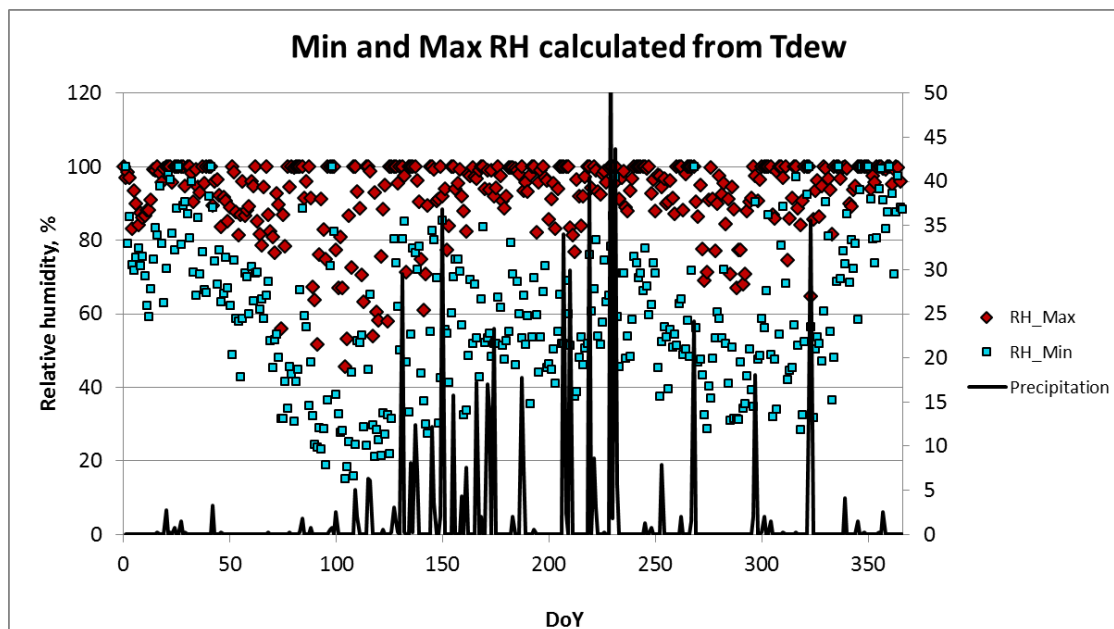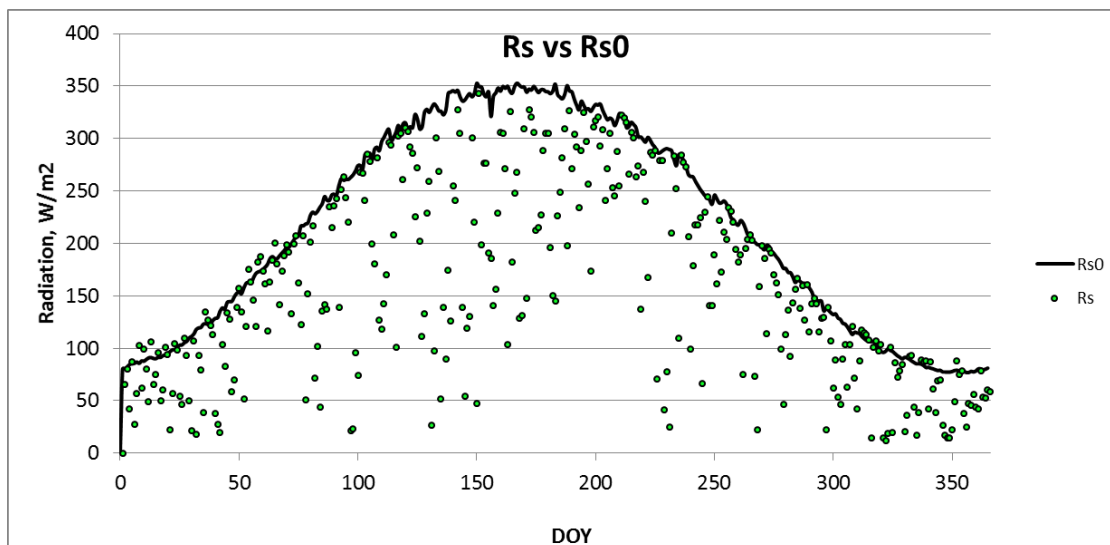

Figure A.1 Hourly quality control samples for Rs, Ta, and Td.

Example of output of daily quality control for solar radiation (Rs), minimum and maximum relative humidity (RH), minimum and maximum air temperature (Ta), and wind speed (WS) for 2016 growing season.
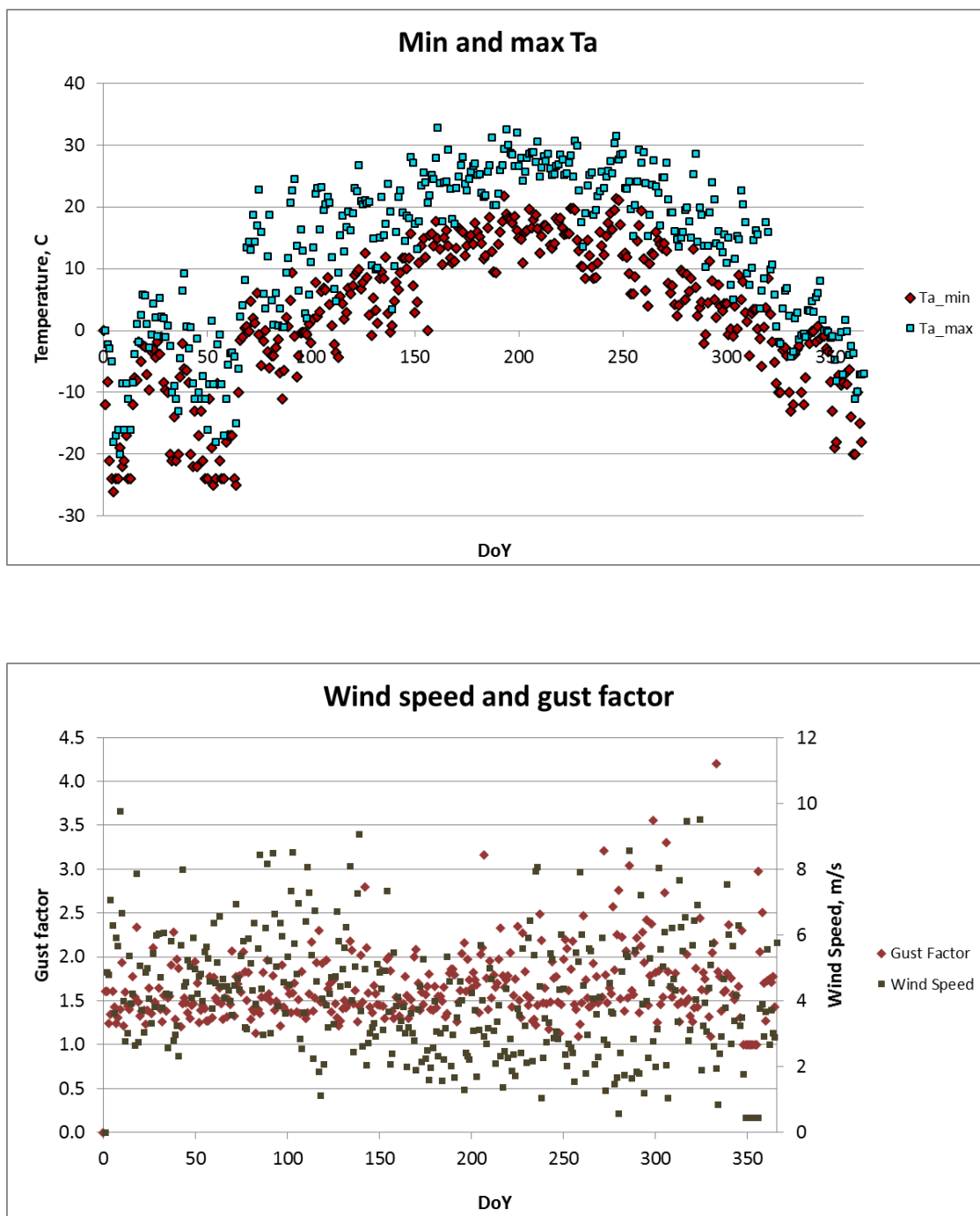
Figure A.2 Daily quality control for solar radiation (Rs), minimum and maximum relative humidity (RH), minimum and maximum air temperature (Ta), and wind speed.

The weather data used in this research did not require any adjustment to solar radiation, relative humidity, air temperature, and wind speed. For example, on clear sky days solar radiation (Rs) should approach the theoretical clear sky solar radiation (Rs0)

curve, 3 - 5% upper or below of Rs0 curve need calibration. Maximum relative humidity

(RH) should be between 95 - 100% and minimum RH stay above ±15%. Minimum air

temperature and dew point temperature are within 2 - 3°C. Wind speed generally average

about 2 ms^{-1} for agricultural setting, less than 1 ms^{-1} may indicate problems.

Hot and cold pixels selected during the 2016 growing season.

Table A.1 Hot and cold pixels used for the analysis.

| DOY | Pixel | Coordinates | | ETrF | Elevation (m) | Albedo | NDVI | LAI | Ts (K) |
		X (UTM)	Y (UTM)						
154	Cold	687390	4931490	1.05	584	0.19	0.82	6.00	296.56
	Hot	691470	4928280	0.35	597	0.15	0.22	0.18	309.83
187	Cold	676860	4918080	1.05	508	0.19	0.83	4.78	300.75
	Hot	687480	4908330	0.35	505	0.18	0.41	0.47	312.94
194	Cold	667652	4907809	1.05	492	0.23	0.84	5.34	296.63
	Hot	688784	4914143	0.35	526	0.17	0.39	0.42	306.97
202	Cold	680222	4867647	1.05	497	0.21	0.83	6.00	299.93
	Hot	675631	4914700	0.35	512	0.18	0.46	1.85	308.06
218	Cold	693029	4904941	1.05	514	0.21	0.89	6.00	296.8
	Hot	672877	4912705	0.35	500	0.18	0.49	2.39	303.85
234	Cold	692517	4928836	1.05	591	0.16	0.78	6.00	294.05
	Hot	689106	4923735	0.35	558	0.15	0.47	1.96	299.46
258	Cold	675770	4914916	1.05	516	0.19	0.84	5.16	289.86
	Hot	683416	4922914	0.35	532	0.14	0.28	0.16	300.16